# ABSTRACT

Title of dissertation: MECHANOBIOLOGY OF T CELL ACTIVATION

King Lam Hui
Doctor of Philosophy, 2015

Dissertation directed by: Professor Arpita Upadhyaya
Department of Physics

Cells can sense and respond to the physical environment through generation and transmission of mechanical forces from the surroundings to the cell interior and from one cell to another. This dissertation focuses on mechanosensing by T cells, key players in the adaptive immune system, which form a strong line of defense against infections by their ability to recognize foreign molecules and develop an appropriate response. T cells form close contact with an opposing antigen presenting cell upon recognition of protein fragments derived from infecting pathogens (antigens). Recent studies have shown that externally applied forces can trigger biochemical signaling in T cells. How forces are internally generated by T cells, involved in signaling and transmitted at the level of the cell interface, remains unclear. In this thesis, we investigate the molecular mechanisms of force generation by T cells and their response to forces and the stiffness of the opposing surface.

We have quantitatively characterized the initial phase of T cell contact with a model of antigen-bearing surfaces. We observe that T cells spread on such sub-

strates and that the kinetics of spreading follows a universal function, with the spreading rate dependent on actin polymerization and myosin II activity. Altering cell-substrate adhesions leads to qualitative changes in cell spreading dynamics and wave-like patterns of actin dynamics. We then used soft elastic substrates with stiffness comparable to that of antigen presenting cells, to measure the forces generated by T cells during activation.

Perturbation experiments reveal that these forces are largely due to actin assembly and dynamics, with myosin contractility contributing to the development of traction forces but not its maintenance. We find that Jurkat T-cells are mechanosensitive, with both traction forces and signaling dynamics exhibiting sensitivity to the stiffness of the substrate. We further demonstrate that dynamics of the T cell microtubule cytoskeleton also participates in regulating forces at the cell-substrate interface, through the Rho/ROCK pathway which regulates myosin II light chain phosphorylation.

Overall, this work highlights physical force as an essential mediator that connects stiffness sensing to intracellular signaling, which then directs gene expression and eventually the immune response in T cells.

# MECHANOBIOLOGY OF T CELL ACTIVATION

by

King Lam Hui

Dissertation submitted to the Faculty of the Graduate School of the
University of Maryland, College Park in partial fulfillment
of the requirements for the degree of
Doctor of Philosophy
2015

Advisory Committee:
Professor Arpita Upadhyaya, Chair
Professor Helim Aranda-Espinoza
Professor Wolfgang Losert
Professor Garegin A. Papoian
Professor Wenxia Song, Dean's Representative

# Acknowledgments

There are many people who I wish to thank for the completion of this dissertation. I will start with my family, especially my parents, for their upbringing and provision of precious resources and support all these years. I am really grateful to my sister, who has grown up and is taking good care of and providing support to my family while I am studying abroad. I owe a lot to them.

I would like to thank my advisor, Prof. Arpita Upadhyaya, for her guidance, encouragement and support all these years. She has been patient and forgiving, as I had little knowledge of biology and cells when I started my doctoral studies. I would also like thank the committee members: Prof. Wolfgang Losert, Prof. Garyk Papoian, Prof. Helim Aranda-Espinoza and Prof. Wenxia Song for reviewing my manuscript and providing invaluable comments.

As biophysics is an interdisciplinary science, I have been getting generous help from my collaborators. I would like to thank Dr. Larry Samelson and Dr. Lakshmi Balagopalan for providing the opportunity of predoctoral training in their laboratory for a year. I am grateful to Dr. Janis Burkhardt and Dr. Nathan Roy, who just started a new collaboration with our laboratory and are providing us with primary cells and reagents. In addition, I have received reagents and enthusiastic help from Dr. Morgan Huse and Dr. Sudha Kumari. I have met many excellent intellectuals and have learned a lot from discussions: my coworkers Dr. Jessica Wayt, Dr. Brian

Grooman, Dr. Mikheil Azatov, Ms. Christina Ketchum and Mr. Ivan Adolfo Rey Suarez; and my colleagues Dr. Chao-Hong Liu, Ms. Chenlu Wang and Ms. Saein Kwak.

I am indebted to my long time friend, Dr. Tommy So, who shares a common background with me as a physics student getting into biology. He has been giving me valuable comments and we shared our thoughts and daily life through online chats between experimental steps. Another friend dear to me is Dr. Kan Leung Cheng, who accompanied me during my most frustrated days, when he was busy preparing his dissertation defense. Conversation with him has changed my view on and get me interested in religion, evolution and psychology. I also wish to thank the fellow Hong Kong doctoral students in Maryland, including Dr. Benedict Chan, Dr. Stephen Ho, Dr. Horace Ip, Dr. Waishing Lee, Mr. Anthony Law and Mr. Chau-Wai Wong. Their company to dinners and gatherings has given me much warmth in the heart. Last but not least, I would like to thank my friends in Hong Kong and Maryland, especially fellows of the Hong Kong Harmonica Association. Despite the long period I was absent from Hong Kong, they still remembered me and invited me for a performance back in Hong Kong in August 2012.

The work in this thesis was supported in part by National Science Foundation, National Cancer Institute and University of Maryland. The information in this dissertation does not necessarily reflect the position or policy of the funders, and no official endorsement should be inferred.

# Contents

# List of Figures

# List of Abbreviations

| | |
|---|---|
| CLP | Common Lymphoid Progenitor |
| APC | Antigen Presenting Cells |
| TCR | T Cell Receptor |
| BCR | B Cell Receptor |
| MHC | Major Histocompatibility Complex |
| RAG | Recombination Activating Gene |
| CD | Cluster of Differentiation |
| ITAM | Immunoreceptor Tyrosine-based Activation Motif |
| RSS | Recombination Signal Sequence |
| NHEJ | nonhomologous end-joining |
| HLA | Human-Leukocyte-Associated |
| ER | Endoplasmic Reticulum |
| CDR | Complementarity Determining Region |
| pMHC | peptide-MHC complex |
| BFP | Biomembrane Force Probe |
| NMR | Nuclear Magnetic Resonance |
| IS | Immunological synapse |
| scFv | single-chain variable fragment |
| MTOC | microtubule organization center |
| TIRF | Total Internal Reflection Fluorescence |
| PLC$\gamma$1 | Phospholipase C $\gamma$1 |
| PKC | protein kinase C |
| LAT | Linker of activated T cells |
| SMAC | SupraMolecular Adhesion Complex |
| F-actin | Filamentous actin |
| RhoGEF | Rho GTPase Guanine nucleotide Exchange Factor |
| NMII | Non-muscle myosin II |
| NMHC II | Non-muscle myosin II heavy chain |
| RLC | Regulatory light chain |
| RT-PCR | Reverse transcription polymerase chain reaction |
| MLCK | Myosin light chain kinase |
| STIM1 | Stromal interaction molecule 1 |
| SOCE | Store Operated Calcium Entry |
| $Ca^{2+}$ | Calcium ions |
| $PIP_2$ | phosphatidylinositol-4,5-biphosphate |
| $IP_3$ | inositol 1,4,5-trisphosphate |
| DAG | Diacylglycerol |
| CRAC | Calcium release activated current |
| SCID | severe combined immunodeficiency |
| SLE | systemic lupus erythemantosus |
| TFM | Traction force microscopy |
| OGB-1 | Oregon Green 488 BAPTA-1 |
| EGTA | ethylene glycol tetraacetic acid |
| FAK | focal adhesion kinase |
| Lck | lymphocyte-specific protein tyrosine kinase |

| | |
|---|---|
| Fyn | Proto-oncogene tyrosine-protein kinase |
| ZAP-70 | Zeta-chain-associated protein kinase 70 |
| LAT | Linker of activated T cells |
| SLP-76 | Lymphocyte cytosolic protein 2 |
| Grb2 | Growth factor receptor-bound protein 2 |
| WASp | Wiskott-Aldrich syndrome protein |
| Nck | non-catalytic region of tyrosine kinase |
| Gads | GRB2-related adapter protein 2 |
| LFA-1 | Lymphocyte function-associated antigen 1 |
| PKC$\theta$ | protein kinase C $\theta$ |
| WAVE2 | Wiskott-Aldrich syndrome protein family member 2 |
| AFM | atomic force microscope |
| FA | focal adhesion |
| ECM | extra-cellular matrix |
| FACS | Fluorescence-activated cell sorting |
| VLA-4 | Very Late Antigen-4 |
| ICAM-1 | Intercellular Adhesion Molecule 1 |
| DMSO | Dimethyl sulfoxide |
| IL-2 | interleukin 2 |

# Chapter 1

# Introduction

## 1.1 Overview of the thesis

Mechanobiology is the study of how physical stimuli, for example, substrate stiffness, mechanical stretching etc. are sensed by the cell through physical forces, which then converts the signal into biochemical signal and drives biological outcomes (Figure 1.1). Cells from diverse tissue types had been shown to be sensitive to physical forces [97]. In the case of immune cells, forces were suggested to be essential for arrest and extravasation from blood vessels [4]. Importantly, recent *in vitro* studies have established that many cell surface receptors [116, 111, 132, 46] and intracellular molecules [177] are mechanosensitive and some exhibit catch-bond behaviour, in which interaction lifetime increases under forced condition.

This thesis will focus on physical forces generated and maintained by T cells when they get activated. We will first characterize the cellular and membrane

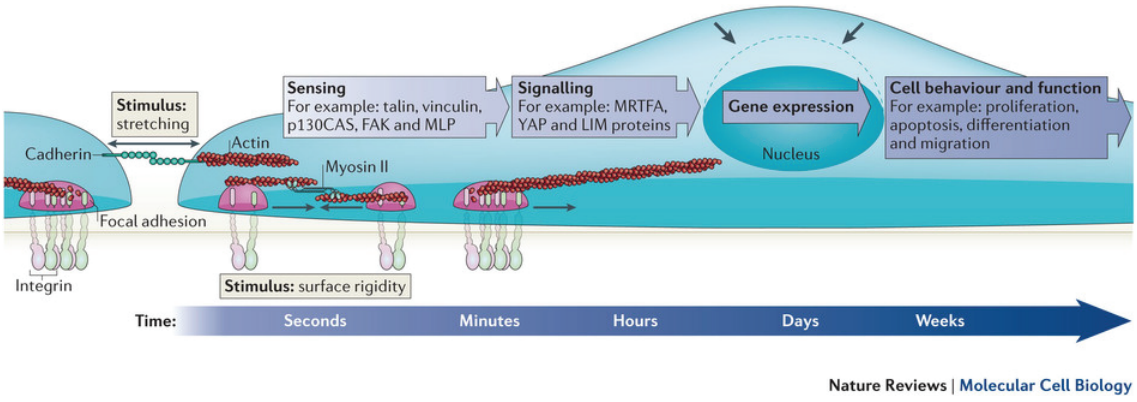


Figure 1.1: **Mechanotransduction.** Mechanotransduction converts mechanical stimuli into chemical signals to regulate cell behaviour and function. Actin, myosin II and other mechanosensitive proteins all take part in force sensing. Image is from [97]. Image used with permission.

dynamics when T cells are activated on rigid substrate (chapter 2), then measure traction forces involved during activation (chapter 3), investigate on the molecular mechanism of generation of these traction stresses (chapter 4), and finally as ongoing work, how the signaling output is related to the physical parameter input during T cell activation (appendix A). We will start with a brief account of T cell biology and discuss on why understanding mechanobiology of T cell activation will contribute to understanding T cell's *in vivo* immune response.

## 1.2 T cell as a part of mammalian immune system

Our body is exposed to constant threats from infection by bacteria, viruses, fungi and parasites in the environment. To face this challenge, different organisms

develop their own line of defence, known as the immune system. Researchers have identified two major subsystems in our immune system: **innate immunity** and **adaptive immunity**. These two systems cooperate to fight pathogens (Figure 1.2a): innate immunity forms the front barrier, whereas adaptive immunity provides pathogen-specific immune response and long term immunological memory.

### 1.2.1 Innate immunity provides the front barrier to pathogen invasion

The innate immune system provides both physical and chemical barrier to pathogens. Our skin, tight junctions between epithelials cells, acidic pH in our stomach and antimicrobial peptides present in mucus layers etc., all inhibit entrance of pathogens and maintain sterility in our body [2]. When one of these barriers is breached, chemical signals (bacterial peptides, cytokines released by immune cells in vicinity etc.) drive chemotaxis of different types of immune cells, including macrophages, neutrophils, dendritic cells etc to sites of infection (Figure 1.2b). These immune cells carry pattern recognition receptors which recognize conserved features on pathogens: formylated methionine in bacterial peptides, CpG motifs in bacterial and viral DNA etc. Upon recognition of invading microbes, professional phagocytes such as macrophages and neutrophils carried out phagocytosis, a process during which their cell surface protruded and engulfed the microbe into phagosomes (Figure 1.2c). Neutrophils can even emit their chromatin together with granule proteins to trap and kill invading bacteria [20]. Apart from direct attack

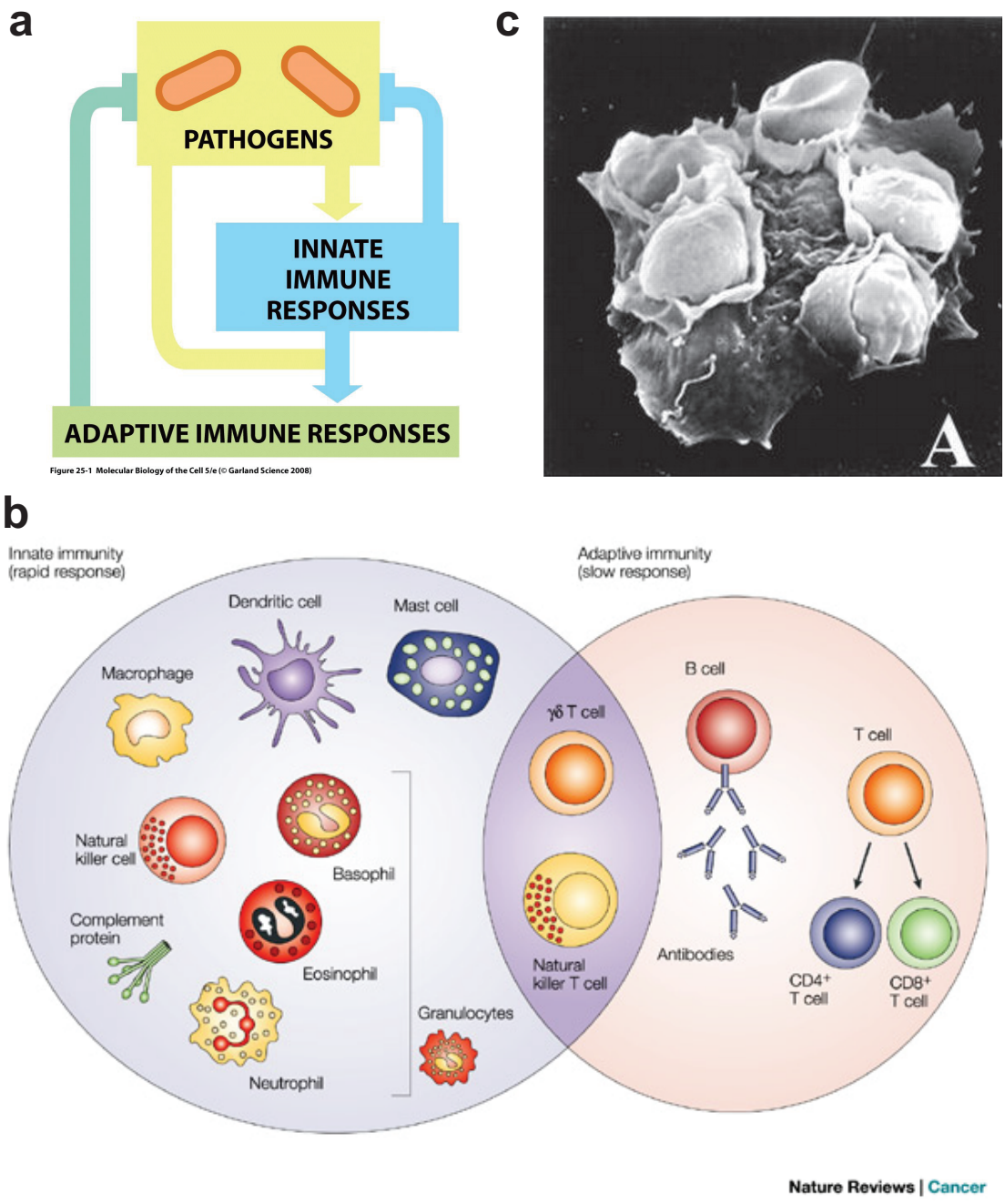


Figure 1.2: **Immune system comprises of innate and adaptive immunity.** (a) Innate and adaptive immunity cooperate to fight pathogens. (b) Cells and accessory proteins comprising our immune system. (c) Macrophage phagocytizing red blood cells opsonized with antibodies. Images are from [2, 56, 76]. All images used with permission.

on invaders, these immune cells secrete signaling proteins and lipids, such as cytokines and prostaglandins to generate an **inflammatory response**. This results in recruitment of more immune cells to the infected site and triggering of fever, a rise of body temperature. Finally, macrophages and more importantly, dendritic cells, act as a critical link between innate and adaptive immunity, to inform T and B cells about identity of invading pathogens and thereafter enable pathogen specific immune response and memory.

### 1.2.2 Adaptive immunity provides specific immune response and memory

From an evolutionary point of view, adaptive immunity was developed later than innate immunity, and was only found in Gnathostomes (jawed vertebrates) and Agnathans (jawless fish)[39, 40]. In contrast, innate immunity was found even in single cell organisms, and studies of how nermatodes (*Caenorhabditis elegans*), bacteria and archaea fight viral infections had led to important breakthroughs in biomedical science and biotechnology [66, 84]. The main difference between innate and adaptive immunities lies in the **specificity** towards individual antigens and the development of **memory** of previous infection. These two characteristics are demonstrated in Figure 1.3. The first encounter with a particular antigen generates a **primary immune response** which takes two weeks to develop, whereas later infection leads to a faster and stronger **secondary immune response**. To achieve that, adaptive immunity uses genetic recombination to generate enormous antigen

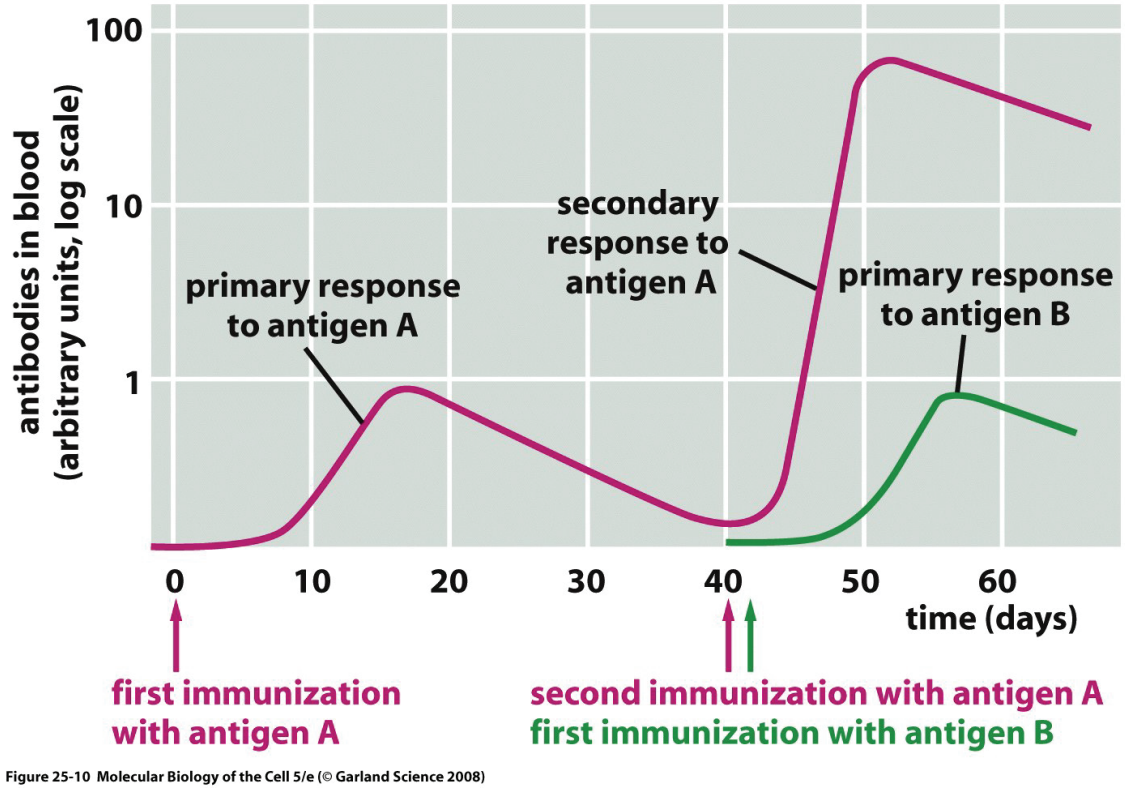


Figure 1.3: **Adaptive immunity provides specificity and memory.** Antibody level in blood after first and second immunization for two different antigens (Red and green). Image is from [2]. Image used with permission.

receptor diversity, to the extent that almost any potential pathogen or toxin can be recognized. The cost in return, is the maintenance of a delicate balance between responses towards self and foreign antigens, in which dysregulation can lead to autoimmune diseases. Also, adaptive response acts slower than innate response, and the primary response takes two weeks to peak, although secondary responses take shorter time (Figure 1.3).

In the human adaptive immune system, two major lineages of white blood cells called lymphocytes detect and respond to pathogen invasion in a specific manner. They are the thymus derived T lymphocytes (T cells) and the bone marrow derived B lymphocytes (B cells) (Figure 1.4a). Thymus and bone marrow are called central lymphoid organs where lymphocytes develop from common lymphoid progenitor (CLP) cells (Figure 1.4b). While B cells develop from CLP in the bone marrow, some CLPs migrate through the blood to the thymus and develop to become naïve T cells, T cells which have not encountered their cognate antigen within the periphery. As shown by the flow chart in Figure 1.4c, lymphocytes continuously leave the bloodstream and enter lymph vessels at peripheral lymphoid organs (lymph nodes, spleen etc.). After percolation through various nodes, lymphocytes rejoin the blood through the thoracic duct.

As demonstrated in Figure 1.5a, after dendritic cells phagocytose microbes (section 1.2.1), the phagosomes get fused with lysosomes, which carry acid hydrolases to kill the microbes and degrade their biomatter. Such dendritic cells are said

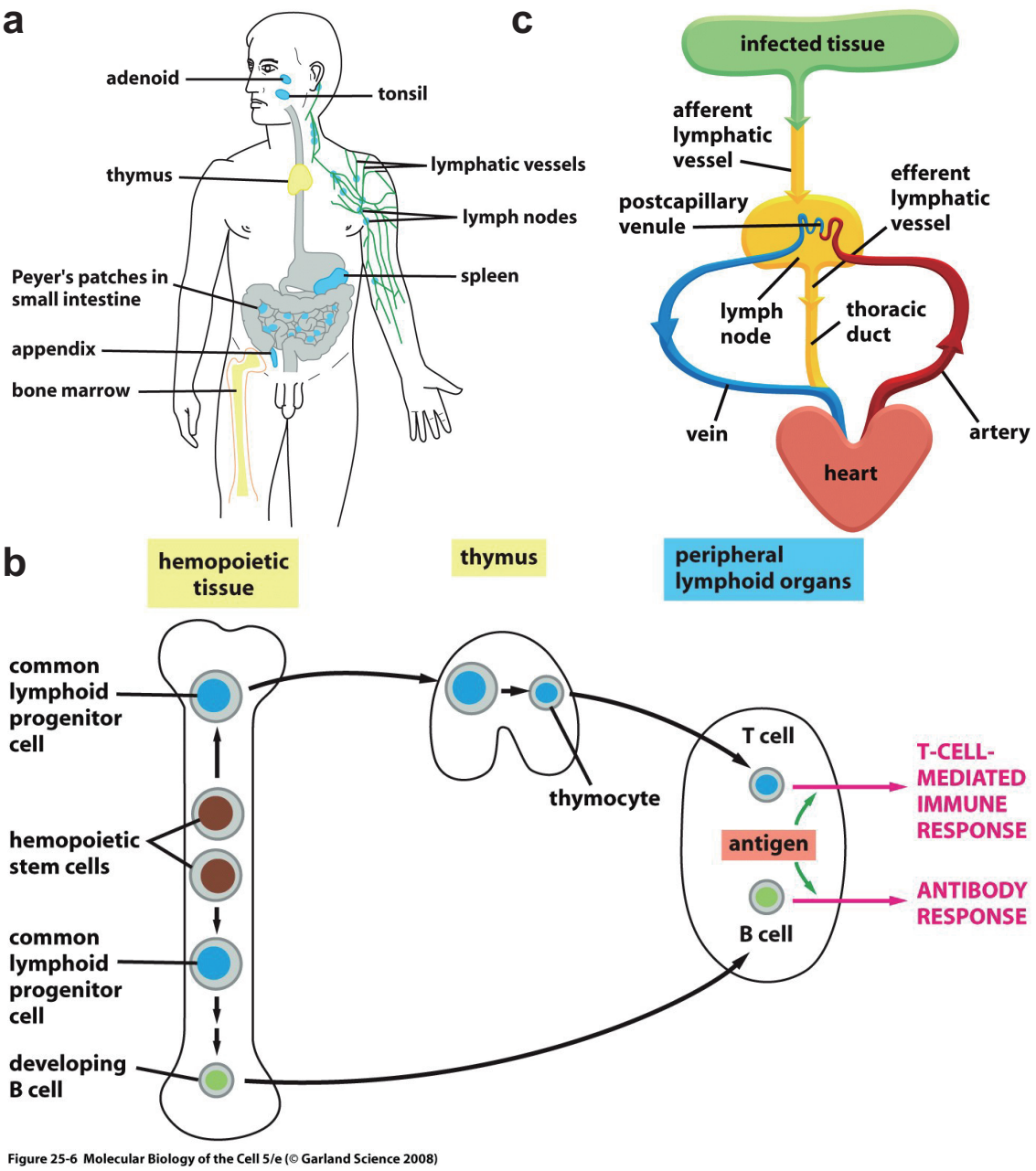


Figure 1.4: **Life cycle of T and B cells.** (a) Human lymphoid organs. Central lymphoid organs are labelled in yellow, peripheral lymphoid organs in blue and lymphatic vessels in green. (b) Development of T cells and B cells. (c) Lymphocytes circulate between the blood and the lymph. Image is from [2]. Image used with permission.

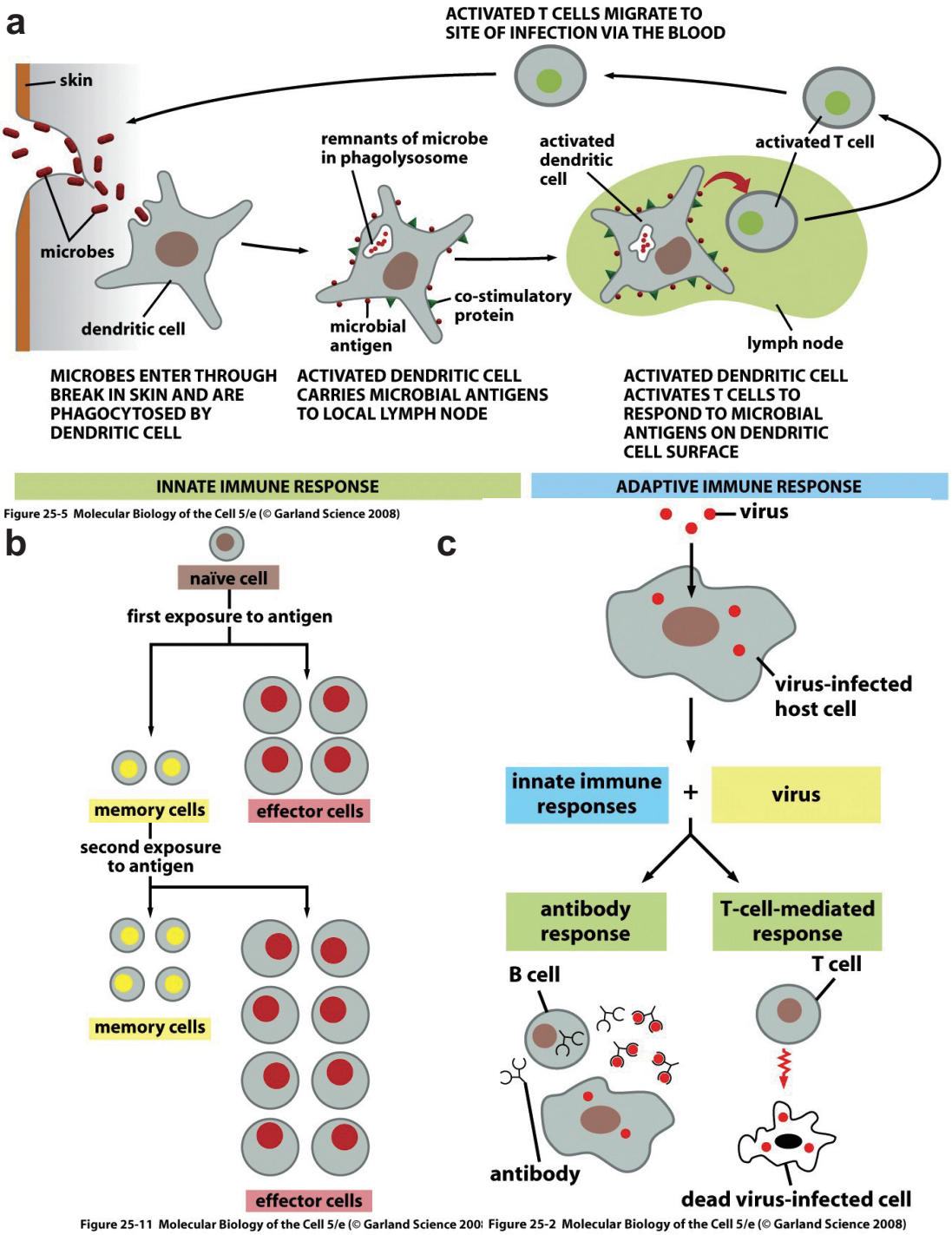


Figure 1.5: **Innate and adaptive immunity cooperate to fight pathogens.** (a) Dendritic cells destroy phagocytosed microbes, and present to T cell. (b) T and B cells proliferate and differentiate into effector and memory cells. (c) T and B cells orchestrates adaptive immune response. Images are from [2]. Images used with permission.

to be activated. They migrate to a nearby lymph node and upregulate their expression of costimulatory proteins. In the lymph node, they present protein peptides (antigen) from the microbe to T cell recognizing that specific antigen, and activate the T cell. For this reason, dendritic cells, macrophage and B cells are called professional antigen presentation cells (APC), as they are particularly efficient at presenting antigens to activate T cells. The molecular basis of this process is discussed in section 1.3.3.

In order to orchestrate an intact immune response as shown in Figure 1.3, naïve lymphocytes proliferate and differentiate into effector and memory cells upon activation (Figure 1.5b). T and B cells operate in different manner: when stimulated, B cells produce antibodies which bind specifically to virus and microbial toxins to deactivate them and to mark for destruction by phagocytic cells; on the other hand, stimulated T cell patrol the body, destroy virus-infected host cells, and produce signal molecules called cytokines to activate macrophages and B cells for microbe destruction and antibody production respectively (Figure 1.5c).

## 1.3 T cell activation: a molecular perspective

Modern immunology is interwined with molecular biology. For example, subtypes of lymphocytes are defined by molecular markers on their cell surface. More importantly, understanding of proteins expressed in T and B lymphocytes and their interactions is indispensable to explain adaptive immunity. The basic molecular

constituents of adaptive immunity are surprisingly few: T Cell Receptor (TCR), antibodies, Major Histocompatibility Complex (MHC) molecules, and Recombination Activating Gene 1 and 2 (RAG1/RAG2) proteins [39]. In this thesis, we will focus on T cells and how TCR triggering leads to cellular response.

### 1.3.1 TCR is a multimeric protein complex binding specifically to MHC

The key protein interaction in T cell biology is undoubtedly the TCR-MHC interaction (Figure 1.6a). TCR is a multimeric protein complex comprising of various transmembrane protein subunits: TCR $\alpha$ and $\beta$ chains, which bind to peptide-MHC (pMHC) and have short cytoplasmic tails; CD3$\delta$, $\epsilon$, $\gamma$ and $\zeta$ chains (CD for Cluster of Differentiation) which are called invariant chains, and contain immunoreceptor tyrosine-based activation motif (ITAM) in their cytoplasmic tails, motifs with a tyrosine separated from a leucine or isoleucine by any two other amino acids (signature sequence of YxxL/I). TCR $\alpha\beta$ heterodimer binds noncovalently to CD3$\epsilon\gamma$, CD3$\epsilon\delta$ and CD3$\zeta\zeta$ dimers in 1:1:1:1 stochiometry, forming the TCR complex. In addition, the key protein kinase that phosphorylates the ITAMs of CD3 proteins, lymphocyte-specific protein tyrosine kinase (Lck), is associated with the cytoplasmic tail of co-receptors CD4 and CD8. These coreceptors have extracellular domains recognizing the invariant part of the MHC molecule. A more realistic molecular view of the TCR-MHC interaction is shown in Figure 1.6b.

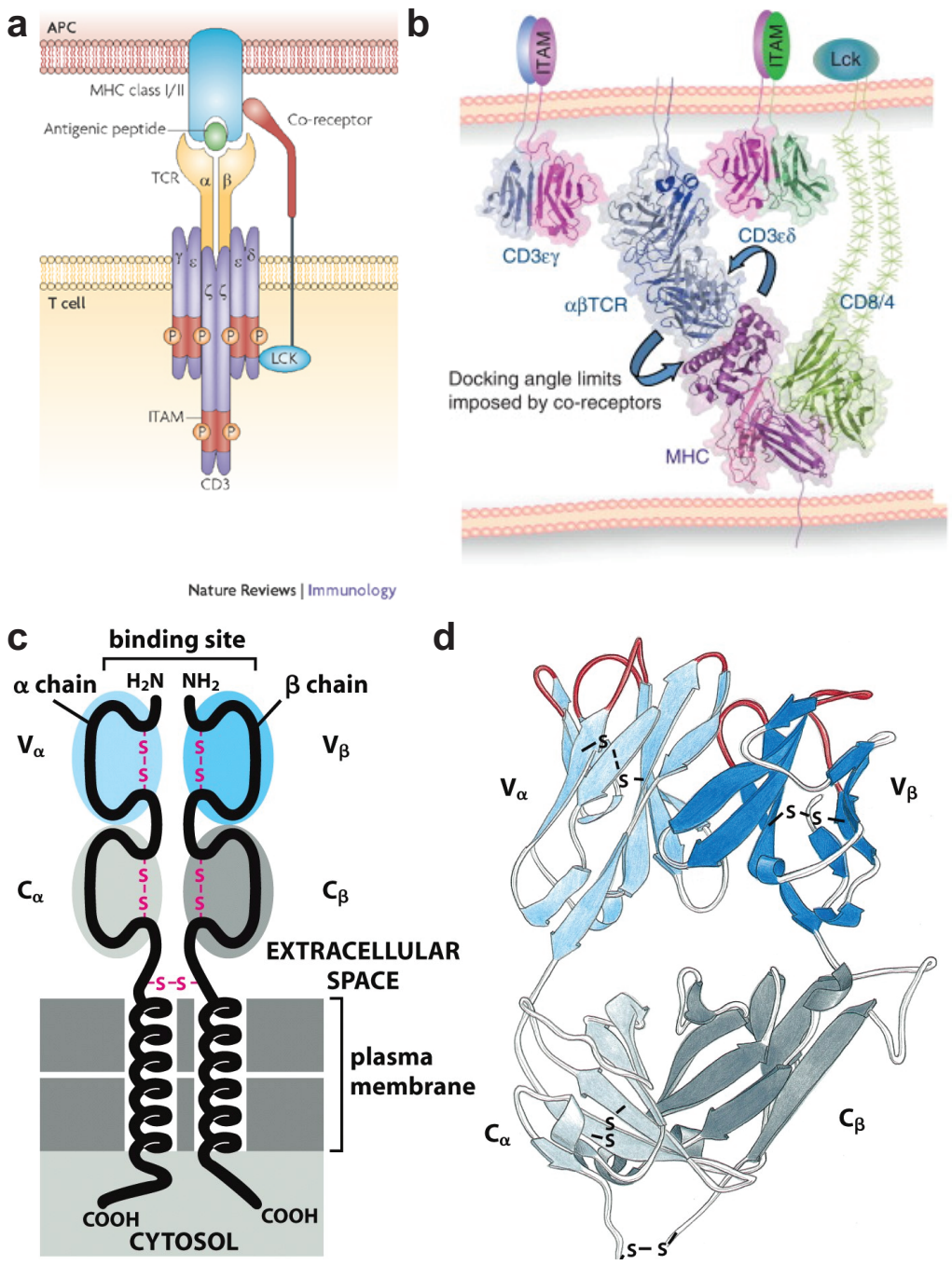


Figure 1.6: **TCR-pMHC interaction.** (a) Cartoon view of core proteins in T cell-APC interaction. (b) Molecular view of TCR-MHC interaction. (c) Schematic of TCR $\alpha\beta$ structure. (d) Three-dimensional view of extracellular domain of TCR $\alpha\beta$. The hypervariable loops are shown in red. Images are from [72, 69, 2] respectively. All images used with permission.

TCR $\alpha$ and $\beta$ chains form a heterodimer as shown in Figure 1.6c and d. Both chains are composed of two separate immunoglobulin (Ig)-like domains: variable (V) and constant (C). The key region for antigen recognition are 3 hypervariable loops in both $V_\alpha$ and $V_\beta$ domains as shown in Figure 1.6d: their amino acid sequence varies among TCRs from different T cells from the same animal. These loops are called complementarity determining regions (CDRs), and the individual loops are called CDR1, CDR2 and CDR3. Their binding position relative to pMHC is discussed in section 1.3.3.

### 1.3.2 MHC presents protein peptide to TCR

MHC molecules can be categorized into 3 different classes, class I, class II and class III, among which class I and II are the most important for antigen presentation to T cells. Class I and II MHC molecules differ in structure, tissue expression and binding partners. As shown in Figure 1.7, in class I, the $\alpha$ chain is folded into three extracellular globular domains $\alpha_1$, $\alpha_2$ and $\alpha_3$, with a separate $\beta_2$ microgobulin domain binding noncovalently to $\alpha_3$. On the other hand, class II MHC is a heterodimer of $\alpha$ and $\beta$ chains. The key regions for antigen presentation are the peptide-binding groves between $\alpha_1$ and $\alpha_2$ in class I and between $\alpha_1$ and $\beta_1$ in class II respectively. A zoomed-in view of TCR-peptide-MHC interface is shown in Figure 1.8b.

In terms of expression pattern, class I is expressed in all tissue cells while

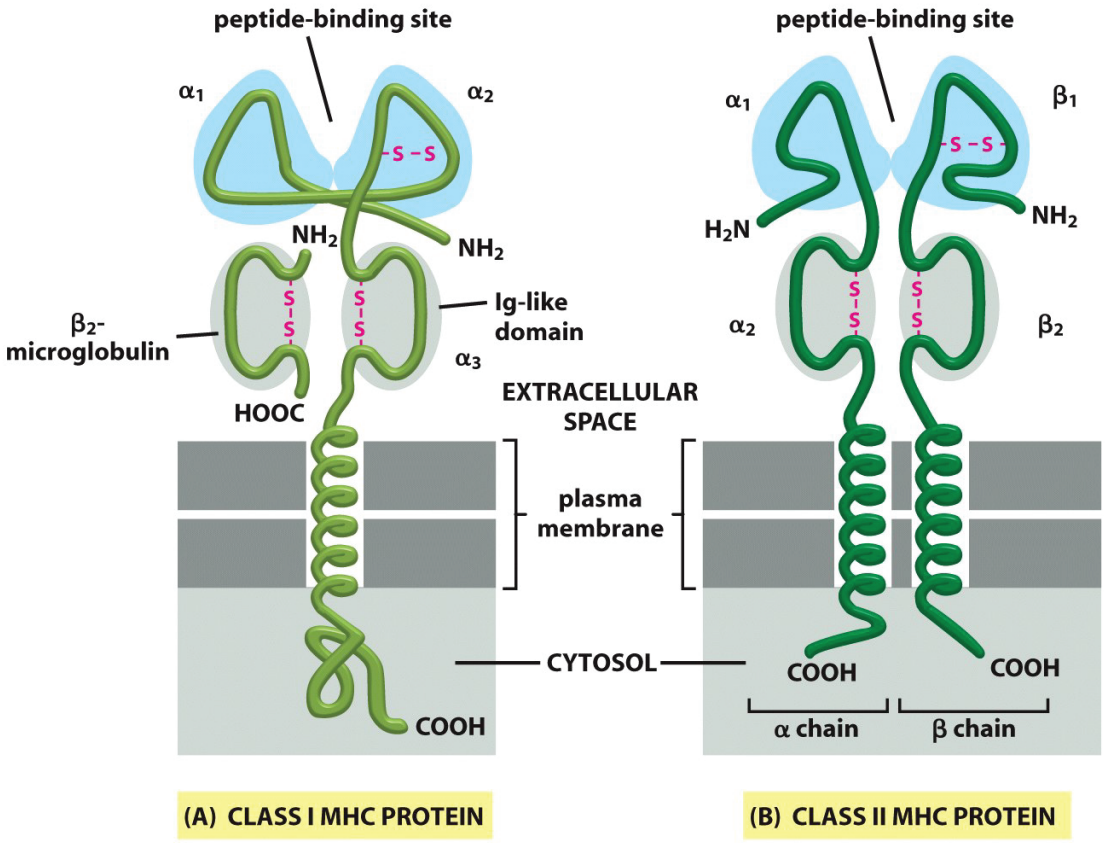


Figure 1.7: **Molecular structure of MHC.** Schematic of class I and II MHC structure. Image is from [2]. Image used with permission.

class II expression is limited to professional APCs (section 1.2.2). Tissue cells regularly transport cytosolic peptides (self/foreign) into endoplasmic reticulum (ER) and bound to $\alpha$ chain of MHC I, which finally presents the peptide to the extracellular space; for professional APCs, endocytosed/ phagocytosed microbial proteins are cleaved by proteases in the endosome, the resultant peptides bind to MHC II molecules targeted to the endosome from Golgi apparatus and finally are presented to cell surface. Therefore, class I presents endogenous while class II presents exogenous antigens. Moreover, class I and II have different binding partners to coreceptors expressed on T cells at their membrane proximal domain: CD4 binds to $\beta_2$ domain of class II and CD8 binds to $\alpha_3$ domain of class I. These two interactions define functions of peripheral T cell species: mature naïve, effector and memory T cells are expressing only one of the two coreceptors, $CD4^+CD8^-$ T cells are the helper cells ($T_h$) and $CD4^-CD8^+$ T cells are the cytotoxic cells.

### 1.3.3 TCR-pMHC binding: a structural view

The first crystal structure of TCR-MHC binding was determined in 1996 [70]. An example is shown in Figure 1.8a, which a HIV-1 peptide (KK10) is presented by MHC to TCR [212]. The peptide is bound in a groove between $\alpha$ helices of $\alpha_1$ and $\alpha_2$ domains in class I and $\alpha_1$ and $\beta_1$ domains in class II respectively. The docking topology of CDR relative to pMHC is conserved among TCR bindings with both class I and II pMHC, and among different peptides presented [69]. The canonical

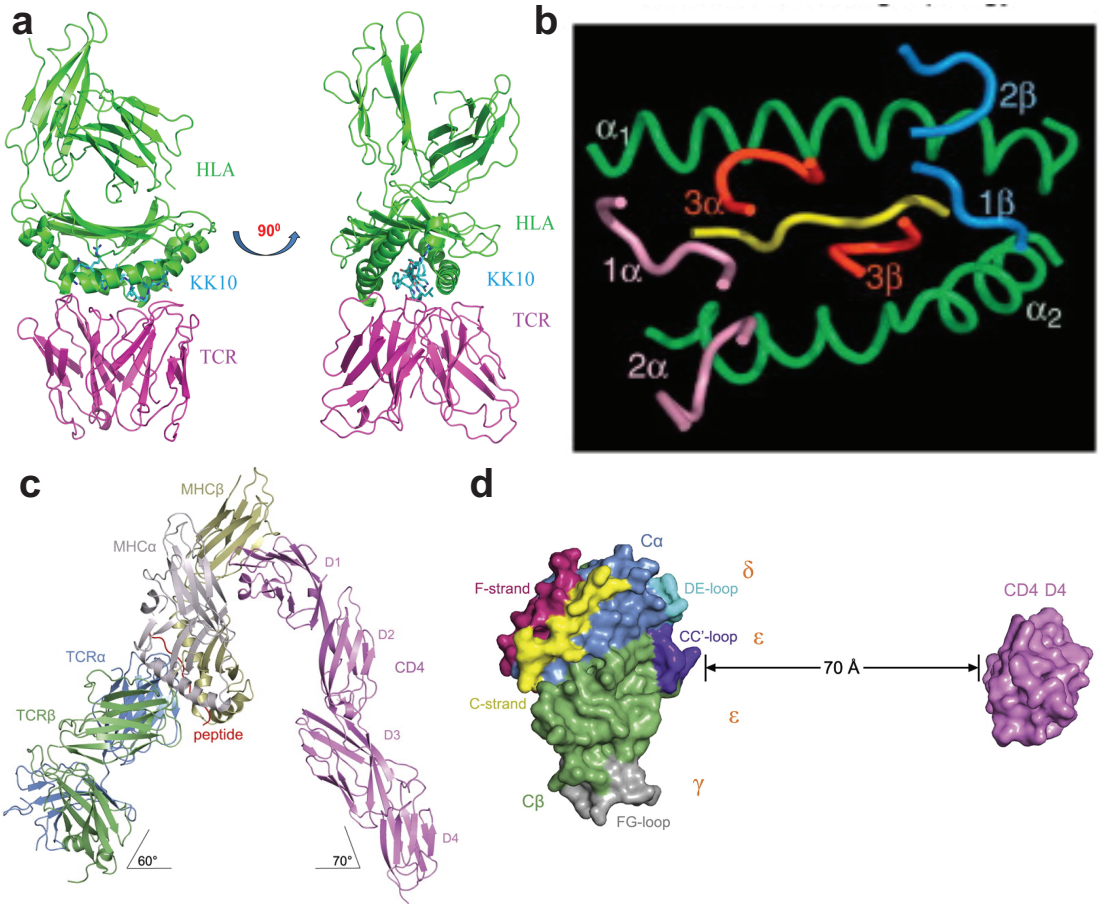


Figure 1.8: **TCR-pMHC binding.** (a) Three dimensional view of a TCR-pMHC complex: HLA-B*2705 in green, KK10 viral peptide in cyan and TCR in magenta. (b) Canonical docking topology of TCR CDRs on pMHC. Green: $\alpha$ helices of the peptide-binding groove. Yellow: peptide. Red, pink, blue: CDRs of TCR. (c) Structure of TCR-pMHC-CD4 complex. The individual protein domains are labelled. (d) Top view to the T cell membrane. On the left is the membrane-proximal TCR C domains and on the right is the CD4 membrane-proximal D4 domain. The interaction site between TCR, CD3$\epsilon\delta$ and CD3$\epsilon\gamma$ are denoted. Images are from [212, 69, 217] respectively. All images used with permission.

TCR-pMHC docking configuration is shown in Figure 1.8b, with the TCR tilted with respect to the groove by an angle between 40° - 85° [170]. CDR1 and CDR2 on both $\alpha$ and $\beta$ chains interacted with the surface of the MHC and the amino and carboxyl termini of the peptide, while CDR3 mainly interacts with the center of the peptide.

Recently the structure of the TCR-pMHCII-CD4 complex was determined, as shown in Figure 1.8c [217]. Both TCR-pMHC and CD4-pMHC interactions were shown to be tilted relative to the T cell plasma membrane, by an angle of around 60°. Therefore these two protein interactions formed an arch above the T cell membrane, and the CD3$\epsilon\delta$ and CD3$\epsilon\gamma$ interaction sites of C$\alpha$ and C$\beta$ domains faced the CD4 membrane-proximal D4 domain, lying under the arch (Figure 1.8d). Such positioning is hypothesized to be essential for efficient signal transduction upon antigen recognition, as discussed in section 1.3.5.

### 1.3.4 TCR stimulation leads to signaling, cytoskeletal remodelling and synapse formation

It has been measured that there are 20-200 $CD4^+$ and 80-1200 $CD8^+$ naïve T cells specific to a particular antigen in lymphoid organs over the whole mouse [149, 160]. Therefore, routine patrolling of naïve and memory T cells in our body, as shown in Figure 1.4c, is necessary to launch an immune response efficiently. Upon contact with antigen presented either on a professional APC or a virus-infected tissue

cell, the T cell stops migration and TCR-pMHC binding leads to **TCR triggering**. T cells are extremely sensitive: they can detect single cognate pMHC on APC [95].

TCR triggering results in exposure of ITAMs, whose tyrosine is phosphorylated by Src kinases Lck and proto-oncogene tyrosine-protein kinase (Fyn). They then recruit zeta-chain-associated protein kinase 70 (ZAP-70) which further phosphorylate the adapter proteins linker of activated T cells (LAT) and lymphocyte cytosolic protein 2 (SLP-76). Phosphorylated LAT and SLP-76 recruit multiple adaptor proteins and downstream signaling molecules into multimolecular signaling complexes located near the site of TCR engagement, including phospholipase C$\gamma$1 (PLC$\gamma$1) and growth factor receptor-bound protein 2 (Grb2), GRB2-related adapter protein 2 (Gads) etc., and generate a tyrosine phosphorylation signaling cascade (Figure 1.9a). Immediate downstream targets of TCR signaling include the non-catalytic region of tyrosine kinase (Nck) adaptor protein, Wiskott-Aldrich syndrome protein (WASp) [10] and Wiskott-Aldrich syndrome protein family member 2 (WAVE2) [157]. These actin regulators activate the Arp2/3 complex, which promotes branched actin polymerization [23, 22, 10, 78, 117]. This leads to cytoskeletal remodeling, morphological changes and cell spreading over the antigen presenting surface (Figure 1.9b, [60, 218]). TCR activation also leads to sustained calcium influx and ultimately gene expression over longer timescales . Signaling proteins transmitting the TCR signal are recruited to TCR within seconds of TCR triggering, and form multi-protein clusters known as signaling microclusters, as they act as hubs for rapid recruitment of downstream signaling proteins (Figure 1.10, [22]).

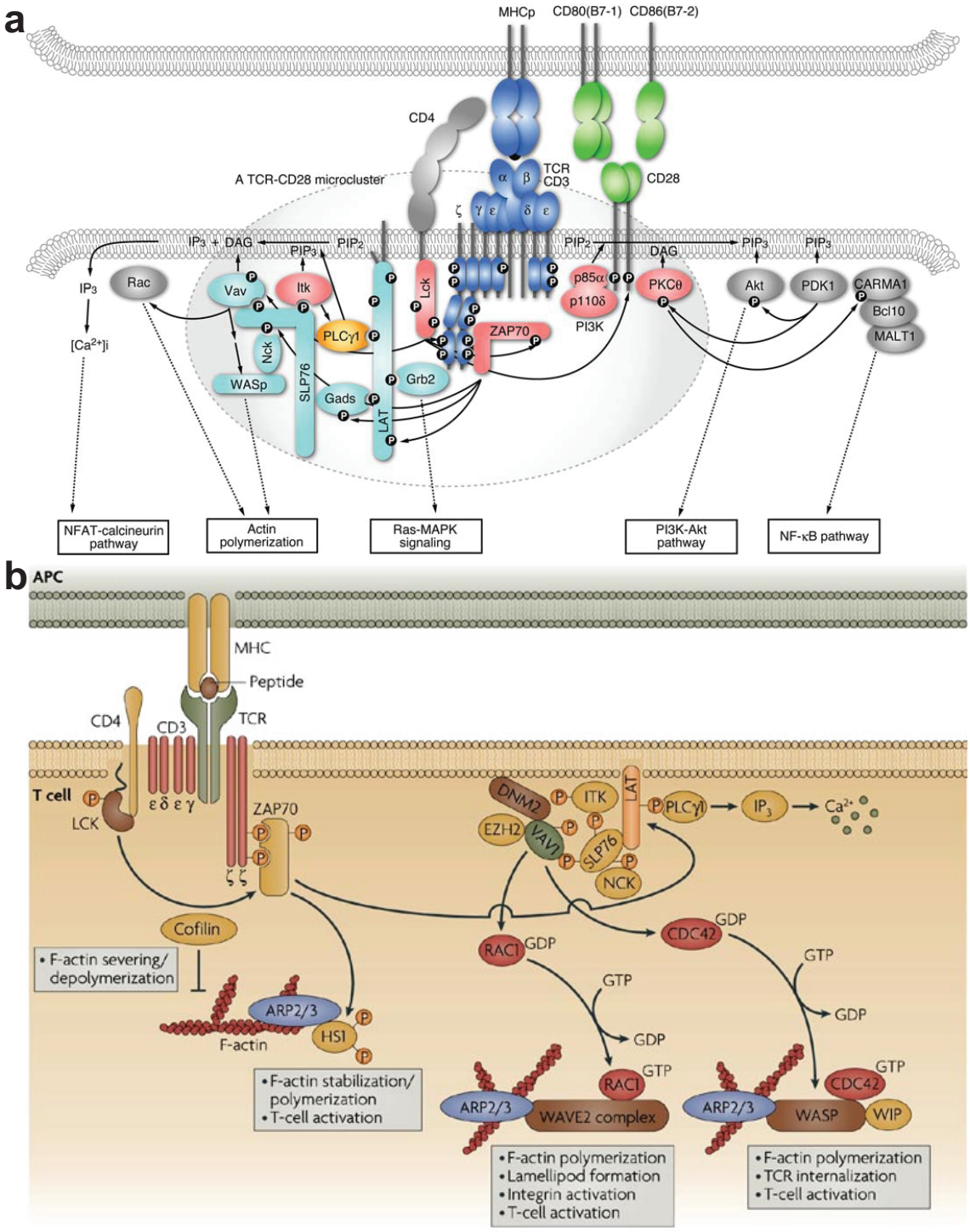


Figure 1.9: **TCR triggering induces tyrosine phosphorylation cascade and cytoskeleton remodelling.** Images are from [218, 16] respectively. All images used with permission.

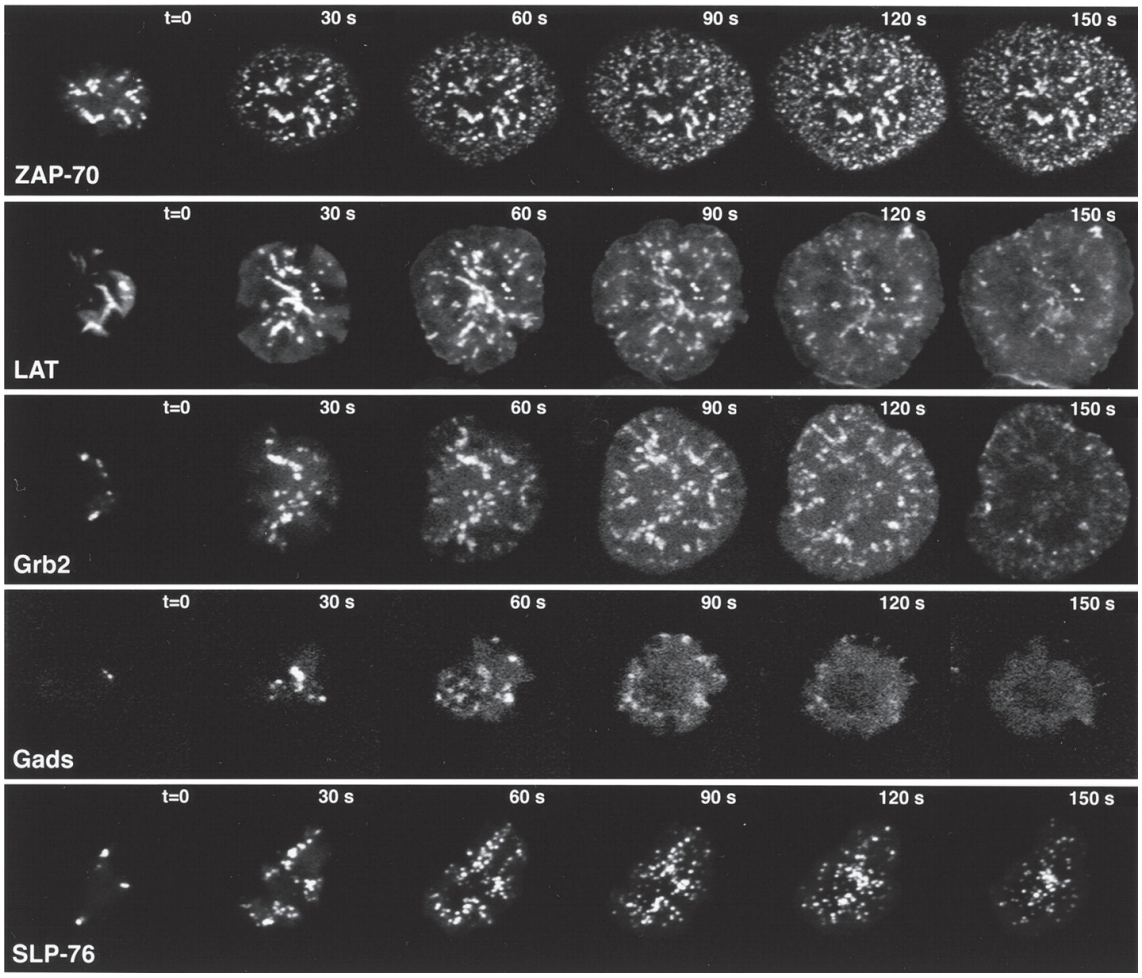


Figure 1.10: **TCR triggering induces formation of signaling microclusters.** Image is from [22] . All images used with permission.

Formation of these microclusters was found to be independent of phosphorylation by Lck, but was dependent on an intact actin cytoskeleton. In addition, appearance of first microcluster after cell-substrate contact was found to precede calcium influx by a few seconds, validating that TCR triggering is a prerequisite for signaling initiation [28, 219].

Within 30 minutes after initial TCR triggering, signaling proteins and other molecules at the cell-cell junction spatially organize into a macromolecular structure called the Immunological Synapse (IS). Reported in 1998 by Kupfer and coworkers (Figure 1.11a, [148]), the structure is characterized by large scale segregation of biomolecules at the interface, with TCR and costimulatory molecules (e.g. CD28) concentrated at the center (also known as central supramolecular adhesion complex (cSMAC)) and adhesion molecules (e.g. lymphocyte function-associated antigen 1 (LFA-1)) located in an annular region outside the cSMAC (known as peripheral SMAC (pSMAC)), together forming a 'bull's eye' pattern (Figure 1.11b, [88]). The most distal region is known as distal SMAC (dSMAC), which is enriched in F-actin, CD43 and the tyrosine phosphatase CD45 [199].

The immune synapse was soon reconstituted in an *in vitro* lipid bilayer system [79] after its discovery. Subsequently, extensive work has been done to study the dynamics of IS formation [167], mechanism of formation [103, 48, 82, 216] and how the structure is related to cellular signaling [152, 199]. cSMAC was initially thought to be the signaling center, but it was soon realized that tyrosine phosphorylated

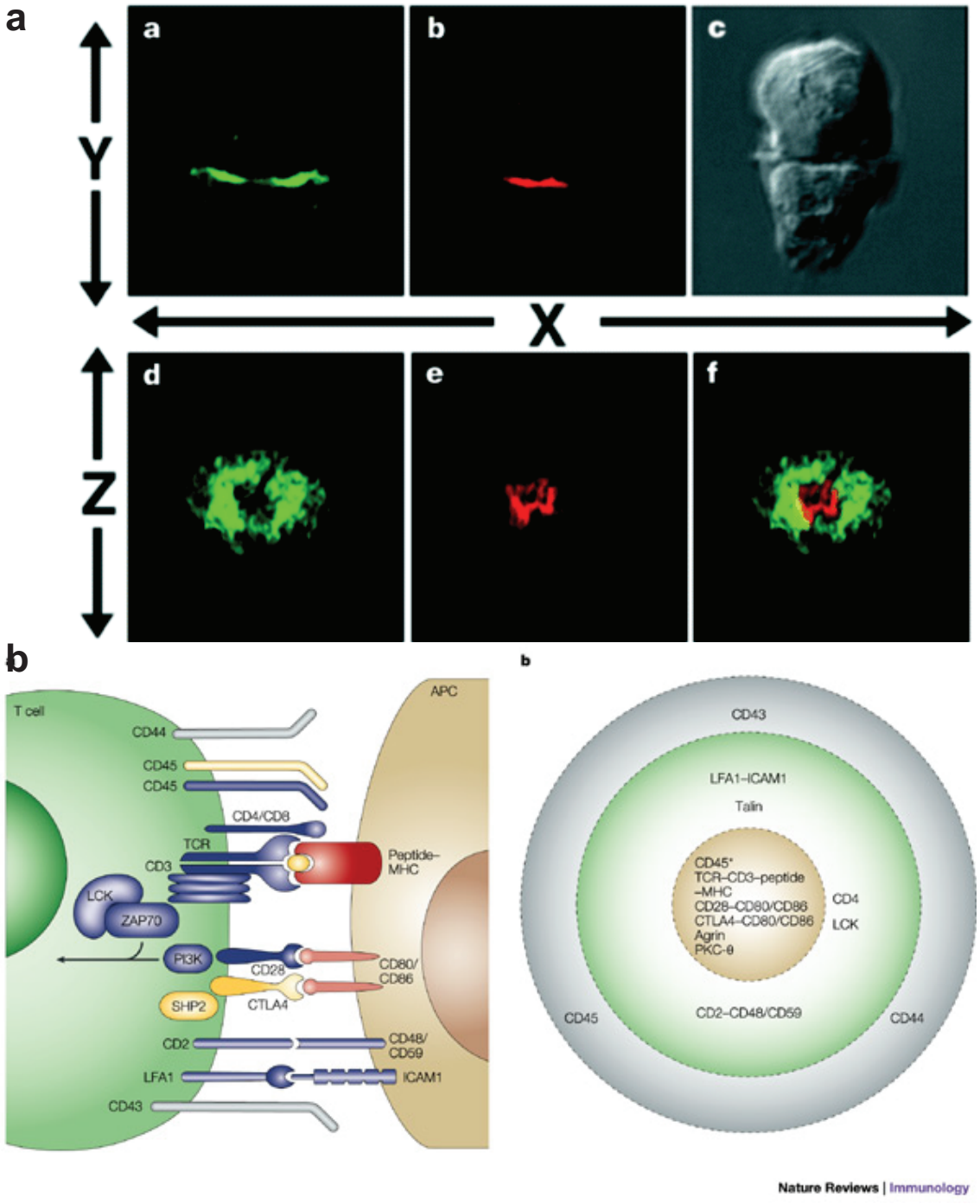


Figure 1.11: **Immunological synapse.** (a) T cell-B lymphoma conjugate. Green: talin. Red: protein kinase C$\theta$ (PKC$\theta$). (b) Molecular organization in mature IS. Images are from [148, 88] respectively. All images used with permission.

signaling proteins were localized in pSMAC [28, 199] and TCR proximal signaling preceded and started to decay before the IS was established [124]. However, stable conjugation and continuous TCR signaling are required for the T cell to achieve its full effector potential [89].

### 1.3.5 Models of TCR triggering

In spite of extensive studies, the exact mechanism of TCR triggering remains unknown and is a subject of intense research and controversy. Numerous models have been proposed to explain how TCR triggering is achieved. There are three categories of models [197]:

1. Aggregation: TCR engagement promotes aggregation of TCRs into clusters, with coreceptor from self-peptide MHC binding to agonist-MHC and therefore brings the associated Lck into the vicinity of ITAM (pseudodimer model, [95]).

2. Segregation: TCR engagement produces close contact zones enriched in signaling microclusters, and are segregated from inhibitory tyrosine phosphatases that dephosphorylate signaling proteins and hence promoting stable phosphorylation (Figure 1.12a, [100]).

3. Conformation change: a mechanical force was transmitted across the TCR complex and this induces signaling by causing a conformational change in ITAM-containing CD3 molecules, exposing them for phosphorylation. The source of the force could be from the APC, from T cell's own cytoskeleton, or

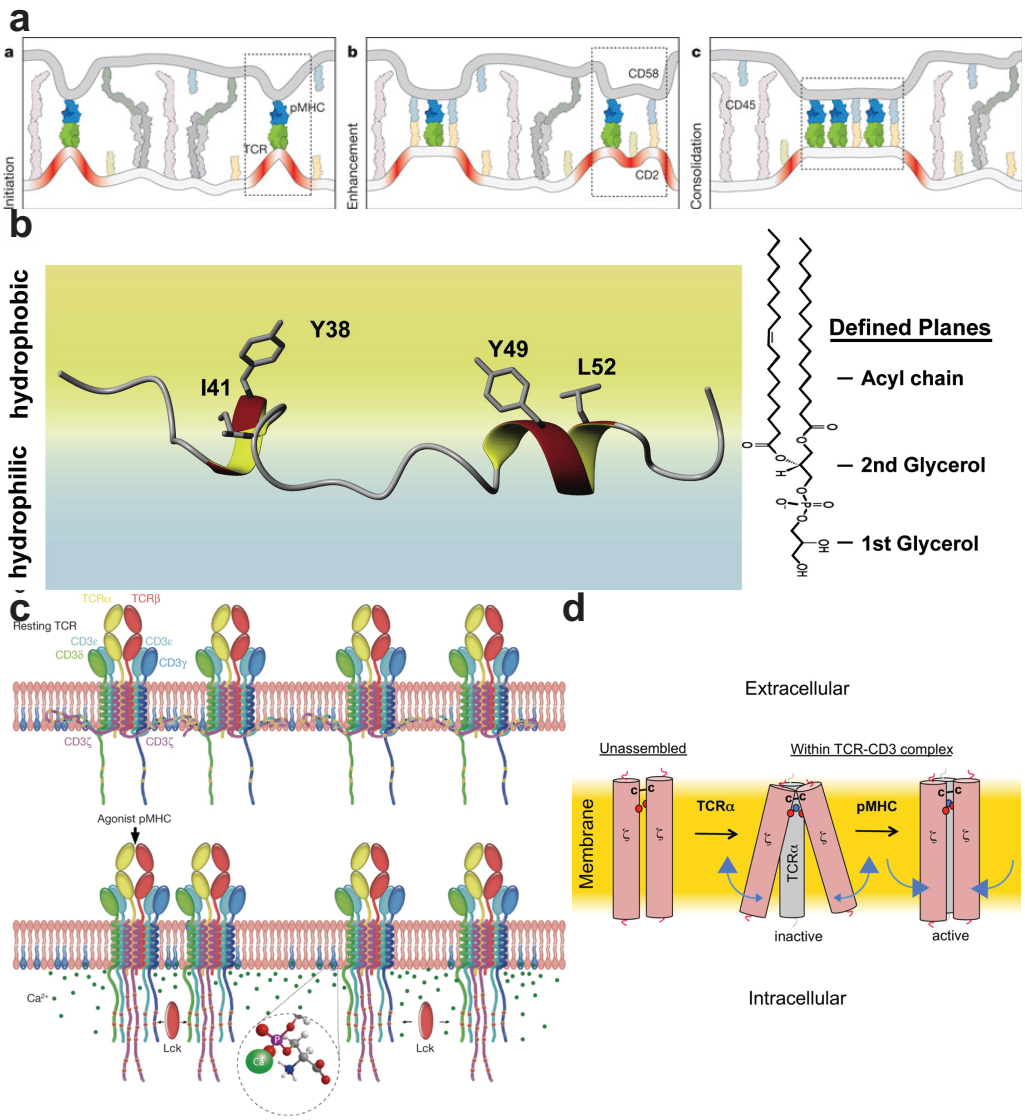


Figure 1.12: **Models of TCR triggering.** (a) Segregation model of TCR triggering. Binding of single TCR-pMHC was enhanced by costimulatory molecule binding which promoted membrane bending, excluding CD45 which had large extracellular domain. (b) Cartoon view of ITAMs of CD3$\epsilon$ residing in hydrophobic leaflet in bicelle inferred from Nuclear Magnetic Resonance (NMR) data. (c) Intracellular calcium elevation dissociates the ITAMs of CD3$\zeta$ and CD3$\epsilon$ from lipid bilayer to facilitate phosphorylation. (d) 'Closing' of the two CD3$\zeta\zeta$ chains upon TCR triggering. Images are from [100, 213, 183, 125] respectively. All images used with permission.

both [136].

It should be noted that these models are not mutually exclusive, and each has its own evidential support. Noteworthy is the mechanical force model of TCR triggering, as there is mounting evidence for it in recent years.. In terms of data related to structural configuration of TCR-CD3 complex, it has been shown that CD3$\epsilon$ and CD3$\zeta$ has their ITAM buried in the lipid bilayer in resting T cells, sequestered from cytoplasmic kinases (Figure 1.12b [213]). Elevated intracellular calcium level releases these ITAMs and facilitate their phosphorylation by kinases (Figure 1.12c, [183]). Interestingly, a recent report using proximity probes and Förster resonance energy transfer (FRET) to study distance between intracellular domains of CD3$\zeta\zeta$ chains suggested that the two chains were brought together upon cognate pMHC binding, acting like a mechanical pivot (Figure 1.12d [125]).

## 1.4 Mechanobiology of T cell activation: a new perspective

Conventional immunology has focussed on elucidation of the roles of different genes in regulating and defining our immune system [2]. In the last 5 years, there has been growing interest in the interplay between mechanical force and biological processes during T cell activation [197, 110]. T cells, by their role of immunosurveillance, routinely encounter opposing cells with various mechanical properties [4].

Whether the forces T cell generates and experiences take part in signaling generation and modulation during T cell activation is poorly understood. Here we discuss three different aspects of why mechanical forces and mechanical properties of the opposing cell might be important in determining T cell's immune response. A short introduction of mechanobiology observed in nonimmune cells will be given in section 1.5.

### 1.4.1 TCR triggering is sensitive to applied physical forces

The role of physical forces in TCR triggering has come into focus after the receptor deformation hypothesis was proposed in 2008 [136]. In this model, cytoskeletal forces deform the membrane at the IS, and thereby push or pull on the TCRs. TCRs binding with agonist are deformed and signal initiation is facilitated by the conformational change caused by the forces.

Several experimental works have followed up on the idea since then. A study in 2009 [111] made use of a nonactivating antibody targeting the cleft between CD3$\epsilon$ and CD3$\gamma$, which would not stimulate calcium influx in force-free conditions. Calcium influx was observed upon tangential shear applied to the antibody through an optical tweezer. The authors argued that the FG loop in C$\beta$ domain of TCR (Figure 1.8d) acts as a lever, which transmits a torque to the CD3$\epsilon\gamma$ and CD3$\epsilon\delta$ ectodomain to stimulate signaling (Figure 1.13a). The efficacy of shear or pull on the TCR to

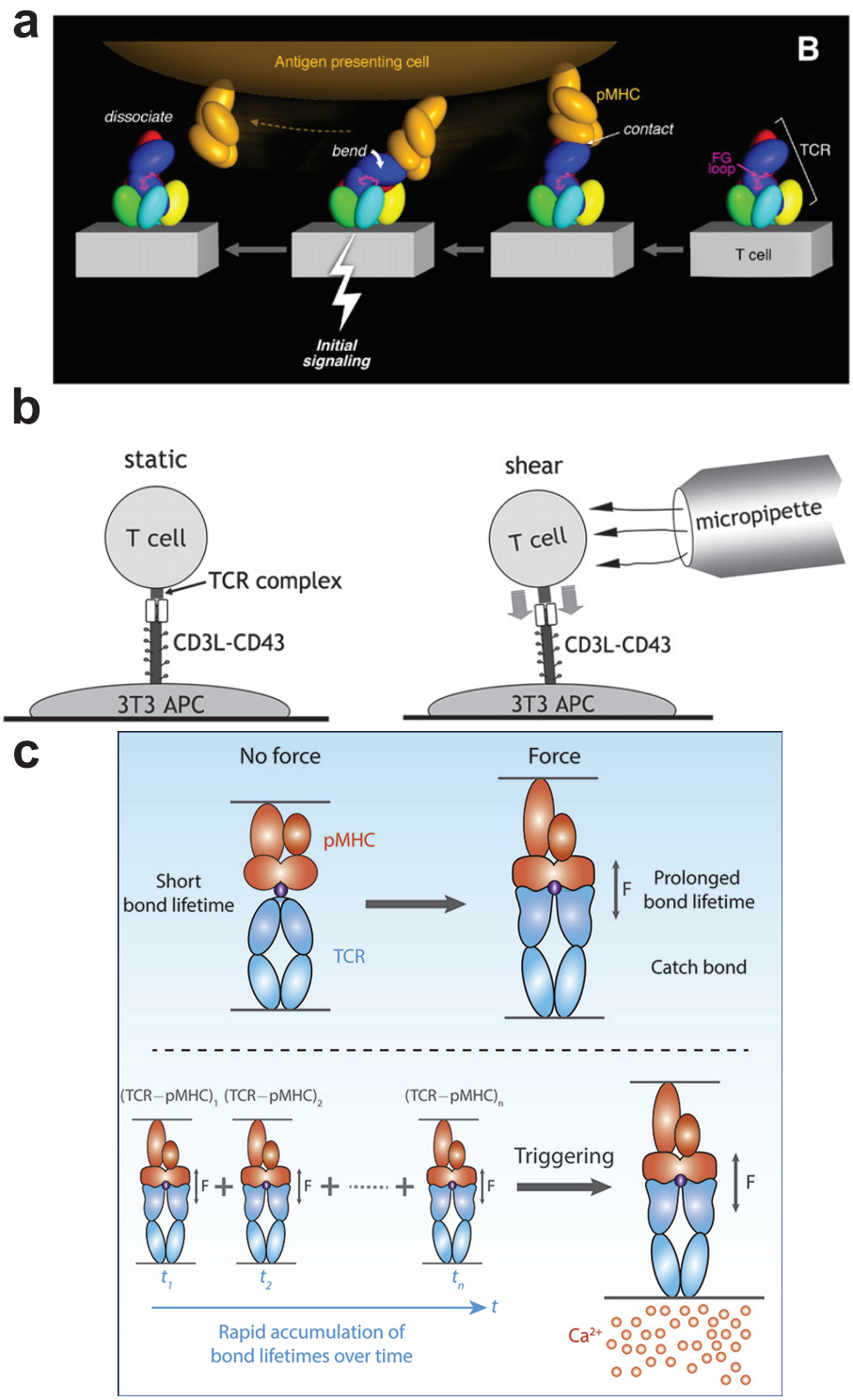


Figure 1.13: (Continued on the following page.)

Figure 1.13: **Physical forces take part in TCR triggering.** (a) Engagement by cognate pMHC generates a torque that transfer to CD3 signaling subunits through the FG loop of C$\beta$. (b) Experimental setup used in [131] to apply shear to TCR. Copyright 2010. The American Association of Immunologists, Inc. (c) TCR-pMHC interaction was found to be a catch bond, and forces help accumulate interaction lifetime to induce calcium influx. Images are from [111, 131, 132]. All images used with permission.

trigger calcium influx is demonstrated again in later study which used single-chain variable fragment (scFv) tethered to 3T3 fibroblast as an artifical APC [131]. The tether was through extracellular domain of the CD43 molecule, which is a large glycoprotein usually excluded from signaling TCR microclusters in the IS (Figure 1.11, [88]). At resting, force free condition, conjugated T cell does not take in calcium but is triggered when the T cell is sheared or pulled by a micropipette (Figure 1.13b).

A major breakthrough was reported in 2014, in which TCR-pMHC interaction is demonstrated to be a catch bond [132],with lifetime increasing with force application. The lifetime of the TCR-pMHC bond peaked at 10 pN of applied force (Figure 1.13d), and calcium influx into the cell correlated strongly with accumulated lifetime in the first minute of force application (Figure 1.13c,e). The catch-bond nature of TCR-pMHC was confirmed in a later single molecule study by another group, who demonstrated that the TCR C$\beta$ FG loop allosterically controls both the lifetime

and peptide discrimination via force-driven conformational transition [46].

### 1.4.2 Flow of actin cytoskeleton is essential to organize IS and signaling

It was appreciated early since the discovery of the IS that the actin cytoskeleton plays an important role in organizing the molecular architecture at the IS [16]. Initial TCR engagement triggers rapid and isotropic actin polymerization to spread the cell membrane onto the stimulatory surface [23]. Studies showed that treatment with actin depolymerizer latrunculin A inhibits TCR microcluster formation and inward movement but does not dissipate preexisting microclusters (Figure 1.14a, [199]). Later studies tracking actin flow and microcluster speeds confirmed their correlation (Figure 1.14b, [103, 8, 216]). Finally, TCR microclusters were reported to recruit actin foci through WASp and cotranslocate into the cSMAC [117].

A series of studies have investigated the interactions between actin dynamics, TCR movements and signaling by using physical barriers to constraint TCR movements during IS formation [152, 48, 220]. It was found that constraining TCR microclusters to the periphery enhanced phosphotyrosine signaling, supporting the notion that pSMAC rather than cSMAC is the region of active signaling [152, 199]. Importantly, by tracking actin retrograde flow around regions of trapped TCR microclusters, it was found that actin flow slowed down in the vicinity of the clusters,

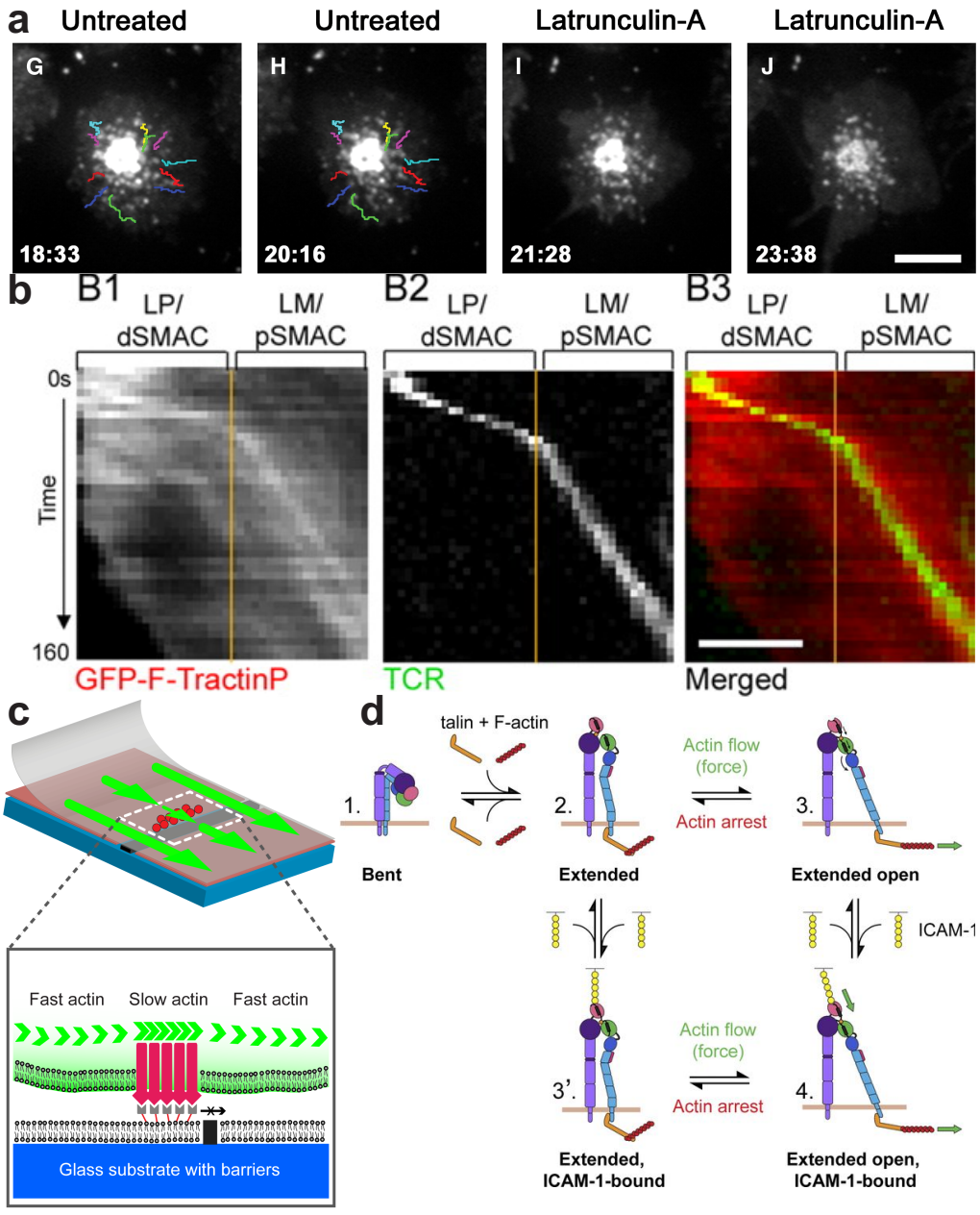


Figure 1.14: **Actin dynamics reorganizes IS.** (a) Abrupt treatment with latrunculin A inhibited formation and movement of TCR microcluster but did not disrupt preexisting microclusters. (b) TCR and actin flow move with same speed in both d-SMAC and p-SMAC. (c) Trapped TCR microclusters slow down actin retrograde flow. (f) Force from actin flow and ICAM-1 binding promoted LFA-1 affinity maturation. Images are from [199, 216, 220, 38] respectively. All images used with permission.

again suggesting that TCR and actin cytoskeleton are coupled and that TCRs are potentially pulled by the actin flow [220].

Lastly, small molecules were used to perturb actin and myosin dynamics to characterize roles of actin flow in organizing the IS and maintaining signaling. Studies from two groups simultaneously reported that the actin flow in T cells can be stopped completely by inhibiting myosin II activity and actin depolymerization [216, 8]. This abrogated calcium signaling [8] and affiniy maturation of LFA-1 [38]. The importance of actin depolymerization in organizing the IS was later demonstrated in two different cytotoxic T cells studies [12, 167].

### 1.4.3 T cell immune response is sensitive to substrate stiffness

Application of physical forces to cells and conversely, cells exerting physical forces to the environment, inherently involve the concept of stiffness. Stiffness is the resistance to deformation in response to applied force. Different materials respond to applied force in different ways. The study of rheological properties of various biomaterials is still an active area of research, and there is no common consensus regarding which category of matter a living cell belongs to. One possible candidate is the poroelastic model, as poroelasticity and intracellular fluid flow have been demonstrated and were shown to be important in cell migration and blebbing in living cells [34, 168, 109, 147].

However, biomaterials are conventionally considered to be viscoelastic: their stiffnesses contain a viscous and an elastic component. In a viscous response, the material resists shear flow and strains linearly with time when a stress is applied. In an elastic response, the material returns to its original state rapidly once the stress is removed. Experimental measurements of immune cells' stiffness/elasticity have been scarce. The first measurement of T cell stiffness was by AFM of trapped immune cells (neutrophil and Jurkat T cells) in microfabricated wells [169]. It was found that Jurkat T cells are among the softest cells, with Young's modulus of 48 Pa. A new study in 2015 focussed on stiffnesses of professional APCs (Figure 1.2b) before and after inflammation [21]. The measurements showed that APCs are soft cells with Young's moduli below 1 kPa, and inflammations with different cytokines change the stiffness in a different manner.

Since APCs and T cells were both measured to be soft, this implies substrate stiffness might play an important role in directing T cell activation. Two previous studies have used elastic substrates with well defined Young's moduli to study how T cell's immune response depends on substrate stiffness. The first study used anti-CD3 and anti-CD28 coated polydimethylsiloxane (PDMS) to stimulate primary T cells [161]. It was found that softer substrates (≈50-100 kPa) enhanced proliferation, IL-2 production, and naïve $CD4^+$ cell differentiation into type 1 helper T cells. The second study used polyacrylamide gels as stimulatory surfaces for naïve $CD4^+$ cells [102]. The stiffness range tested was 10-200 kPa. It was found that in contrast

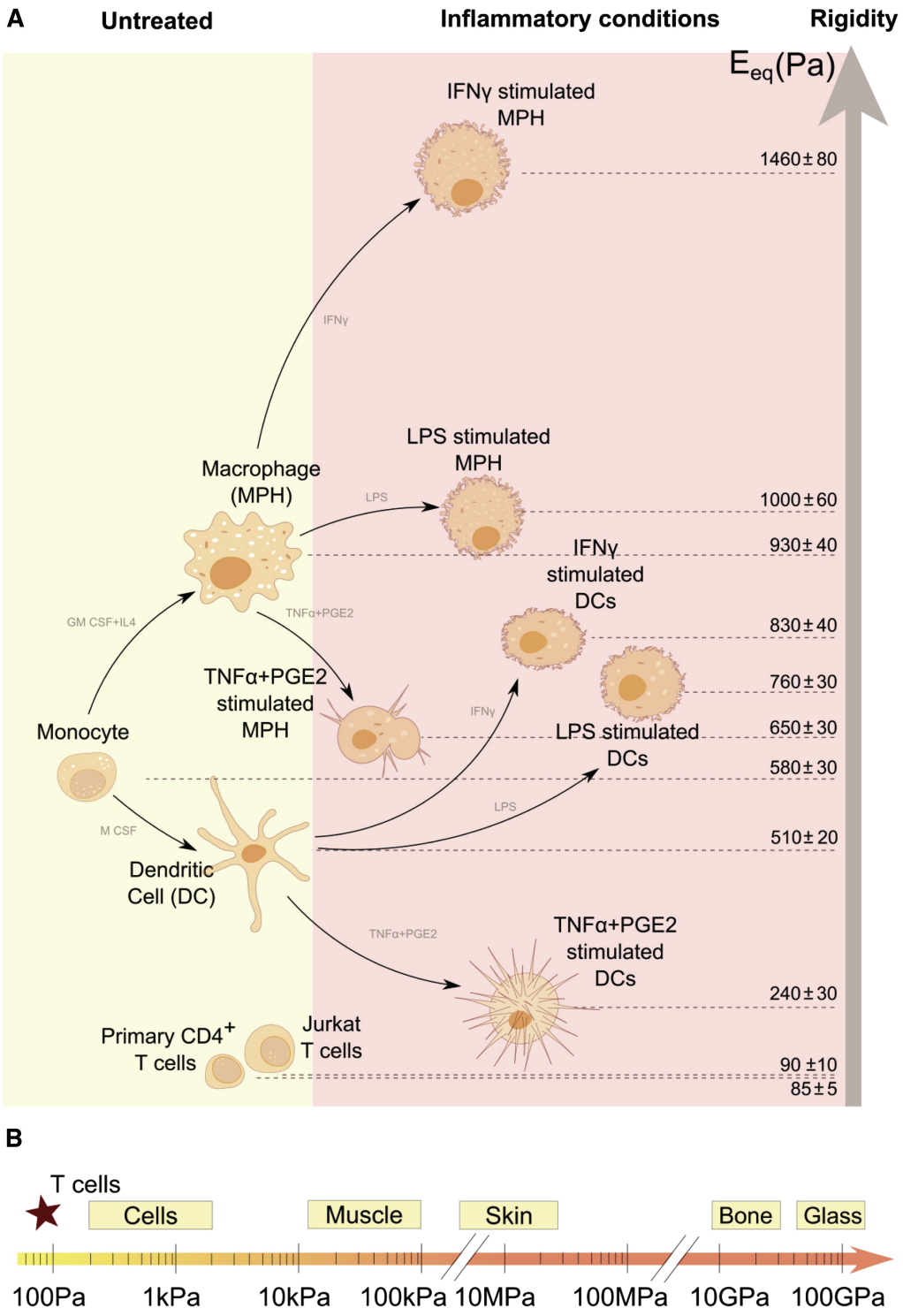


Figure 1.15: **Antigen presenting cells are soft.** (a) Macrophages and dendritic cells' stiffnesses before and after inflammation. (b) Stiffness scale for cells and tissues. Image is from [21]. Image used with permission.

to the first study, IL-2 production was enhanced on stiffer substrates. In addition, proximal signaling was also higher on stiffer substrate. Unfortunately, the stiffness range of substrates in both studies was much higher than stiffness of APC ($< 1$ kPa).

## 1.5 Mechanobiology in nonimmune cells

Mechanobiology has been studied more actively in non-immune adherent cells that interact with extracellular matrix (ECM), compared to immune cells. Although they are drastically different in mechanical properties and gene expression profiles, knowledge of the molecular components that make up the force generating and mechanosensing apparatus in non-immune cells provides useful guidelines to think about possible players and molecular mechanisms of mechanosensing in immune cells. We will be discussing traction forces different types of cells are able to generate, how they generate forces, and finally how stiffness information obtained by the cell is transmitted and integrated to arrive at cellular decision and to determine cell fate.

### 1.5.1 Force generation by nonimmune cells

It is well known that mesenchymal cells exert larger stresses with increasing substrate stiffness and can generate stresses up to 10 kPa on stiff substrates (Figure 1.16a, [194]). This is associated with an increasingly organized actin cytoskeleton such as alignment of contractile actin bundles called stress fibers, which originate

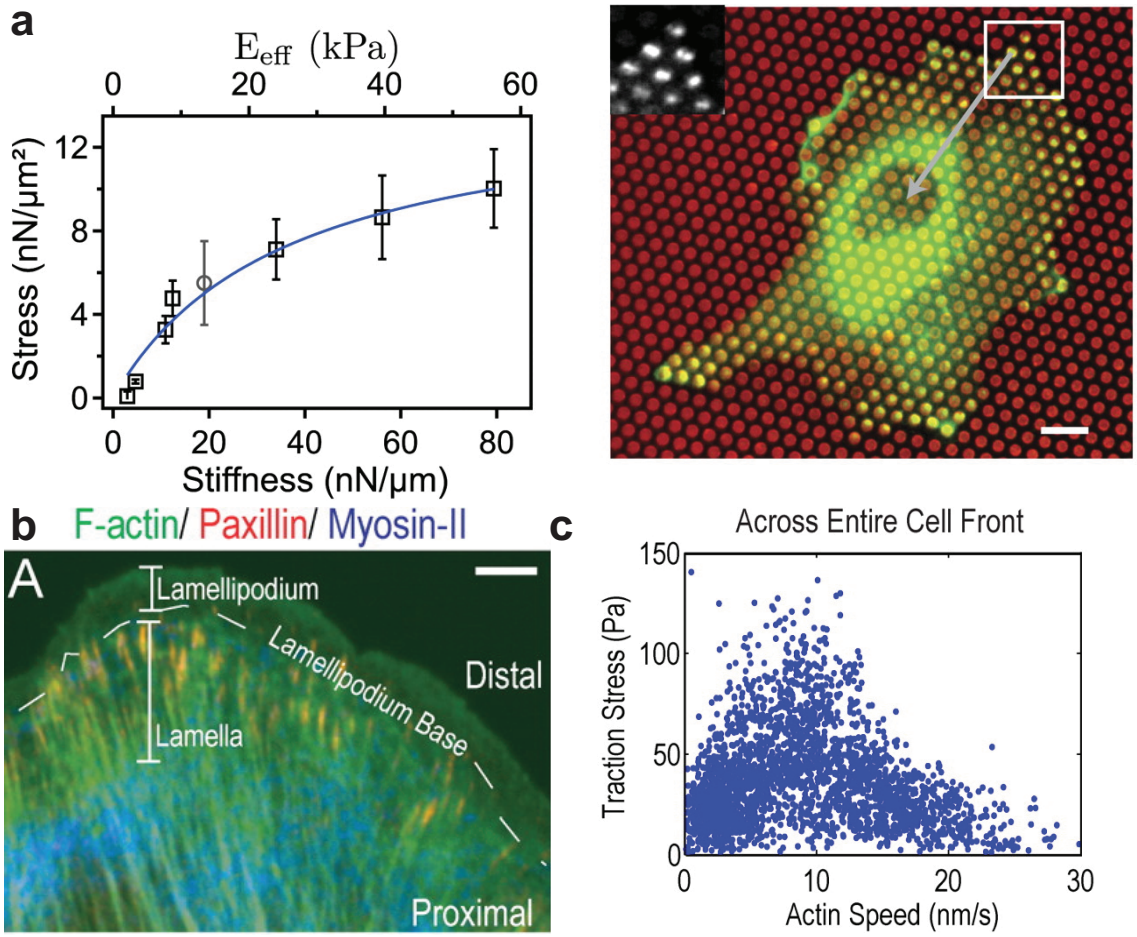


Figure 1.16: **Traction force exerted by nonimmune cells.** (a) REF52 fibroblasts exert increasing stress on higher stiffness. Right: red: micropillars; green: paxillin. (b) Cytoskeletal organization at the leading edge of epithelial cells. Green: actin; red: paxillin; blue: NMII. (c) Traction stress versus F-actin speed for all points throughout the cell front. Scalebar: 10 $\mu$m. Images are from [194, 71] respectively. All images used with permission.

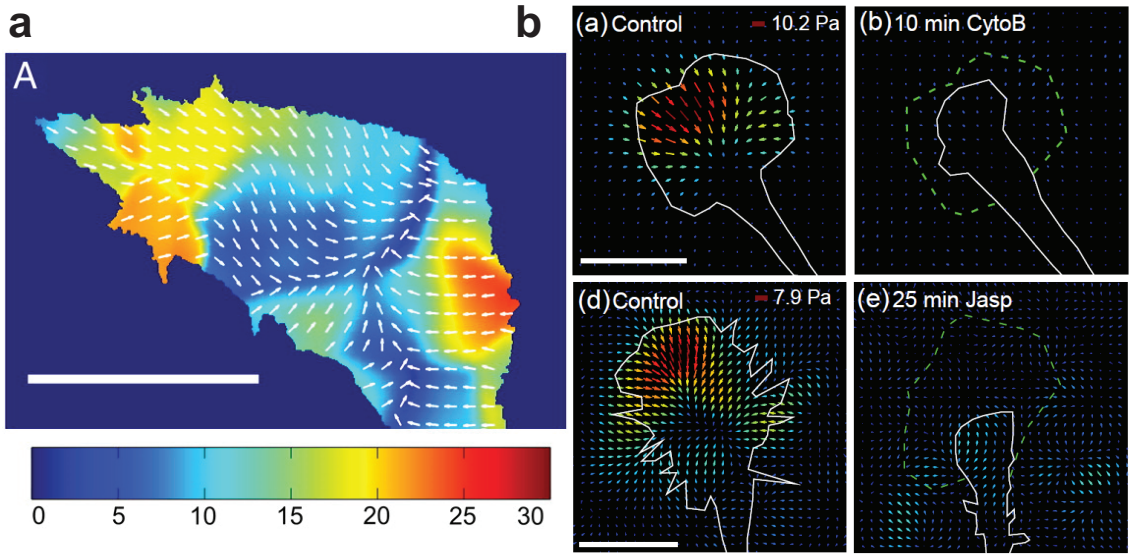


Figure 1.17: **Actin dynamics is essential to traction stress.** (a) Traction stress profile of NG108-15 neuronal growth cone. Scalebar: 10 $\mu$m. (b) Inhibition of actin dynamics abrogated traction stress in growth cone. Images are from [92, 15] respectively. All images used with permission.

and terminate at molecular structures known as focal adhesions (Figure 1.16b, section 1.5.2, [71, 223, 145]). Nonmuscle myosin II (NMII) contractions are known to be essential to organize the actin network [14], and NMII knowndown experiments have shown that NMIIA and NMIIB contribute 60 % and 30 % of stresses in mouse embryonic fibroblasts [27]. Recently, it was found that local traction stress varies biphasically with actin flow speed in epithelial cells (Figure 1.16c, [71]).

On the other hand, neuronal growth cones exert much weaker traction stresses, in range of 5-50 Pa (Figure 1.17a, [15, 114, 92]). Rapidly migrating cells like fish keratocytes also generate significant traction stresses during migration, up to 200 Pa [68]. A significant amount of research has focused on the molecular mechanisms of traction force generation. The dynamics of actin cytoskeleton is considered essential for stress generation and maintenance for all the cell types described above. For example, inhibition of actin polymerization in keratocytes reduced traction stresses by 50 % [68]. This was also observed in growth cone when subjected to actin dynamics inhibitions (Figure 1.17b, [92]).

### 1.5.2 Focal adhesion: force-transducing molecular clutch

Focal adhesions (FA) are macromolecular structures which connect and transmit forces from the actin cytoskeleton to integrins [30]. Through advances in 3D superresolution microscopy, its structure was revealed in 2010, as shown in Figure

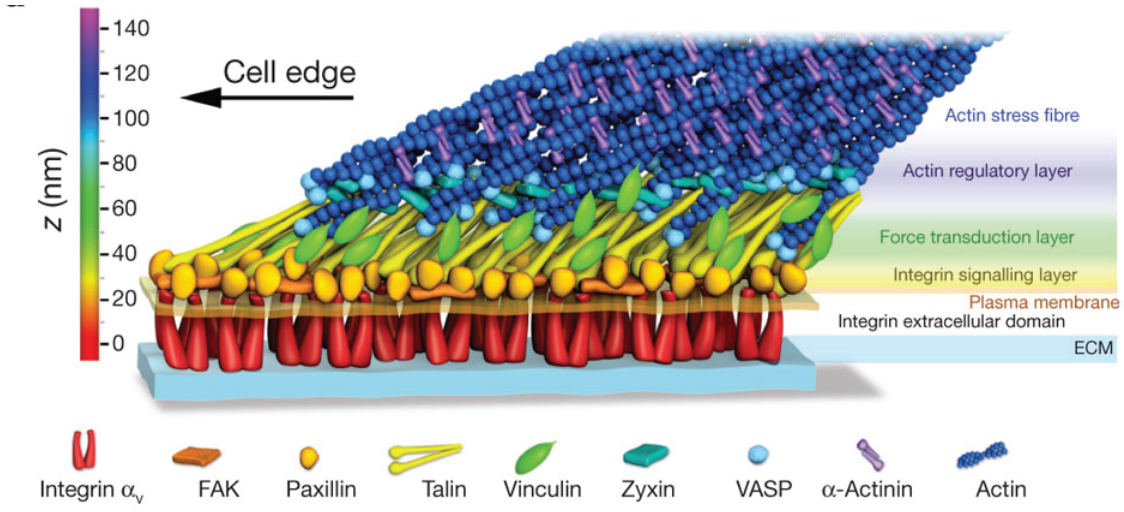


Figure 1.18: **Focal adhesion: a molecular clutch.** Image is from [106]. Image used with permission.

1.18a. Stratified in the $z$ direction, the bottom layer of FA is the membrane protein integrin, which different subtype of integrins recognizes and binds to recognition sequences in different extracellular matrix (ECM) proteins. Integrins do not bind to actin filaments directly, but rather recruit FA associated proteins, for example, paxillin, focal adhesion kinase (FAK), talin and vinculin etc. that assemble into two distinct layers (integrin signaling and force transducing layers) (Figure 1.18a). Actin filaments and crosslinkers like $\alpha$-actinin then bind to these proteins on top.

As shown in Figure 1.17c, FAs (labelled by paxillin staining) are located behind the leading edge, and are separated from a region called lamellipodium composed of a dense meshwork of actin. In live cells, the actin cytoskeleton persistently polymerizes at the leading edge, membrane tension pushes back the f-actin network and

f-actin depolymerizes when it moves backward relative to the underlying substrate [42]. Balancing membrane tension and rates of these two processes, f-actin treadmills and flows retrograde. By catching this flow with FA associated proteins, FA represents a physical link and provides pulling force to integrins, which further pull on the ECM proteins. This is known as the molecular clutch hypothesis [30].

By fluorescent speckle microscopy, it was found that the retrograde flow speed at FA decreases from top layer to bottom layer, with actin being the fastest and integrin being almost stationary [86]. Therefore, the different FA-associated proteins are expected to be under mechanical tension with respect to each other when assembled in FA. This was shown directly by a FRET sensor measuring extension of vinculin in FA that vinculin in stable FA are under 2.5 pN force [80]. These intramolecular forces can unfold proteins and expose cryptic binding sites. p130Cas, an adaptor protein recruited to FAs, was shown to expose its Src phosphorylation site upon isotropic cell pulling [177]. More recently, it was shown in an elegant *in vitro* experiment that actomyosin contraction pulls on talin to expose its vinculin-binding sites and recruits vinculin [37]. Secondly, mechanical forces can increase interaction lifetime if the bond of interest has a catch-bond behaviour. For example, integrin-fibronectin binding has been demonstrated to be a catch bond [116].

To conclude, FA is a classic example of an organelle which carries out mechanosensing and mechanotransduction. The multi-protein nature of FA bears strong resemblance to signaling microclusters that are present in T cell IS (Figure 1.10). Inter-

estingly, CasL, a homologue of p130Cas, colocalizes with microclusters during IS formation and its phosphorylation is sensitive to NMII activities [221, 118]. This raises the interesting possibility that these signaling microclusters might also be mechanosensitive like FAs.

### 1.5.3 Substrate stiffness drives diverse cellular processes

As illustrated in Figure 1.15, tissue cells and ECMs are inherently soft materials compared with glass coverslips or tissue culture dishes, and can have a diverse range of stiffnesses in different physiological contexts. Given that cells can sense the rigidity of the environment with traction forces, it is not surprising that stiffness differences can lead to diverse biological outcomes. Three different examples will be discussed here to illustrate why understanding force sensing is essential to a better understanding of cellular behaviour.

Elastic substrates have been commonly used to mimic the cells mechanical environment and study cellular responses to changes in stiffness. When fibroblasts were plated onto a polyacrylamide gel with a gradient of stiffness, it was found that fibroblasts migrate towards a stiffer substrate, a phenomenon called durotaxis [134]. Secondly, it is well known that cancer cells and tumors have significantly different stiffnesses from normal healthy tissue. For example, it was shown in mouse breast cancer that metastatic potential of a tumor correlates inversely with its stiffness [64, 133].

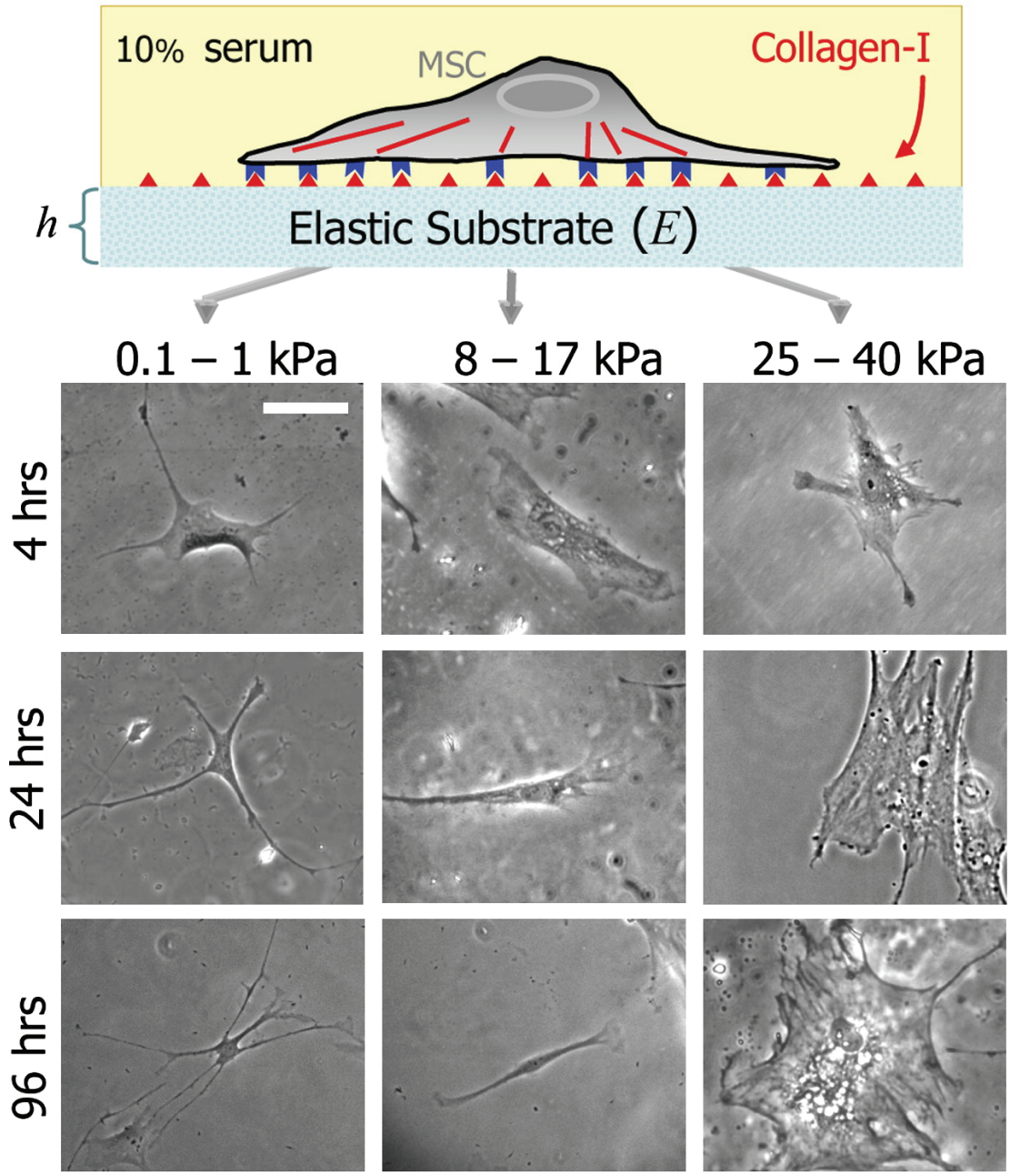


Figure 1.19: **Stiffness drives mesenchymal stem cell differentiation.** Image is from [61]. Image used with permission.

A dramatic example of stiffness driven determination of biological fate is found during differentiation of mesenchymal stem cells (Figure 1.19, [61]). Human mesenchymal stem cells were plated on polyacrylamide gels of stiffnesses that mimic brain, muscle and bones, and were cultured in identical media. After 4 days, these cells differentiated into lineages of cells from tissues of corresponding stiffnesses (neurons, myoblasts, and osteoblasts), and showed the corresponding mRNA transcription and gene expression patterns. Such differentiation was completely blocked upon inhibition of NMII, indicative of the role of force sensing in the process.

### 1.5.4 Objectives of this study

Given the available data in the T cell literature and knowledge in mechanobiology of nonimmune cells, this thesis focuses on the following questions and attempts to fill in the gaps between roles of physical forces during T cell activation at molecular and cellular level:

1. Does T cell exert significant traction stress during formation of IS?

2. If so, does the stress depend on stiffness of the stimulatory substrate and how?

3. How does T cell generate and maintain traction stress? Do the actin and microtubule cytoskeletons play a role?

4. How does proximal T cell signaling (tyrosine phosphorylation, calcium signal-

ing) depend on substrate stiffness? Does active stress generated by T cell help maintain calcium signaling as suggested by the catch-bond behaviour [132]?

By using elastic substrates with stiffnesses that fall in the range of APC stiffnesses (Figure 1.15a), we ask if mechanosensing contributes to T cell activation, in terms of signaling, gene expression and differentiation etc., and compare with immobilized, bilayer and cell-cell conjugate studies [9]. Below is a brief overview of the different chapters:

1. In chapter 2 , we characterize spreading kinetics, membrane and actin dynamics during T cell activation on coverslip.

2. In chapter 3, we measure traction forces exerted by T cell during activation, highlight the importance of actin dynamics in generating and maintaining these forces, and show that T cell display distinct morphological and signaling responses to different stiffnesses.

3. In chapter 4, we show that microtubule dynamics regulate traction force maintenance through Rho-ROCK-NMII pathway at IS.

4. In appendix A. we use the calcium influx during T cell activation as a signaling output readout to characterize how inputs of substrate stiffness and traction forces regulate signaling.

# Chapter 2

# Spreading kinetics, membrane and actin dynamics in Jurkat T cell activation

# Abstract

Contact formation of T cells with antigen presenting cells (APCs) results in the engagement of T cell receptors (TCRs), recruitment and aggregation of signaling proteins into microclusters and ultimately, T cell activation. During this process, T cells undergo dramatic changes in cell shape and reorganization of the cytoskeleton. While the importance of the cytoskeleton in T cell activation is well known, how its dynamics correlates with spreading kinetcs during the early stages of spreading is not well understood. In this study, we observed two modes of spreading during activation of Jurkat T cells on anti-CD3-coated substrates. The cell edge exhibited repeated protrusions and retractions, which were driven by wave like patterns of actin. Our results suggest that cell membrane morphology at the cell-substrate interface may be a critical constraint on signaling and the actin cytoskeleton in Jurkat cells is capable of organizing into spatial patterns.

*This chapter is adapted from Hui, Wang, Grooman, Wayt and Upadhyaya [87] and Hui, Kwak and Upadhyaya [119]. Jessica Wayt and Chenlu Wang both contributed to data acquisition in Figure 2.1-2.3 and Saein Kwak contributed to data acquisition in Figure 2.4-2.5.*

## 2.1 Introduction

Cellular responses to environmental stimuli involve large scale changes in morphology, primarily driven by reorganization of the actin cytoskeleton [101, 107, 108]. One striking example of this occurs during cell-cell recognition in immune cells, where T lymphocytes rapidly spread to establish contacts with antigen-presenting cells (APCs) [148, 210]. These contacts allow T cell receptors (TCRs) to bind to peptide- major histocompatibility complex (pMHC) displayed on the APC surface. TCR-pMHC binding results in the activation of TCRs and the formation of signaling microclusters that consist of activated TCR and various downstream signaling molecules [22, 28, 54, 219, 199]. This subsequently activates actin nucleation promoting factors (NPFs) such as WAVE2, HS1, and WASP [16]. These NPFs in turn activate the Arp2/3 complex, nucleating actin polymerization, which provides the necessary force for membrane deformation, cell spreading, and microcluster transport [16, 24, 13].

Arp2/3-nucleated actin polymerization has been intensely studied in many cell types owing to its importance in chemotaxis, cell motility, endocytosis, mem-

brane ruffling, and ventral F-actin waves [207, 77, 184]. These studies show that polymerizing actin can form stationary or moving spots, or propagate as waves under a broad variety of conditions. In particular, ventral F-actin waves have been extensively observed in neutrophils [206], *Dictyostelium* [202, 18, 17, 74, 179] and adherent cells [29], suggesting that the underlying mechanisms of their formation are largely conserved. However, despite the engagement of a similar complement of actin regulators as other cells, it is not known if T cells exhibit such dynamic structures and whether these play a role in microcluster assembly.

The formation of contacts between a cell and another surface is driven by deformations occurring at multiple length scales. Large-scale deformations of the cell membrane, driven by cytoskeletal reorganization, allow the formation of cellular contacts over micrometer length scales [31, 44, 57, 75, 166, 180]. Recent work has devoted considerable attention to cell adhesion and spreading during the first few minutes of cell-substrate contact [31, 44, 180, 50, 62, 181]. In particular, theoretical and experimental studies have focused on the kinetics of spreading. An emerging consensus view is that cell spreading occurs in phases, where the growth of spread area (or contact) follows a power law in time with distinct exponents [44, 180, 50] or other distinct functional forms [31, 32].

We have used simultaneous interference reflection microscopy (IRM) and total internal reflection fluorescence (TIRF) microscopy to analyze the dynamics of the cell periphery and actin cytoskeleton, using Jurkat cells as a model system. We

found that the contact area of spreading cells is characterized by a common function of time with a characteristic timescale, which is determined by the dynamics of the actomyosin cytoskeleton but is largely insensitive to ligand density. In addition, we found two distinct modes of cell spreading with similar kinetics but striking differences in membrane topography and dynamics. Actin organizes into spatiotemporal patterns such as traveling waves and spirals, which are driven by polymerization. These waves appear to be associated with moving membrane folds suggesting that a coupling between chemical and mechanical factors. Our studies demonstrate an intricate relationship between membrane and F-actin dynamics, during activation and spreading of Jurkat T cells and may have implications for theoretical models of actin dynamics.

## 2.2 Results

### 2.2.1 Kinetics of cell spreading

To examine the biophysical factors that determine spreading kinetics and the role of membrane dynamics in signaling we studied the spreading of Jurkat cells on glass substrates coated with anti-CD3$\epsilon$. Antibody binding to CD3 leads to induction of signaling and activation of actin polymerization. This model system has been shown to induce robust spreading of T cells, recapitulating many aspects of T-cell signaling and activation [23, 10, 154, 22, 54] while facilitating multimodal imaging of the cell-substrate interface. Cells were allowed to contact an antibody-

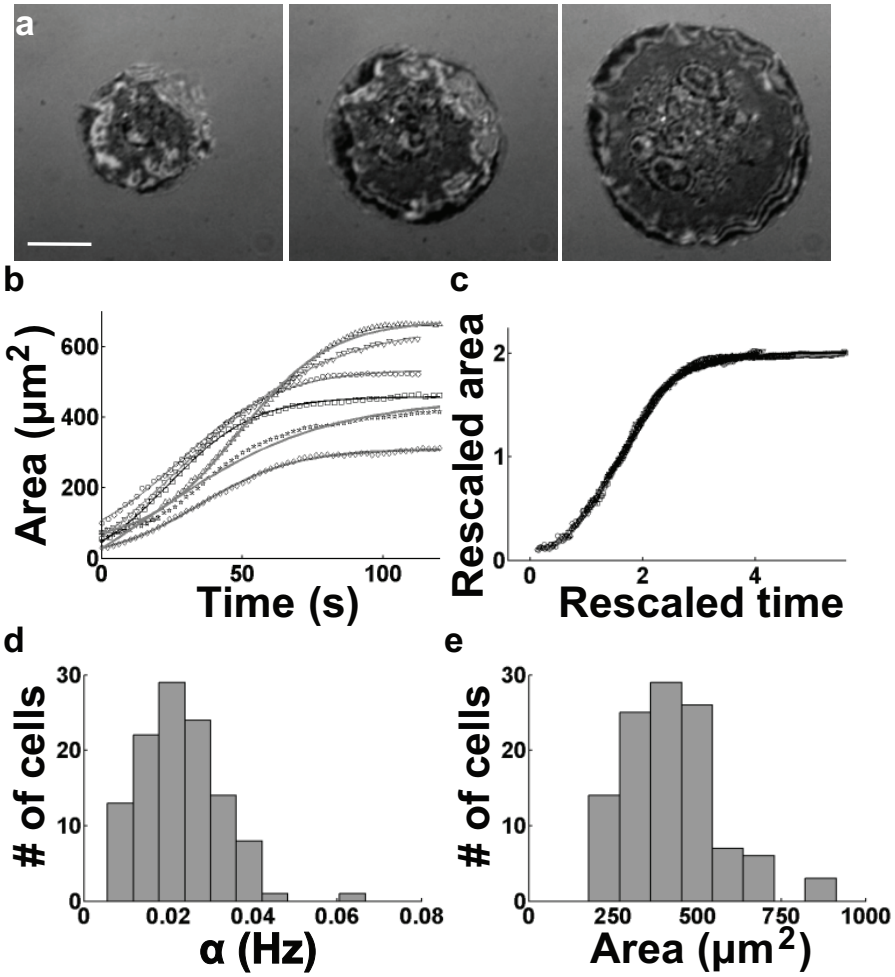


Figure 2.1: **Spreading of Jurkat T lymphocytes on antibody-coated substrates.** (a) Time-lapse IRM images showing the increasing contact zone as the cell spreads out. Scale bar, 5 $\mu$m. (b) Contact area as a function of time for six representative cells. The smooth lines are fits to a tanh function, $A(t) \sim A_0 \tanh(\alpha t)$. (c) Rescaled graphs showing that the spreading of all cells can be described by a common spreading function. (d) Histogram of the spreading rate, $\alpha$ ($n = 88$). (e) Histogram of the final spread area $A_0$.

coated glass substrate in serum-free media and imaged with brightfield microscopy and IRM. Within seconds of incubation, cells started forming contacts with the coated substrate. The contacts appeared as fluctuating light and dark IRM patterns and interference rings. After initial contact, the cells started spreading and rapidly increased their contact area (Figure 2.1a). The contact zone of a spreading cell appeared as a predominantly dark gray patch that increased in size isotropically, with the cell boundary being relatively smooth and circular, until the spread area saturated in 2-3 min (Figure 2.1a). Cells displayed limited spreading on poly-L-lysine coated glass or plain glass, suggesting that T cell spreading requires specific adhesion.

We found that the cell-substrate contact area showed a rapid growth after a small initial lag period, and eventually saturated (Figure 2.1b). The overall time course of the spread area supports a recent model [31, 32]. This model predicts that growth of the contact area as a function of time follows a hyperbolic tangent function and highlights the requirement of actin polymerization to drive spreading. Accordingly, we found that the area was well fit by a hyperbolic tangent function, $A(t) \sim A_0 \tanh(\alpha t)$ (Figure 2.1b), as indicated by the fit residuals. This allowed us to extract a characteristic timescale of spreading to saturation, as well as the asymptotic spread area. Upon rescaling the area of each cell with the final area $A_0$, and the time by $\alpha$, all the data from the cells fell on a single universal curve (Figure 2.1c) showing that a common mechanism likely underlies the spreading of all these cells. From the fits, we obtained a typical spreading rate of $\alpha \sim 0.02 \pm 0.01$ s$^{-1}$ and

a final spread area of $A_0 \sim 430 \pm 160$ $\mu$m$^2$. Both these parameters showed some degree of heterogeneity across the cell population (Figure 2.1d).

Recent model of active spreading [32] predicts that the spreading rate should be independent or weakly dependent on the density of adhesive ligands on the substrate. To test this for T cell spreading, we examined the effect of the antibody coating density by changing the antibody concentration in solution from 0.01 $\mu$g/ml to 10 $\mu$g/ml. At concentrations $> 0.2$ $\mu$g/ml, cell spreading was similar to that at 10 $\mu$g/ml (the control concentration), with similar spreading rates and final areas (data not shown). At concentrations $< 0.2$ $\mu$g/ml, cells established adhesive patches but did not spread. However, for the small fraction of cells that did spread, the mean $\alpha$ value was the same as that of control cells. Thus, spreading kinetics of T cells are robust, with a characteristic timescale that does not change over a range of antibody density.

### 2.2.2 Role of the actomyosin cytoskeleton on cell spreading

Previous work has shown that the binding of TCRs to anti-CD3$\epsilon$ antibodies on the substrate leads to the activation of signaling cascades that regulate actin polymerization [23, 10, 78, 157, 24]. Cells treated with very high doses (500 nM and higher) of actin polymerization inhibitor latrunculin A (lat-A) do not spread. At 100 nM lat-A, cells can spread but with lower spreading rates and final areas as compared to the control population (Figure 2.2a,b). At even lower concentrations of

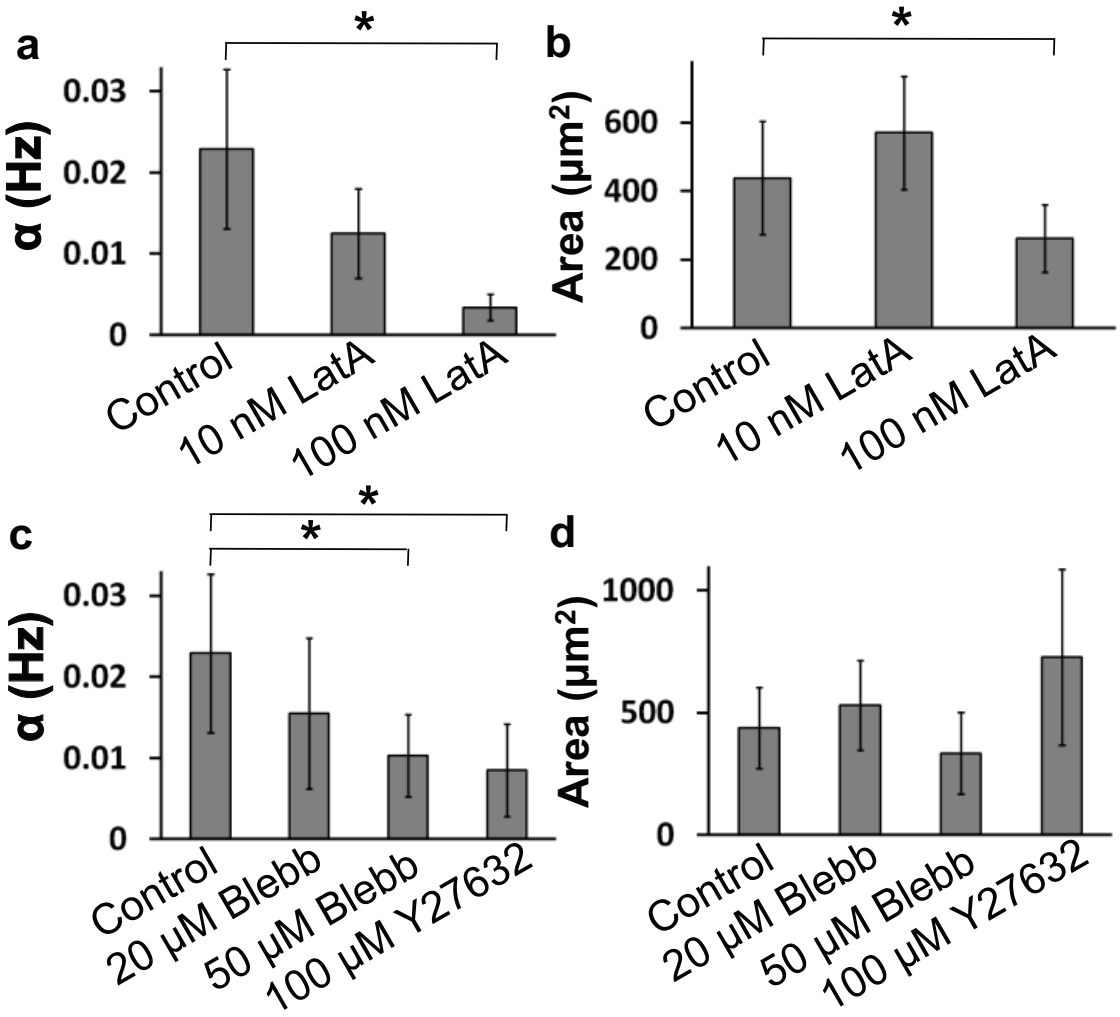


Figure 2.2: **Cells with compromised actin polymerization do not spread efficiently.** (a) Spreading rate $\alpha$ decreases as the concentration of Lat-A increases ($p < 0.01$, t-test). (b) The final spread area is unaffected for small concentrations of Lat-A, but is much smaller for higher concentrations ($p < 0.05$, t-test). (c) Spreading rate is diminished upon inhibition of the activity of NMII or Rho kinase (ROCK). (d) Final spread area is not affected by inhibition of NMII or ROCK. The number of cells analyzed was $> 18$ in all conditions.

lat-A (10 nM), the final areas of spread cells were similar to those for control cells, but spreading occurred with significantly slower rates (Figure 2.2a,b). The dose-dependent effect of Lat-A on spreading rate indicates that the rate of spreading is largely determined by actin polymerization kinetics, and distinguishes it from the passive spreading described by [44].

Previous studies have shown that nonmuscle myosin II (NMII) regulates the rate of cell spreading in fibroblasts (33,34). In T cells, NMII (specifically the IIA isoform) knockdown or inhibition alters signaling in the immune synapse (35). However, its role in the initial spreading of T cells has not been investigated. Cells treated with blebbistatin (a specific inhibitor of the ATPase action of NMII [3]) were able to spread, and the contact area growth over time followed a hyperbolic tangent function, as in the case of control cells. For low concentrations of blebbistatin (20 $\mu$M), the rate of spreading was only weakly reduced and the maximal spread area showed no significant change (Figure 2.2c,d). In 50 $\mu$M blebbistatin, the spreading rate was reduced compared to the control case, but the maximal areas were largely unaffected (Figure 2.2c,d). To assess the roles of distinct signaling pathways that might control the activity of NMII, we investigated the role of the Rho-associated protein kinase (ROCK), which is essential for phosphorylation of myosin light chain (MLC), in turn essential for NMII activity. We found that the ROCK inhibitor Y-27632 (100 $\mu$M) significantly reduced the spreading rate of cells but not their final area.

### 2.2.3 Effect of serum on cell spreading

In the experiments described so far, cells were cultured in growth medium, and then withdrawn from serum 15 min before imaging. These conditions are used routinely to study T-cell activation and signaling [78, 157]. To test whether TCR mediated spreading behavior depends on the presence of serum, a more physiological condition, we imaged cell spreading in medium supplemented with 10% FBS. As in serum-free medium, cells in medium with 10% FBS rapidly established contact with the substrate and started spreading (Figure 2.3a). The growth of contact area as a function of time for a spreading cell could be well fit by a hyperbolic tangent function, similar to the case for serum-free conditions. However, the kinetics were characterized by an irregular growth of the projected cell area (Fig. 2.3b). The spreading rate $\alpha$ for cell populations was the same in the presence and absence of serum (Figure 2.3c) ($p > 0.1$, t-test, $n = 88$, serum-free, $n = 45$ with serum), although the final spread area, $A_0$, was lower in the serum-supplemented than in the serum-free case ($p < 0.05$). However, there was a remarkable difference in the nature of spreading. Kymographs of the cell edge (Figure 2.3d) showed that the cell-substrate contacts were highly dynamic, with the cell edge undergoing repeated protrusions and retractions during spreading. In contrast, cells spreading in the absence of serum showed a smooth movement of the cell periphery (Figure 2.3e). Across the population, in the presence of serum, most cells showed an irregular anisotropic pattern of spreading ($> 75\%$), whereas nearly all cells in serum-free medium ($> 95\%$) showed smooth isotropic spreading.

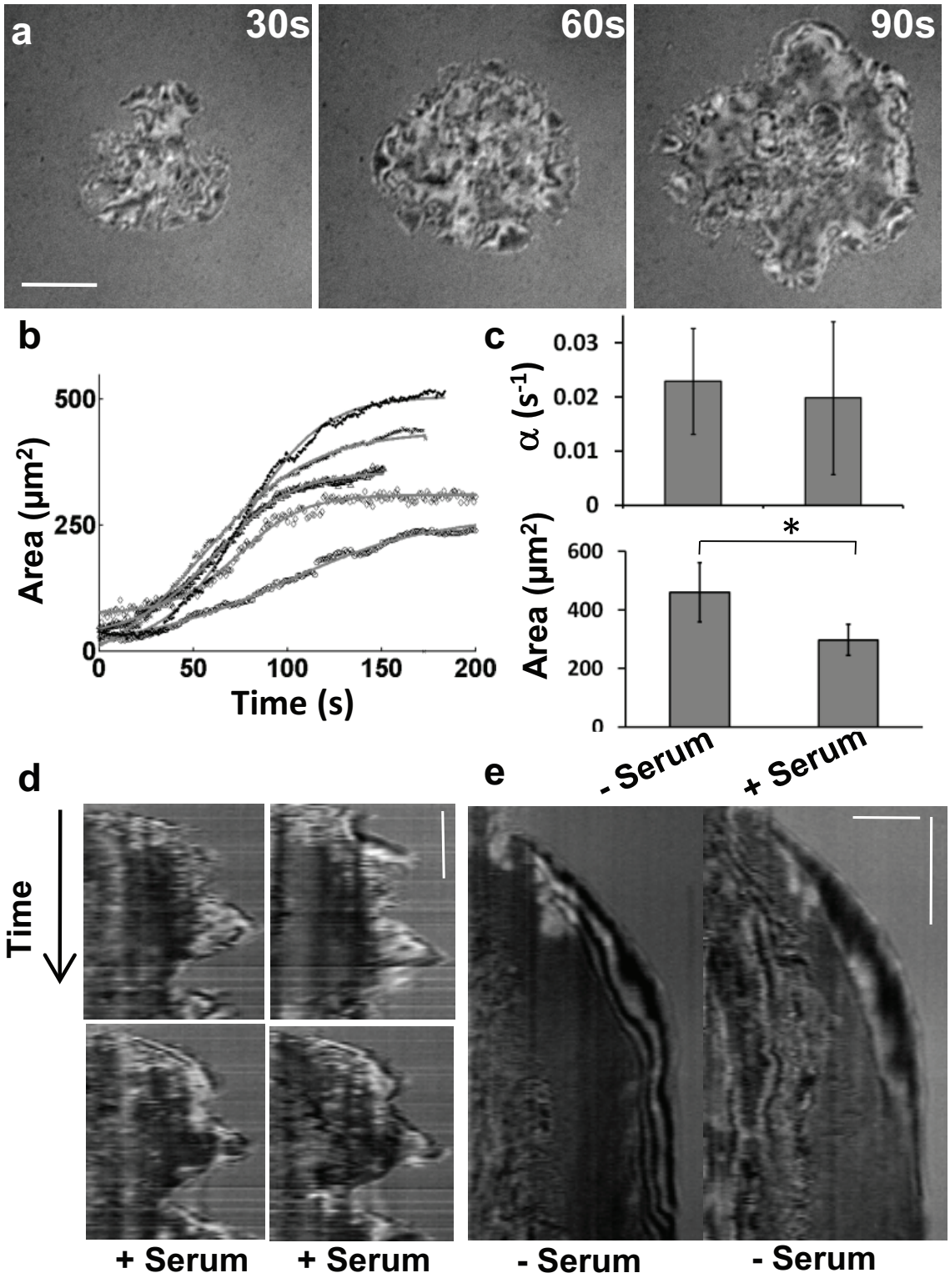


Figure 2.3: (Continued on the following page.)

Figure 2.3: **Spreading in the presence of serum is qualitatively different.** (a) Time-lapse IRM images of a T cell spreading on antibody-coated glass substrate in the presence of serum. Scale bar, 5 $\mu$m. (b) Contact area of the cell as a function of time. Each graph corresponds to a different cell. The solid gray lines show a fit to a hyperbolic tangent function. (c) Comparison of spreading rate $\alpha$ and final spread area $A_0$, for serum and serum-free cases shows that these parameters are very similar in the two conditions. (d) Kymographs of four representative sections in serum. (e) Kymographs of two representative sections in serum-free conditions (scale bars, 3 $\mu$m, 30 s).

### 2.2.4 Actin waves correlate with edge protrusions

We then used Jurkat T cells expressing EGFP-actin to visualize the actin cytoskeleton when cells spread in the presence of serum, in order to examine its role in the dynamics of the cell edge. Following initial contact, the cells spread, rapidly increasing their contact area (Figure 2.4A). Simultaneously collected timelapse TIRF images of EGFP-actin (Figure 2.4B) showed that the leading edge was associated with radially moving fronts of actin. Figure 2.4D shows a traveling bump of actin intensity at the cell periphery as it moved radially outwards. Kymographs (Figure 2.4C) show that the cell edge underwent repeated protrusions and retractions throughout spreading before establishing a clear lamellipodium, which was marked by the formation of a ring of actin and the establishment of retrograde flow. The protrusion-retraction events were not strictly periodic, and the average time inter-

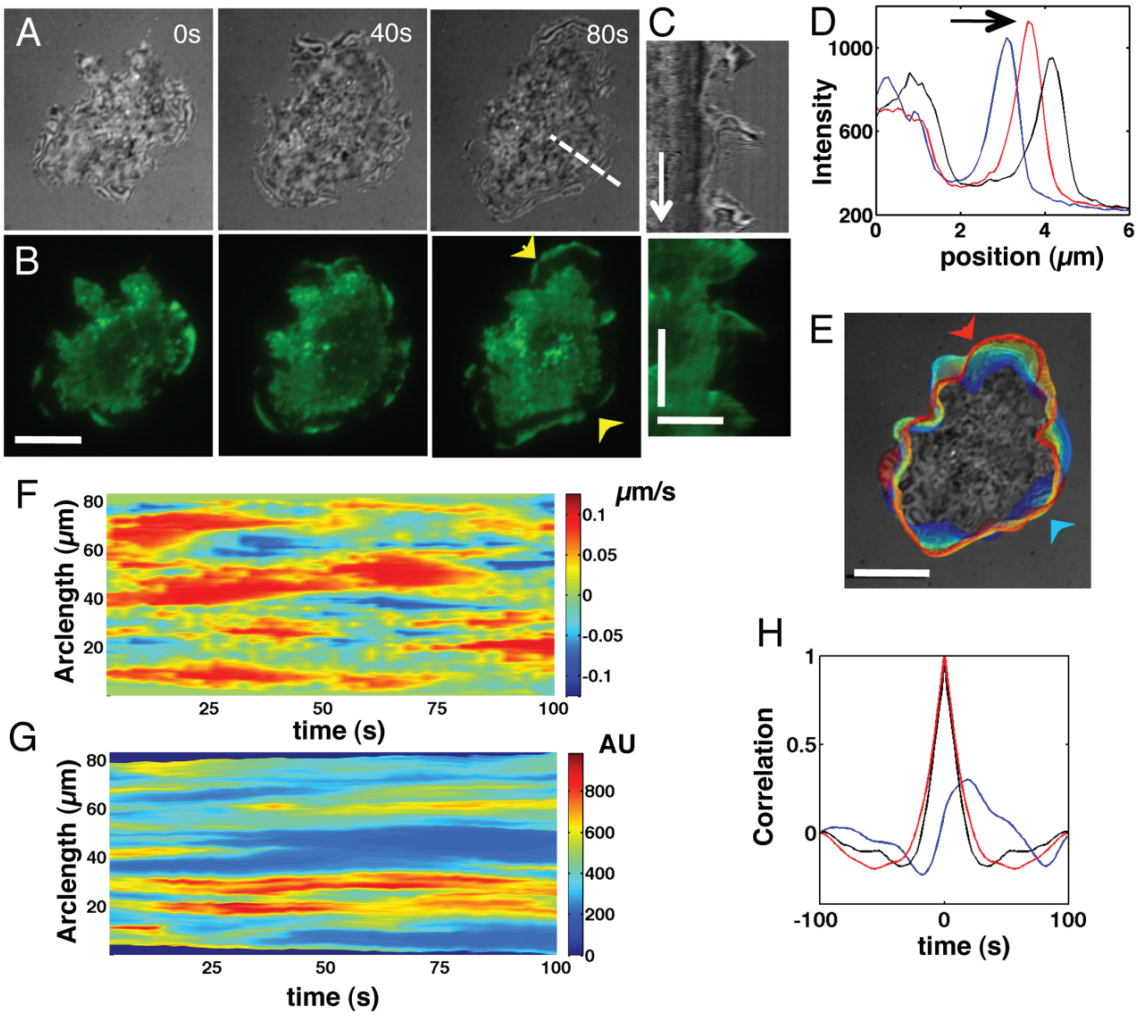


Figure 2.4: **Spreading T cells display dynamic edge movement and actin waves.** (A,B) Time-lapse (A) IRM and (B) TIRFM images of a Jurkat T cell spreading on anti-CD3-coated substrates. Yellow arrows: actin waves. Scale bar is 10 $\mu$m. (C) Kymograph of a radial line across the cell edge (dashed line in (A)) in IRM (top) and TIRF (bottom). Scale bars: horizontal 5 $\mu$m; vertical 2 min. (Continued on next page.)

Figure 2.4: (D) Line profile corresponds to the wave marked by the top yellow arrow in (B). Direction of the arrow corresponds to time. (E) Cell outlines at multiple time-points in different colors, going from blue (earlier in time) to red (later in time) for 0 to 5 min. (F,G) Heat maps of (F) edge velocity and (G) actin intensities in the normal direction along the cell edge as a function of time. (H) Temporal autocorrelation of leading edge velocity (black), EGFP-actin intensity (red), and their cross-correlation (blue).

val between successive protrusion peaks was $80 \pm 17$ s ($N = 56$ intervals from 10 cells). Successive cell contours extracted from the IRM images (Figure 2.4E) also show that the cell edge around the entire cell periphery was dynamic with extensive protrusions and retractions. The time evolution of the leading-edge position as obtained from the IRM images was tracked using a level-set method [137] to determine the local protrusion and retraction velocities normal to the leading edge. A relatively irregular sequence of protrusion and retraction events was observed with typical velocities on the order of 100-120 nm/s (Figure 2.4F).

While similar oscillations have been observed in primary T cells spreading on stimulatory bilayer substrates [51], the relationship between actin and edge dynamics is not well understood. To quantify this, we calculated the intensity profile of EGFP-actin by summing the intensity of pixels within a 2 $\mu$m band around the cell edge obtained from the IRM images (Figure 2.4G). Brighter F-actin intensities appeared

to weakly correlate with slower protrusion velocities while lower intensities were associated with larger protrusion velocities. To further quantify the relationship, we computed auto- and cross-correlations of the edge velocity and the local actin signal. While the temporal autocorrelation of the leading edge velocity and actin intensity showed a pronounced dip, the cross-correlation indicated a slight offset of $\sim$ 15 s (Figure 2.4H). This indicates that the leading edge velocity peaks several seconds ($15 \pm 4$ s, $n = 5$ cells) earlier than the actin intensity, similar to observations in adherent cells [171].

### 2.2.5 Actin Waves correlate with membrane folds

In addition to the peripheral actin waves (Figure 2.5A), we also observed dynamic actin structures interior to the cell periphery, such as traveling waves moving radially outwards and inwards towards the cell center (Figure 2.5B,C), as well as spiral patterns (Figure 2.5C). The movement of these structures was visualized as shown in a representative kymograph (Figure 2.5D). The average velocity for the entire population was $7.1 \pm 2.0$ $\mu$m/min ($n = 80$, Figure 2.5E) consistent with the edge velocities observed in Figure 2.5F. Internal actin structures typically had an average velocity of $6.7 \pm 2.1$ $\mu$m/min ($n = 27$), similar to that of the peripheral actin waves, $7.1 \pm 1.8$ $\mu$m/min ($n = 43$), suggesting that all these structures may be driven largely by actin polymerization and share a similar mechanistic origin.

Previous studies have reported the assembly of actin or actin nucleators into

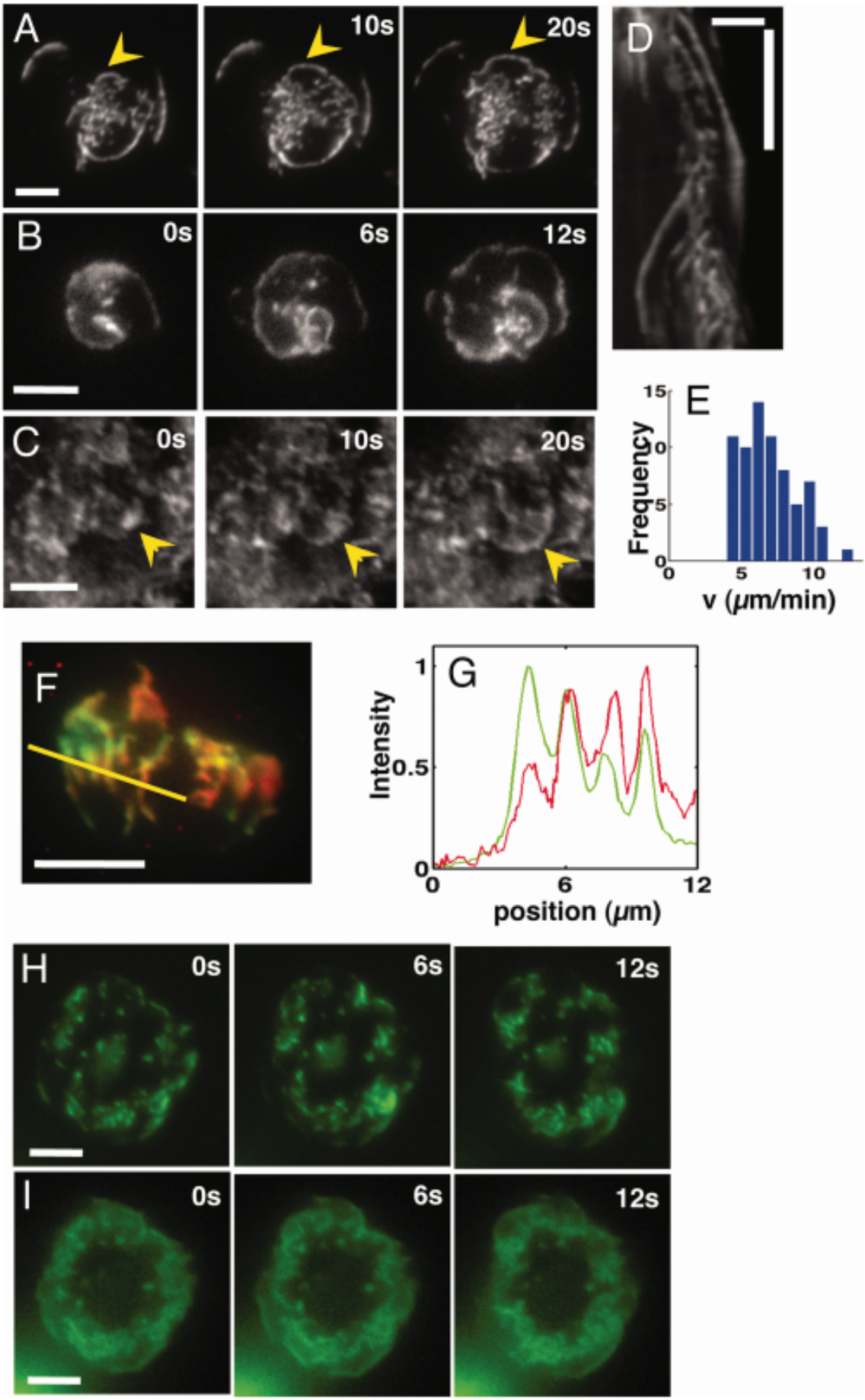
A
10s
20s
B
0s
6s
12s
C
0s
10s
20s
D
E
Frequency
15
10
5
0
0
5
10
v (μm/min)
F
G
Intensity
1
0.5
0
0
6
12
position (μm)
H
0s
6s
12s
I
0s
6s
12s

Figure 2.5: **Spreading Jurkat T cells display membrane coupled actin waves.** (A) Time-lapse image of EGFP-actin expressing cell on anti-CD3-coated substrates showing peripheral actin waves. (B) Time-lapse image showing a spiral wave of actin. (C) Time-lapse TIRF images showing internal actin waves. (D) Kymograph showing multiple types of propagating actin structures. The linear streaks of GFP represent traveling waves. Vertical scale bar: 1 min. (E) Histogram of actin wave velocities across cell populations. The mean velocity is $7.1 \pm 2.0$ $\mu$m/min, $N = 80$. (F,G) (F) Dual-wavelength images and (G) intensity profiles showing snapshots of a spreading cell with EGFP-actin (green) and TagRFP-T cytosol (red). (H,I) Time-lapse (H) TIRF and (I) wildfield images of EGFP-actin cell showing propagating actin waves. All horizontal scale bar: 5 $\mu$m.

wave-like structures of protein density in a variety of cell types, such as neutrophils, *Dictyostelium*, and epithelial cells [18, 17, 73, 206, 6, 29]. To examine whether the internal waves we observed were actin density waves, we stably transfected EGFP-actin labeled Jurkat cells with TagRFP-T as a cytosolic marker to generate two-color cell lines. TIRF images of the red fluorescence show the position of the membrane, which is in closest contact with the substrate, as the TIRF signal disappears when the membrane-substrate distance increases. Dual-wavelength TIRF imaging of actin and cytosol showed a high degree of correlation between the location of actin waves (green) and cytosol (red), which likely corresponds to membrane folds (Figure 2.5F). Direct observation of the membrane by labeling proved to be difficult owing to mem-

brane recycling over the time-scale of spreading. Line profiles of the fluorescence intensities across a region of the cell plotted for the two channels show that the peaks of intensities overlap with each other, indicating that actin is colocalized with membrane folds that are in close contact with the surface (Figure 2.5G). However, the actin and cytosol intensities at each wave do not vary proportionately. In addition to TIRF, we observed actin/membrane structures in simultaneously collected epifluorescence images (Figure 2.5H), indicating that these waves were not a proximity artifact of TIRF imaging. Taken together, these observations suggest that the observed waves are coupled actin-membrane waves traveling on a planar membrane surface. This is consistent with our previous observations using IRM that the membrane topography at the cell substrate interface is not entirely flat, rather it has vertical undulations on the order of 25-50 nm [120].

We finally verified that these actin waves result from TCR activation at the surface to formally rule out the possibility that these structures accompany passive spreading. We imaged cells spreading on substrates coated with the pro-adhesive ligand, anti-CD43, which leads to non-integrin mediated adhesion, without any stimulatory anti-CD3. While cells spread on this surface (though to a smaller extent than on stimulatory antibody), the actin cytoskeleton as imaged in TIRF remained largely uniform with no visible structures such as the propagating waves observed on an activating surface (data not shown). The advance of the cell periphery was slower and not as smooth and efficient as in the presence of stimulatory antibody. These results suggest that the actin structures are dynamically stabilized membrane folds

that require TCR activation and signaling for their formation and maintenance.

## 2.3 Discussion

The initial attachment of cell membranes to a surface plays a key role in the formation of receptor-ligand bonds during cell-cell and cell-substrate junction formation. In the commonly studied 'T cell activation on coverslip' system [23, 22, 54, 8], we identified two modes of spreading that are characterized by marked differences in the dynamics of the cell edge (Figures 2.1,2.3), consistent with previous observations in spreading fibroblasts [57]. Also, we have characterized actin dynamics during early stages of activation, and found that actin organize into rich spatiotemporal patterns such as traveling waves, moving spots, and spirals (Figure 2.4).

We found that the contact area of spreading Jurkat T cells on antibody-coated substrates was well described by a hyperbolic tangent function, with a characteristic timescale of $\sim 45$ s. This is similar to the time over which the initial signaling peaks [85]. Our results are consistent with a recent model of cell spreading, which predicts that the spread area grows as $\tanh(\alpha t)$ [31]. Previous studies have described the kinetics of spreading in different cells as power laws [31, 44, 57, 75, 180, 50, 158]. We note that the early phase of spreading in our observations, after the initial lag period, is compatible with models suggesting linear growth of cell area (since at early times a hyperbolic tangent function is linear). Perturbing the actin cytoskeleton using lat-A in a dose-dependent manner leads to slower spreading, as predicted by

these models. This shows that actin polymerization is essential for spreading and controls its timescale.

The role of NMII in determining the early spreading kinetics in T lymphocytes is not known. Our experiments showed that inhibition of NMMII and ROCK activity slowed down spreading kinetics without significantly altering the maximal spread area. This is in contrast to observations in fibroblasts, where spreading is enhanced by the inhibition of NMII [27, 203], presumably due to the loss of contractile activity of the actomyosin network that applies an inward tension to cells. This suggests that the actomyosin network may not function similarly in the early stages of T cell spreading. It is possible that the contraction of the actomyosin network applies a force that squeezes the lamellipodia outward [121]. Inhibition of myosin would then slow down the outward movement of the cell edge, as we observed. This alternative hypothesis has been postulated before for leukocyte and lymphocyte motility and could also presumably be functional during the spreading of T cells [121].

Actin waves have been observed in *Dictyostelium* [202, 18, 73] and in motile neutrophils during chemotaxis [206]. However, the mobile actin structures we have characterized here in Jurkat cells (Figure 2.4) appear to be distinct from those previously observed. First, TCR activation is obligatory for the formation of the propagating actin waves, unlike in *Dictyostelium* where waves are generated in the absence of G-protein signaling [17]. Second, actin waves in Jurkat cells appear to be associated with membrane undulations and correlated with moving membrane folds

suggesting that a coupling between chemical and mechanical factors is required to generate these waves (Figure 2.5). Previous studies on Jurkat, mouse, and human T cells have not reported such patterns, possibly because these studies either focused on well spread cells in the later stages of spreading or imaged the actin fluorescence using confocal microscopy which has lower axial resolution than TIRF microscopy [23, 78, 103, 8]. Moreover, most studies of T cell spreading on lipid bilayers used ICAM-1 as an adhesive ligand, which may have suppressed such waves.

The central role played by the actin cytoskeleton in T cell signaling has been demonstrated by pharmacological, physical, and genetic perturbations [222]. Collectively, these studies suggest that a dynamic actin network is required for effective TCR-ligand interaction as well as the formation and transport of kinases, scaffolds, and other proteins into micron-sized signaling assemblies around activated TCRs, but the coordinated behavior of the cytoskeletal network and signaling components is not well understood. Our results show that the actin cytoskeleton and regulatory proteins in Jurkat T cells couple with membrane undulations to lead to traveling waves, which are modulated by TCR signaling during activation. These dynamic edge oscillations under conditions of low adhesion and the actin coupled membrane waves may be helpful in the search for antigens on the relatively rough surface of an antigen presenting cell, as well as facilitating TCR triggering through kinetic segregation [100].

# Chapter 3

# Cytoskeletal forces during signaling activation in Jurkat T cells

# Abstract

T-cells are critical for the adaptive immune response in the body. The binding of the T cell receptor (TCR) with antigen on the surface of antigen presenting cells (APCs) leads to cell spreading and signaling activation. The underlying mechanism of signaling activation is not completely understood. Although cytoskeletal forces have been implicated in this process, the contribution of different cytoskeletal components and their spatial organization are unknown. Here we use traction force microscopy to measure the forces exerted by Jurkat T-cells during TCR activation. Perturbation experiments reveal that these forces are largely due to actin assembly and dynamics, with myosin contractility contributing to the development of traction force but not its maintenance. We find that Jurkat T-cells are mechanosensitive, with cytoskeletal forces and signaling dynamics both sensitive to the stiffness of the substrate. Our results delineate the cytoskeletal contributions to interfacial forces exerted by T-cells during activation.

*This chapter is adapted from Hui, Balagopalan, Samelson and Upadhyaya [87].*

## 3.1 Introduction

T lymphocytes are central effectors of the adaptive immune response, circulating through the body and scanning APCs for their cognate antigens [2, 141]. Contact and adhesion between the T cell and the APC results in T cell spreading on the APC, ensuring close proximity between the cells. TCRs recognize peptide-major hiscompatibility complexes (pMHCs) on the APC surface. This results in the activation of TCRs and the formation of signaling microclusters that consist of activated TCR and various downstream signaling molecules [22, 219, 199]. Despite extensive study of the biochemical signaling pathways involved, much further work is required to elucidate the precise mechanism of T-cell activation [197].

Signaling activation of T-cells critically depends upon T-cell adhesion to the APC [215] and extensive rearrangements of the actin cytoskeleton and cell deformation [222]. These observations suggest that physical forces exerted on the TCR may contribute to activation by facilitating conformational changes in the TCR/CD3 complex, resulting in signaling activation, TCR clustering, and the assembly of signaling microclusters [136, 135, 111]. Alternatively, the applied forces may act directly on signaling molecules, resulting in conformational changes that activate additional signaling cascades [221]. In support of these views, direct application of external forces to anti-CD3 or pMHC coated beads or biomembrane force probe can

lead to activation of the TCR [111, 91, 132].

In the literature, two different studies have examined the forces generated by T cells when they are activated. The first one used a biomembrane force probe (BFP) to measure pushing and pulling forces when primary T-cells engulf anti-CD3 coated beads [91]. The small size of the beads precluded spatial resolution of the forces exerted across the cell-substrate contact. The second study plated primary human $CD4^+$ cells on elastomer pillar arrays coated with anti-CD3 or pMHC and showed that T-cells exert traction forces in response to CD3 and CD28 costimulation [11]. Considering the small size of T cell compared with adherent cells, the micropillar assay introduces a high percentage of nonstimulatory empty space between pillars, and artifacts like local assembly of proteins around the pillars.

In most adherent cells, stresses are generated by the coordinated action of actin polymerization and myosin contraction, which drive actin flows. Although several studies suggest that cytoskeletal dynamics plays a crucial role in TCR signaling [8, 12, 222], the delineation of contributions of different cytoskeletal components to force generation is unclear. Regardless of the origin of the force, the overall magnitude of generated forces will depend on the elastic properties of the cellular actin network and the dynamics of actin assembly and disassembly. The effective internal stress generated in the viscoelastic actin network can be estimated from the material parameters of the cell [15]. Independent measures of resting Jurkat cell stiffness suggest that these are soft (Youngs modulus, 50-100 Pa [$pN/\mu m^2$], [169]), which

likely limits the peak internal stresses to 100 Pa at best. Whether these forces are sufficient for activation is unknown.

Here we use traction force microscopy (TFM) to measure the forces exerted by T-cells during activation [47]. We find that Jurkat T-cells are weak force generators on anti-CD3 coated elastic substrates, exerting peak stresses reaching 20-30 Pa on stiff substrates. These forces are largely driven by actin polymerization dynamics. Nonmuscle myosin II (NMII) activity is dispensable for maintenance of traction stress, but contributes to the generation of forces. We find that T-cell signaling activation is sensitive to the stiffness of the activating substrates and this mechanosensitivity is correlated with increased cytoskeletal forces. Our results suggest that forces generated by the actomyosin cytoskeleton are essential for continuous receptor activation and TCR signal maintenance at the immunological synapse (IS) [89].

## 3.2 Results

### 3.2.1 Traction forces generated by Jurkat T-cells

To measure the forces exerted by T-cells, we performed TFM, which allows the measurement of spatially resolved traction stresses. Jurkat T cells expressing enhanced green fluorescent protein (EGFP)-actin were allowed to spread on polyacrylamide gels coated with anti-CD3 and embedded with fluorescent beads on the

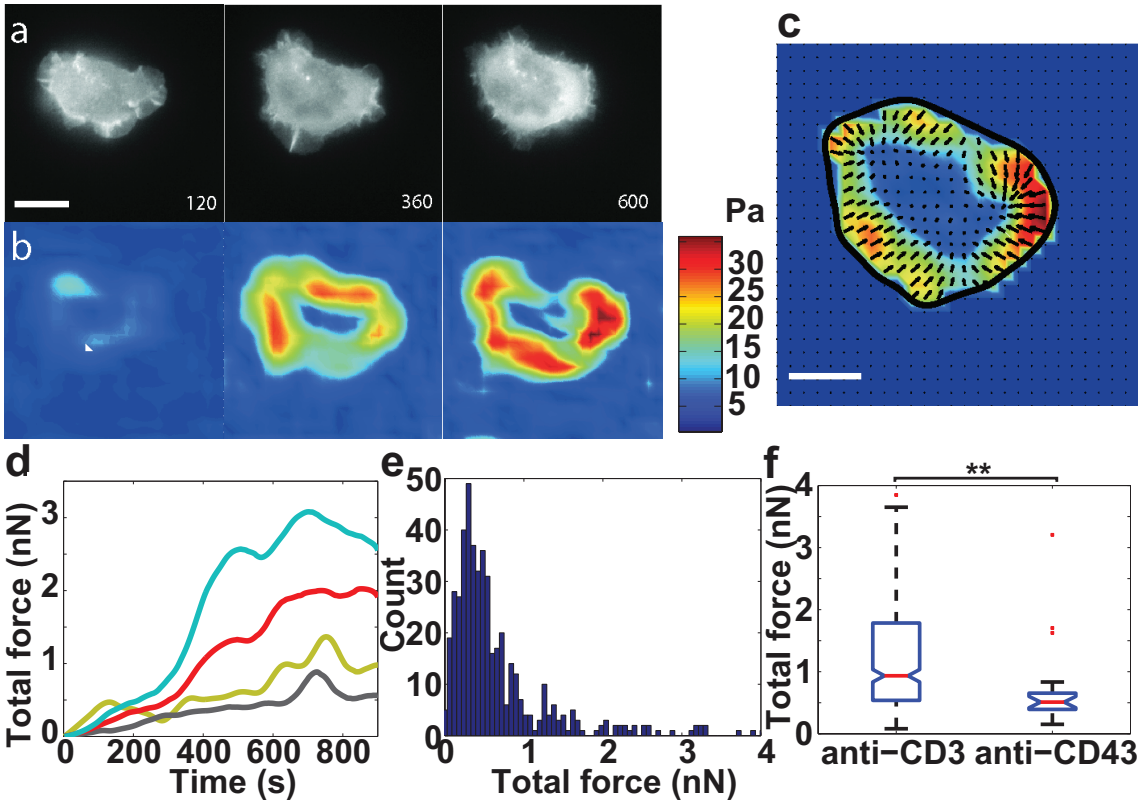


Figure 3.1: **Jurkat T-cells are weak generators of traction force.** (a,b) Time-lapse (a) fluorescence images and (b) traction stress color maps of EGFP-actin expressing Jurkat T-cells spreading on an anti-CD3 coated elastic substrate (of stiffness 1.2 kPa). (c) Vector map of traction forces showing the direction of stresses. Scale bar, 10 $\mu$m. (d) Development of stress as a function of time for four sample cells on substrate with Young modulus ($E$) below 1 kPa. (e) Histogram of stress exerted by Jurkat T-cells on substrate with $E < 1$ kPa ($n = 486$). (f) Comparison of traction stresses on substrates coated with stimulatory antibody anti-CD3 and nonstimulatory antibody anti-CD43.

top surface as fiduciary markers. We imaged the spreading dynamics of cells starting from the earliest time points before the cell established contact with the substrate and continued imaging for at least 15 min. Typically, cells were completely spread before 15 min, as shown in the EGFP-actin montage of a typical cell spreading on a gel of stiffness 1.2 kPa, which approximates the stiffness of APCs, [21] (Figure 3.1a). To measure the traction stresses exerted by cells, we tracked the fluorescent beads using particle image velocimetry (PIV). The first frame of the live-cell image sequence, before the cell exerted traction on the surface, was used as the zero displacement or reference image. Unconstrained Fourier transform traction cytometry (unconstrained FTTC; [26]) was used to calculate the traction stress map from the measured bead displacements at different times (Figure 3.1b). The average traction stresses exerted by cells were in the range of 0-10 Pa, in the same range as stresses exerted by neuronal growth cones [15, 114, 92]. By contrast, rapidly migrating keratocytes and strongly adherent fibroblasts are known to exert traction stresses in the range of 100 Pa to several kPas [47, 68, 194].

We found that the traction stress was concentrated at the periphery of the spread area coincident with lamellipodia and lamella. The stresses exerted were higher a few microns internal to the periphery of the cell, which corresponded to actin-dense regions. Stresses were exerted centripetally and directed toward the cell center, as seen in the spatial map of vectors corresponding to the exerted stresses (Figure 3.1c). We used EGFP-actin images to track cell edges (as shown by the black line in Figure 3.1c) and to obtain the contact area of the spreading cell at

each time point. The total force exerted by the cell rapidly increased over the first 5 min after initiation of spreading, until it reached a maximum and subsequently either saturated over the rest of the observation period or showed a slight decrease (Figure 3.1d). The total force exerted by cells on gels of stiffness below 1 kPa between 14 and 15 min showed considerable variation, with a median value of 0.47 nN (Figure 3.1e).

We further verified that the observed forces were specific to TCR-ligand mediated activation and spreading. On substrates coated with the nonstimulatory antibody anti-CD43, cells established contact and spread but to a smaller extent than on stimulating surfaces. The total force exerted by cells on a nonstimulating surface were significantly lower than the stress exerted on stimulating surfaces (anti-CD3: $0.93 \pm 0.85$ nN, $n = 383$; anti-CD43: $0.51 \pm 0.14$ nN, $n = 20$; $p = 0.002$, $1< E <2$ kPa, Figure 3.1f). This indicates that the observed forces are largely a direct consequence of TCR-ligand binding leading to T cell activation.

### 3.2.2 Role of the actin cytoskeleton in force maintenance

We next sought to examine the molecular basis of force maintenance in Jurkat T-cells. The actomyosin cytoskeleton is likely to be essential to force maintenance in these cells, similar to other cell types [152, 8]. We perturbed the activity of the actomyosin cytoskeleton using small-molecule inhibitors, which are powerful agents

for rapid and reversible inhibition of target molecules [164]. Because preincubation of cells with inhibitors can affect cell spreading, we added inhibitors to cells after they had spread and measured the changes in cellular traction stress after inhibitor application. Unless specified, we added inhibitors to cells after 15 min of stimulation on anti-CD3 coated gels of stiffness in the range of 0-2 kPa and continued to image the bead movements and GFP-actin dynamics simultaneously for an additional 15 min in order to measure the effect of the drug on forces. This method allows us to examine the effects of inhibitors on a single-cell basis and avoid the problems of population averaging that might mask the inhibition effects (Figure 3.1e).

We first focused on the role of actin polymerization and depolymerization dynamics on cellular traction forces with latrunculin-A (Lat-A) to inhibit polymerization of actin, jasplakinolide (Jasp) to stabilize preexisting actin filaments, and CK-666 to inhibit the activity of Arp2/3 complex, an actin-nucleating protein. Inhibition of actin polymerization by Lat-A resulted in the disruption of preexisting lamellipodia and actin-rich structures visible in the cell surface contact zone (Figure 3.2c), with a reduction in traction (Figure 3.2d). Application of Lat-A 5 min after initiation of spreading resulted in similar disruption of actin and loss of traction (unpublished data). As a control, addition of dimethyl sulfoxide (DMSO) carrier alone did not significantly affect the actin structures in the cell or the traction forces generated (Figure 3.2a,b).

Initial TCR signaling upon stimulation has been shown to result in immedi-

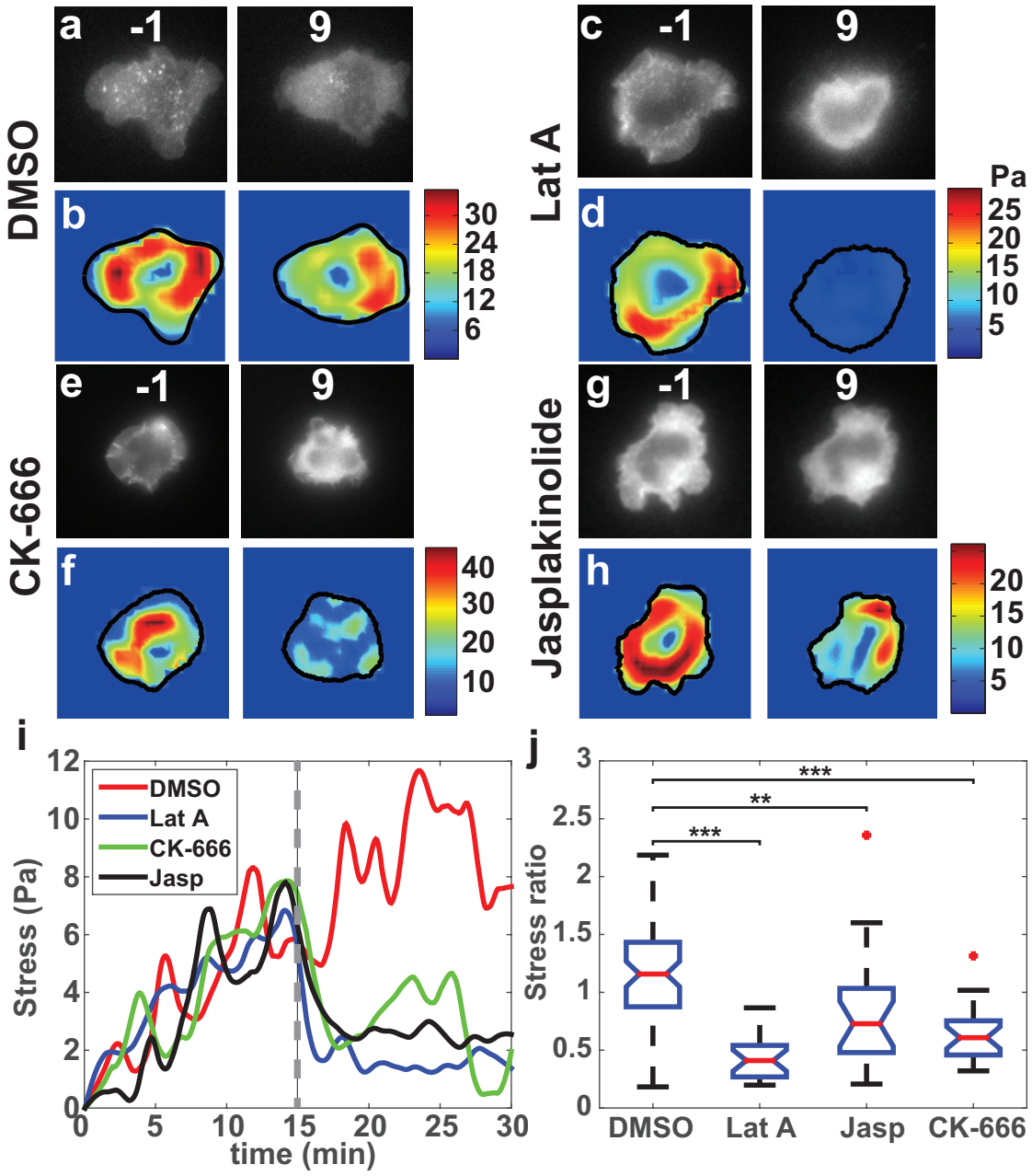


Figure 3.2: (Continued on next page).

Figure 3.2: **Loss of F-actin dynamics reduces cellular force generation.** Fluorescence images (top) and traction color maps (bottom) of EGFP-actin expressing Jurkat T-cells on elastic substrate 1 min before (left) and 9 min after (right) application of (a,b) 0.1 % DMSO, (c,d) 1 $\mu$M latrunculin-A, (e,f) 100 $\mu$M CK-666, and (g,h) 1 $\mu$M jasplakinolide. (i) Average stress as a function of time for a representative cell in each of the conditions described. The dashed line represents the time point at which the drug was added. (j) Comparison of the after-to-before ratios of traction stresses for application of Lat-A ($n = 22$), CK-666 ($n = 24$), and Jasp ($n = 20$) with control ($n = 64$). The average stresses in a 3-min time interval just before addition of drug and in the time interval 9-15 min after addition of drugs were used to compute the ratios. $^{**}p < 0.01$, $^{***}p < 0.001$.

ate recruitment of signaling proteins that subsequently lead to Arp2/3 activation [16, 24, 59, 117]. Inhibition of Arp2/3 activation by addition of CK-666, an inhibitor that locks the Arp2/3 complex in an inactive conformation [156], led to the retraction of lamellipodia and termination of edge dynamics (Figure 3.2e). This is in accordance with previous observation that the Arp2/3 complex is essential for maintaining lamellipodial structure [78]. Consistent with our expectations, addition of CK-666 led to a reduction in the traction forces, as seen from the before-and-after traction maps (Figure 3.2f).

Stabilization of F-actin upon addition of Jasp, which was reported to inhibit

actin retrograde flow in both T cells [8, 216] and neuronal growth cones [198], resulted in the reduction of traction forces in most cells, as shown in the traction maps before and after inhibitor addition (Figure 3.2h). However, the effect of Jasp was somewhat variable, with some cells showing little effect of Jasp on actin flow and edge dynamics. These cells typically did not show a decrease in traction.

Representative curves of the time evolution of average stress upon addition of inhibitors or control (DMSO carrier alone) are shown in Figure 3.2i. To characterize the change in stress upon inhibitor application for a population of cells, we quantified the ratio of mean stress after (between 9 and 15 min) and before (-3 to 0 min) application of drug for each cell. Lat-A treatment decreased the traction stresses by 65 % (stress ratio: $0.41 \pm 0.14$, $p = 9.7 \times 10^{-13}$), whereas CK-666 resulted in a 50 % decrease (stress ratio of $0.61 \pm 0.15$, $p = 1.3 \times 10^{-8}$), and Jasp treatment decrease stress by 40 % (ratio: $0.73 \pm 0.31$, $p = 0.0018$) (Figure 3.2j). All of these were significantly different from the control (stress ratio $1.2 \pm 0.3$).

To characterize the effects of these drugs on the actin cytoskeleton, we used the superior optical resolution of TIRF microscopy to observe the change in F-actin levels at the cell-substrate interface. We allowed the EGFP-actin Jurkat cells to be activated on anti-CD3 coated coverslips for 10 minutes, treated with drugs for 3 minutes, fixed the cells and stained with phalloidin. Jasp treatment resulted in cells that retracted from the coverslip, in accordance to previous reports [8, 216]. On the other hand, Lat A reduced f-actin level at the IS by 35 % (phalloidin intensity:

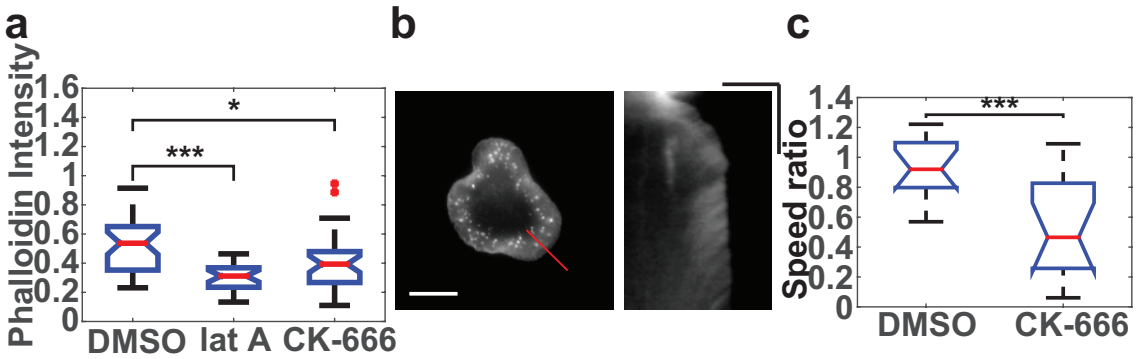


Figure 3.3: **Effects of actin inhibitors on f-actin level and retrograde flow.** (a) Phalloidin intensity of cells treated by actin inhibitors at 10 min after activation for 3 minutes. (b) Snapshot of an EGFP-actin cell spreading (left; scale bar, 10 $\mu$m), and a kymograph (right) drawn along the dashed line. The linear streaks illustrate actin retrograde flow in the cell periphery. Scale bar, 5 $\mu$m (horizontal), 5 min. (vertical). (c) Ratio of retrograde flow speed after to before drug treatment.

$0.42 \pm 0.09$, $p = 4.4 \times 10^{-5}$), and CK-666 reduced f-actin level by 16 % (phalloidin intensity: $0.55 \pm 0.15$, $p = 0.03$) (Figure 3.3a).

Previous studies on neurons established a connection between traction forces exerted by cells, cell stiffness, and internal cellular forces with the rate of actin retrograde flows in the cell lamellipodia [33, 15]. We therefore examined how lamellipodial actin flows in Jurkat T cells were affected by drug treatments, by conducting live cell imaging of EGFP-actin cells activated on glass, adding drugs at 10 minutes and imaged for further 10 minutes. We quantified the rate of actin flow using kymography of actin structures in the lamellipodia of spreaded cells (Figure 3.3b). Upon lat A application, the actin structure in most cells disappeared, forbidding tracking of retrograde flow (data not shown). Fortunately, retrograde flow was still observable after CK-666 treatment. By taking ratio between retrograde flow speed after to before drug treatment, we found that Arp2/3 inhibition significantly slowed down retrograde speed by 50 % compared with the control (Figure 3.3c). Our results indicate that actin polymerization, depolymerization and retrograde flow dynamics are important for the generation and maintenance of forces in activated Jurkat T-cells.

### 3.2.3 Role of NMII activity in force generation

The role of NMII in organizing the IS is controversial. [81]. It was suggested that NMII activity is required for central supramolecular activation cluster (cSMAC) formation [93], while later studies provided evidence contradicting this hypothesis [12, 118, 221]. As TFM provides direct measurement of forces generated by T cells during activation, we therefore investigated the role of NMII in force generation during T cell signaling activation.

We first examined the effect of blebbistatin, which inhibits NMII's ATPase activity, on traction force maintenance. Because blue light inhibits blebbistatin, we turned off the blue illumination just before adding 50 $\mu$M blebbistatin to spreading Jurkat cells and compared the traction stress, as shown in the before and after stress maps (Figure 3.4, a and b) for a representative cell. Qualitatively, we found that the cell edge continued to behave in a dynamic manner upon blebbistatin addition. We measured actin retrograde flow in the presence of blebbistatin using TagRFP-T-actin-labeled cells and found that the flow was largely intact, indicating that NMIIA does not play a significant role in maintaining actin flow in these cells (Figure 3.5a, $n = 11$, $p = 0.08$). We noted that the average stress ratio ($0.94 \pm 0.43$) was not significantly different from the control (stress ratio, $1.18 \pm 0.28$; $n = 66$, $p = 0.57$; Figure 3.4e). On the other hand, treatment with 100 $\mu$M Y-27632 decreased the stresses exerted, as shown in the stress maps (Figure 3.4, c and d). The cell contact area did not decrease upon drug application, and actin lamellipodial structures were

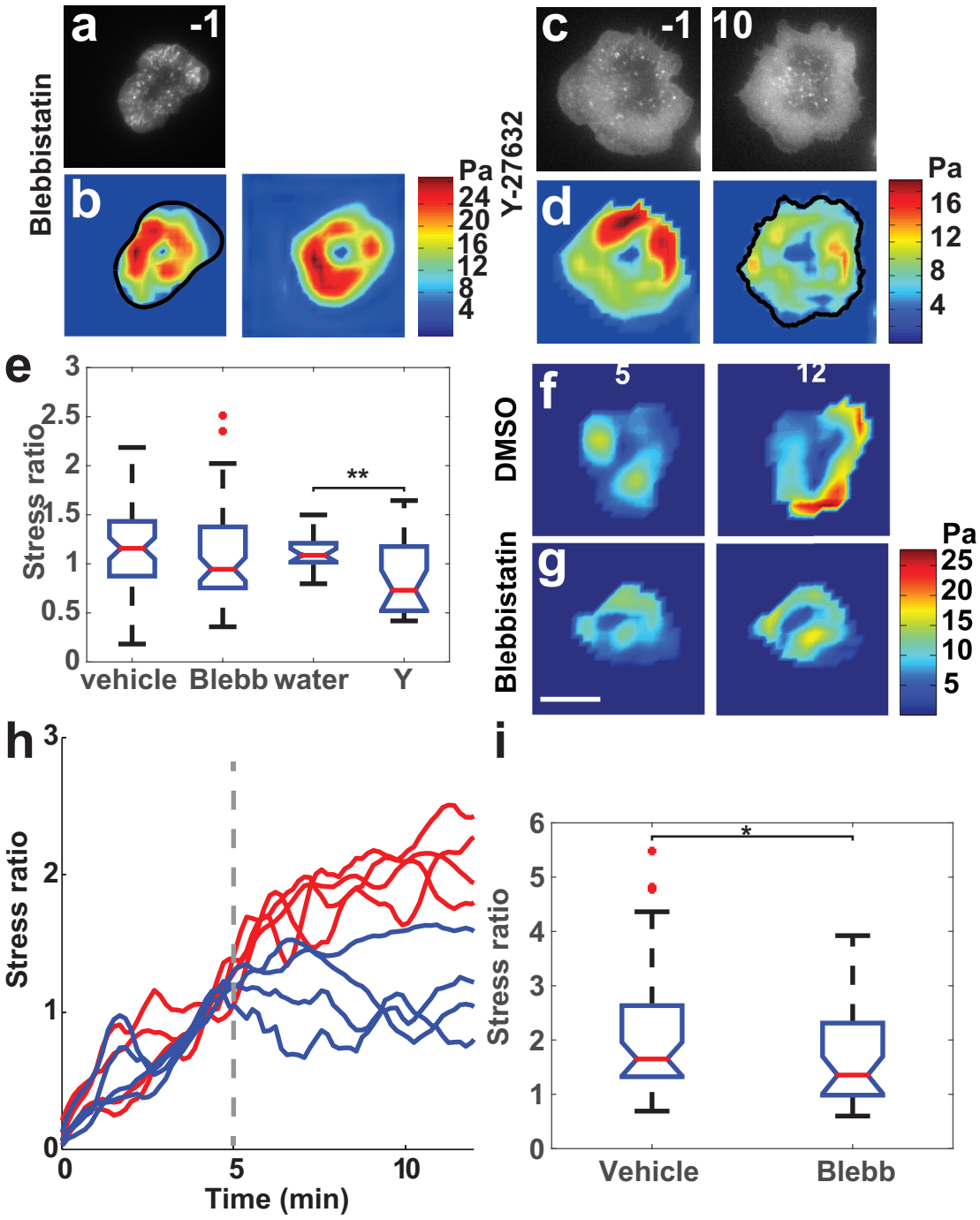


Figure 3.4: **Effect of NMII activity on cellular force generation.** (Continued on next page)

Figure 3.4: (a,c) Fluorescence image and (b,d) Traction stress color map of EGFP-actin Jurkat T-cell on an elastic substrate 1 min before (left) and 9 min. after (right) addition of (a,b) 50 $\mu$M blebbistatin (c,d) 100 $\mu$M Y-27632.(e) After-to-before ratios of traction stresses upon addition of blebbistatin ($N = 66$ cells), control (DMSO carrier), Y-27632 ($N = 25$ cells) and water control ($N = 20$ cells). $^{**}p < 0.01$. (f, g) Traction stress color maps for example cells which f: DMSO and g: Blebb was added at 5 min after stimulation. (h) Traces of the stress ratio exerted by four example cells with drug addition 5 min after stimulation (vertical dashed line). Red lines indicate vehicle, and blue lines indicate blebbistatin addition. (i) Summary statistics of the stress ratio after drug addition for cells averaged between 9 and 12 min after stimulation. $N = 37$ for blebbistatin and $N = 44$ for DMSO (* $p$ <0.05, Wilcoxons rank sum test). Scale bars, 10 $\mu$m.

maintained even after the addition of Y-27632 (Figure 3.4, c and d). The summary data show a 33 % decrease in stresses (stress ratio, $0.73 \pm 0.44$) as compared with the water control ($1.09 \pm 0.12$; $p = 0.004$; Figure 3.4e).

Because myosin II contraction affects conjugate formation [93] and T-cell activation in the early stages [221], it is possible that NMII is required for the initial generation of forces but not at later stages. To test this, we applied blebbistatin 5 min after the initiation of spreading and examined the effect on the exerted forces. We found that whereas the stress exerted by the cell continued to increase until

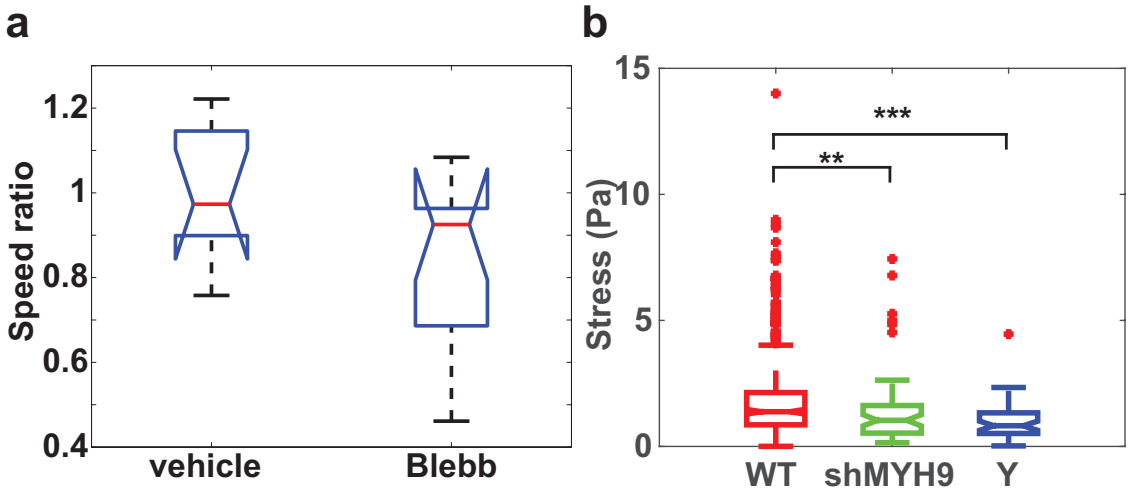


Figure 3.5: **NMII contributes to stress generation by Jurkat T cells, but not through modulating retrograde flow.** (a) Blebbistatin application to E6-1 TagRFP-T-actin cells did not modulate retrograde flow speed. (b) Average stress exerted by cells between 14-15 min on substrate with $E < 1$ kPa. shMYH9: NMII knockdown cells; Y: 100 $\mu$M Y-27632.

saturation upon vehicle application (Figure 3.4f), the total force exerted by the cell plateaued near the value at 5 min or decreased slightly upon blebbistatin application. However, blebbistatin did not abolish the forces (Figure 3.4, g and h), and a few cells continued to show increase in traction. Summary data of the stress ratios after and before treatment show that blebbistatin-treated cells have a significantly lower stress ratio than DMSO (carrier)-treated cells ($n = 37$, $p = 0.04$). This confirms that myosin II is required for the initial phase of force generation but is not involved at later time points (Figure 3.4i).

To further examine the role of NMIIA in force generation, we knocked down NMIIA expression in these EGFP-actin expressing Jurkat cells by RNA interference against NMIIA [162]. The resultant cell line, labelled shMYH9 in Figure 3.5a, had 50 % knockdown of NMIIA (data not shown). These cells exert 25 % less stresses than wildtype cells (Figure 3.5, WT: $1.38 \pm 0.75$ Pa, $n = 486$; shMYH9: $1.04 \pm 0.59$ Pa, $n = 59$; $p = 0.0026$). Alternatively, we allowed the EGFP-actin expressing cells to spread in the presence of 100 $\mu$M Y-27632 [196], which inhibits NMII contractility in these cells [8]. Cells were able to spread and exerted traction forces, but with a 40 % reduction (Figure 3.5b, Y: $0.82 \pm 0.51$ Pa, $n = 49$, $p = 1.2 \times 10^{-6}$). Therefore, we conclude that NMII activities contribute to stress generation in Jurkat T cells at IS.

### 3.2.4 Effect of substrate stiffness on cellular forces, morphology, and signaling

Many types of cells that interact with soft materials have the ability to sense the stiffness of their mechanical environment and respond to it by exerting larger forces on stiffer substrates [101]. Whether Jurkat cells respond similarly to substrate stiffness is not known. Recent experiments suggest that physical forces, such as those generated by the actin cytoskeleton, may be important for T cell signaling [111, 132]. To examine whether Jurkat cells are sensitive to substrate stiffness, we fabricated polyacrylamide gels with varying concentrations of cross-linker to change

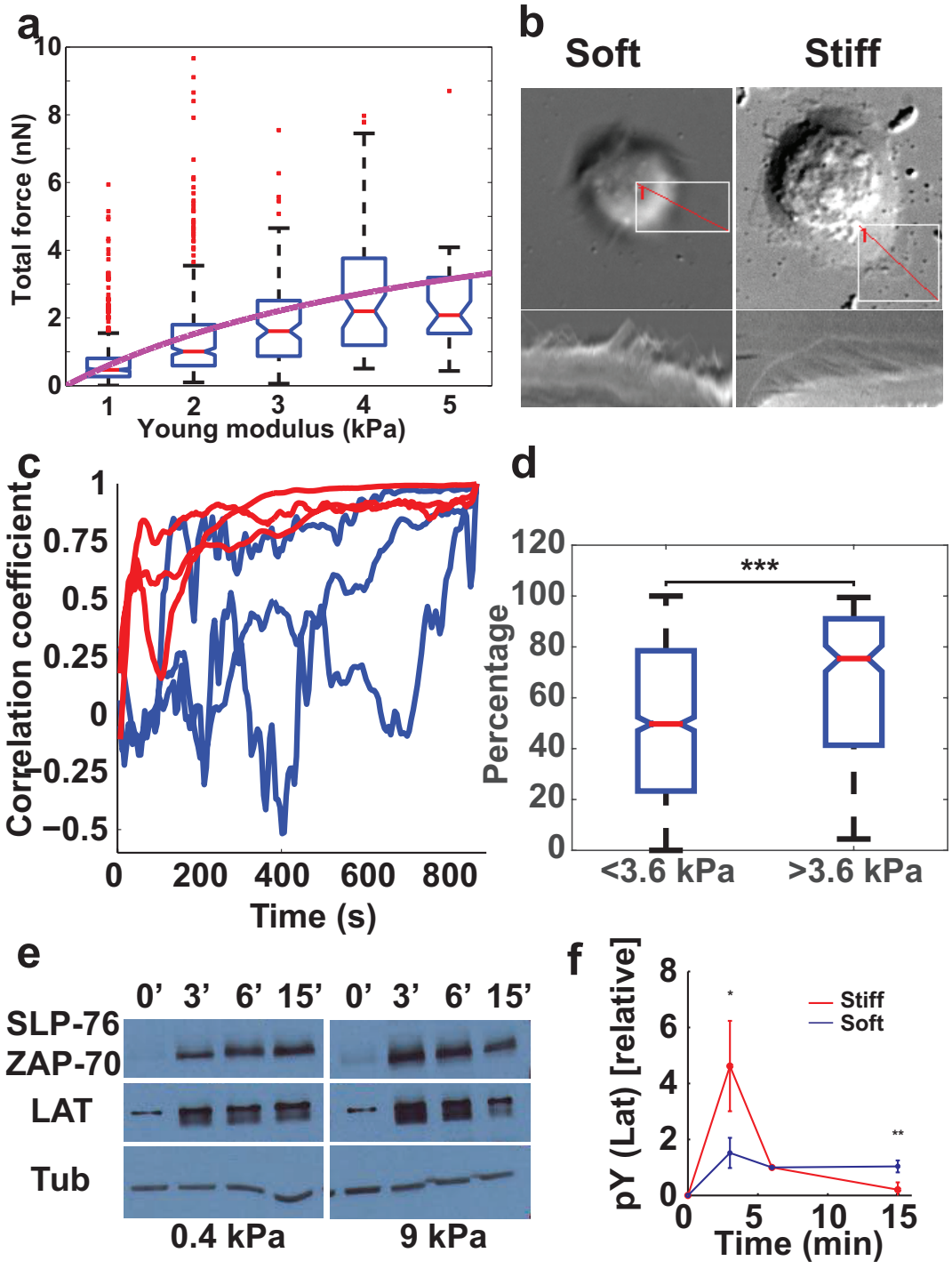


Figure 3.6: (Continued on next page)

Figure 3.6: **Substrate stiffness affects traction forces and signaling.** (a) Total force exerted by cells as a function of gel stiffness. The data are fit to a sigmoidal curve (Eq. 3.1). (b) Top, DIC images of two representative cells spreading on soft (200 Pa) and stiff (10 kPa) gels. Bottom: kymographs of edge dynamics along the red lines. (c) Example time traces of Pearson coefficient between cell edge's radial position profile at 15 min and at earlier time points for cells spreading on soft ($< 3.6$ kPa, blue) and stiff ($> 3.6$ kPa, red) gels. (d) Comparison of the percentage of time for which the cell edge profile had correlation coefficient $> 0.5$ compared with the profile at 15 min for soft and stiff gels. (e) Western blot of pY levels of LAT and ZAP-70 at the indicated times on two different gel stiffnesses (0.4 and 9 kPa). (f) Densitometry analysis of relative pY levels. Analysis represents average of five different experiments.

the elastic modulus of the gels. We used gels that ranged in stiffness from 200 Pa to 5 kPa embedded with beads and imaged for traction force measurements as before. For comparison of forces between gels of different stiffness, we calculated the average traction stress exerted by stably spread cells between 14 and 15 minutes after spreading initiation. We found that the average stress exerted by cells increased for soft substrates and rapidly saturated for stiffer substrates, as shown in Figure 3.6a. Similar results were obtained for earlier time points (unpublished data). Our observations suggest that Jurkat T-cells have the ability to sense the substrate stiffness and modulate the internally generated cytoskeletal forces as a function of substrate

stiffness. We fit our stress-stiffness data to a sigmoidal function from active matter theory (Figure 3.6a, [138]):

$$F_{eq} = F_{sat}\frac{k_{ext}}{k_{ext} + k_C} \tag{3.1}$$

Here $F_{eq}$ is the traction force at equilibrium, $F_{sat}$ is the saturation force, $k_{ext}$ is the stiffness of the external environment, and $k_C$ is the cytoskeletal stiffness of the cell. $k_C$ also represents a characteristic stiffness scale of which $k_{ext} > k_C$ represents stiff regime and otherwise. Fitting results gave $F_{sat}$ of 6.7 nN and $k_C$ of 3.6 kPa. It suggested an operational definition in which gels with stiffness $< 3.6$ kPa could be denoted as soft and gels of higher stiffness as stiff.

We then examined whether cell morphology and edge dynamics showed distinct behaviors depending on gel stiffness. We found that cells were more dynamic, with cell edges displaying extensive protrusions and retractions and cell shape remodeling on soft gels. On stiff gels, cells typically spread out smoothly, with the cell edge advancing in a more isotropic manner. Furthermore, cell edge dynamics continued for a much longer period of time on softer gels, whereas on stiffer gels, cell edges either remained stably spread with minimal edge dynamics or retracted. This is illustrated in Figure 3.6b with kymographs drawn radially across the cell for representative cells on soft (left) and stiff (right) gels. We quantified the dynamics of cell morphology by comparing the radial distance profile (from the cell center around the cell edge as tracked from EGFP-actin images) at 15 min with that at each earlier time point. We calculated the Pearson correlation coefficient of these

two profiles as the cell edge evolved in time. Representative time courses of the correlation coefficient for cells spreading on soft ($< 3.6$ kPa, blue) and stiff ($> 3.6$ kPa, red) gels are shown in Figure 3.6c. On stiff gels, the correlation coefficient was small initially, indicating considerable edge dynamics, but approached 1 as the cell periphery remained stable and persistent. However, on soft gels, the correlation coefficient remained low throughout, indicating ongoing edge dynamics during the movie. To quantify the population response to substrate stiffness, we calculated the percentage of time, $P(t)$, that the correlation coefficient was $> 0.5$, that is, with a shape similar to that at 15 min (Figure 3.6d). We found that cells on soft gels were significantly more dynamic, with low $P(t)$ (Mann-Whitney U-test, $p < 0.001$) compared with those on stiff gels. These observations demonstrate that cell morphologies are more dynamic on soft substrates.

Recent work has shown that primary T-cells show enhanced signaling on stiff elastic substrates compared with softer ones [102]. However, the softest substrates used in that study (10 kPa) were much stiffer than the stiffest ones used in our force measurements (8 kPa), while typical APC stiffness is $< 1$ kPa. We confirmed that Jurkat T-cells showed phosphotyrosine (pY) signaling on the anti-CD3 coated gels of different stiffnesses used in our study and not on poly-l-lysine coated gels (Figure 3.7). We next examined whether the differences in observed forces and morphology at varying gel stiffness were associated with differences in signaling activation. As it is difficult to sample signaling on a continuous range of substrate stiffnesses, we chose two specific stiffness values ($\approx 0.4$ and $\approx 9$ kPa) as representative soft and stiff

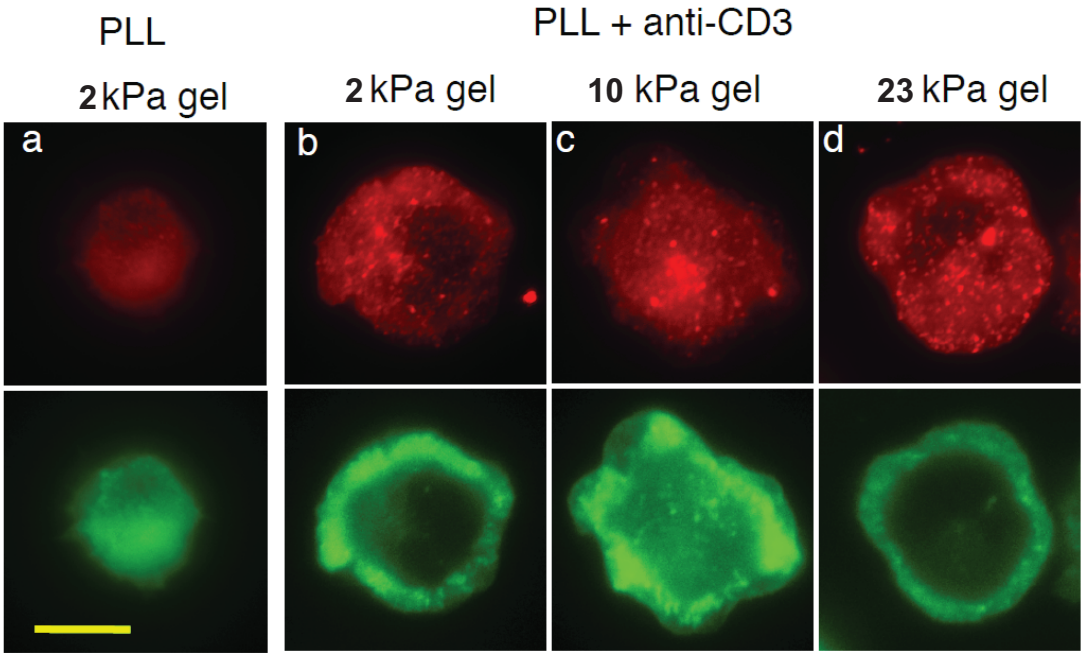


Figure 3.7: (a) Widefield images of EGFP-actin labeled Jurkat cell spreading on an poly-L-lysine coated glass surface with phosphotyrosine staining (top) and actin fluorescence image (bottom). (b-d) Widefield images of EGFP actin cells spreading on anti-CD3 coated substrates of indicated stiffness. Gel compositions were (3:0.1, 5:0.1 and 10:0.1 of acrylamide:BIS). All scale bars are 10 $\mu$m.

substrates, respectively. We allowed the cells to spread on gels for specific times (3, 6, and 15 min) before lysing them *in situ* and used the cell lysates for SDS-PAGE analysis. Western blotting for phosphotyrosine (pY) residues was used to analyze the relative pY levels at various time points on gels of different stiffnesses. Figure 3.6e shows the results of a representative SDS-PAGE analysis for soft and stiff gels. As seen from the bands of pY labeling, signaling is activated in cells spreading on both types of gels and appears to peak within 3 min of contact formation. However, for stiff gels, pY levels decrease after 6 min, whereas for soft gels, the pY levels appear to persist for a longer time (as the band appears more intense even at later time points). To quantify the development of signaling, we calculated the relative pY levels for the 35- to 40-kDa band, likely corresponding to phosphorylated LAT, for soft and stiff gels. We found that pY levels peaked at 3 min on stiff gels and rapidly declined, whereas on softer gels, the levels were lower but sustained even at 15 min after stimulation (Figure 3.6f). We observed the same trend for bands corresponding to ZAP70/SLP76. Our results suggest that the temporal evolution of early signaling in Jurkat T-cells is sensitive to substrate stiffness and soft substrates support signal maintenance.

## 3.3 Discussion

Mechanical forces have been implicated to play a role in TCR signaling and activation. Here we measured the traction stresses generated by Jurkat T-cells and transmitted through TCRs to the contacting surface. We find that T-cells are soft

and weak force generators exerting average stresses on the order of 0-13 Pa during activation by anti-CD3 coated elastic substrates. The stresses are distributed peripherally around the contact zone. The forces increased as the cell spread upon stimulation and are maintained for at least 15 minutes. Moreover, these forces are specifically generated in response to CD3 stimulation similar to human primary $CD4^+$ cells [11]. Overall, the forces are of lower magnitude than those associated with integrins in adherent cells [194].

Previous studies have established that actin cytoskeletal dynamics is essential for TCR signaling and activation [8]. We found that an intact and dynamic F-actin cytoskeleton was essential for the exertion of traction stresses by Jurkat T-cells. As expected, inhibition of actin polymerization with Lat-A substantially decreased the forces generated. Stabilization of F-actin by Jasp consistently led to a reduction in forces in cells in which actin flows and edge dynamics were inhibited upon Jasp treatment. We also found that the Arp2/3 complex was required for force maintenance, suggesting that the biochemical pathway that leads to Arp2/3 activation and actin polymerization [77] might also link activated TCR to the actin cytoskeleton physically [16]. We further found that actin flow speeds were reduced by the inhibition of CK-666 (Figure 3.3c). It is not clear whether the stress relaxation effects of CK-666 are due to disruption of the physical link between TCR and actin, modulation of retrograde flow speed or combination of both.

Myosin II-driven contraction of actomyosin networks is the major contributor

to actin retrograde flow in neuronal growth cones and filopodia [142, 198] and contributes 90% of the traction stress exerted by mouse embryonic fibroblasts, most likely related their contractions on actin to form stress fibers [27]. In contrast, the role of myosin II in TCR signaling and IS formation has not been unequivocally established [81]. The primary form of myosin II present in T-cells is myosin IIA, with a very small fraction of myosin IIB [98, 93]. We find that suppression of NMII ATPase activity by blebbistatin did not affect the maintenance of traction forces in cells that were already spread (Figure 3.4a). In contrast, inhibition of Rho-kinase by Y-27632 modestly decreased the forces (Figure 3.4c). We suspect this is because the mechanism of action of these two commonly used drugs are different, in which blebbistatin is known to weaken NMII-actin binding while Y-27632 promotes NMII light chain dephosphorylation. More in-depth study to distinguish between these two aspects of NMII activities will be the subject of future research.

On the other hand, application of blebbistatin during the early phase of spreading retarded further development of tractions (Figure 3.4g). This agrees with further experiments in which we directly measured traction stress generated by cells under depletion of NMIIA or Rho kinase inhibtion (Figure 3.5b), and found that both reduced the cell's stress. Therefore, we establish that NMII activity is essential to the buildup of traction forces during IS formation.

We found that Jurkat T cells exert larger forces on substrates of increased stiffness (in the stiffness range of 200 Pa to 6 kPa), indicating that they are able to

sense the substrate rigidity over this large range and modulate their force generation accordingly. This appears to be in contrast to a recent study on human primary $CD4^+$ cells spreading on anti-CD3 coated micropillar arrays [11], which did not show any change in traction force per pillar as a function of pillar stiffness. However, our results are consistent with a previous study using biomembrane force probe, which showed that T cells engage anti-CD3 coated beads and pull with loading rates that increased with probe stiffness [91].

Many cell types, including fibroblasts, neutrophils, and neurons, have been shown to be mechanosensitive, being able to exert increasing force on substrates of greater stiffnesses [134, 33, 159]. The characteristic stiffness scale of 3.6 kPa derived from active matter theory (Figure 3.6a, [138]) is substantially higher than measured stiffness of Jurkat T cells [21, 169]. We think that could be due to stiffening of cell cortex after actin polymerization induced by TCR triggering [23], as cell stiffness of the T cell IS is never measured in the literature.

Mouse primary T-cells have been found to respond to the mechanical stiffness of substrates, with increased interleukin-2 production and enhanced tyrosine phosphorylation on stiffer polyacrylamide gels [102]. However, the stiffness range explored in those studies was considerably higher (10-200 kPa), and traction forces were not measured. In vivo, T-cells spread on APCs that are soft (in the stiffness range of a few hundred pascals to 1 kPa; [21]), suggesting that our observations of enhanced dynamics of the cell edge on soft gels may be physiologically relevant to

T-cell function.

The repeated edge dynamics may result from repeated bursts of actin polymerization leading to multiple leading edges and formation of fresh signaling clusters at the nascent cell periphery. In contrast, on stiff substrates, the cell-edge expansion is smoother, without repeated protrusions. Previous studies have shown that the continuous recycling of signaling intermediates (tyrosine kinases and substrates) is essential for maintaining levels of pY after cell spreading [124, 28, 199]. Thus it is likely that the continued cell-edge dynamics of cells on softer substrates may mediate the sustained signaling observed on these substrates.

Hydrostatic pressure interacts with actomyosin contractions to determine the cell shape and the cellular forces during cell blebbing [34] and mitosis [185]. A recent study measured the intracellular hydrostatic pressure in lamellipodia and lobopodia during cell migration and found values of 300 Pa and 2200 Pa respectively [165]. This is comparable in magnitude to stress generated by the cell on a 2D [126] or 3D matrix [127]. Although intracellular pressure of T cell during formation of IS is unknown, we expect that it would be of the same order of magnitude as the stress generated by the cell, and that varying the osmotic pressure can change the stress level significantly. Whether osmotic pressure takes part in mechanosensing, for example, Jurkat T cells activated on soft and stiff substrates might have different osmotic pressures, is still an open question.

The molecular mechanisms that underlie mechanosensing remain a topic of intense study [150]. A number of studies suggest that integrins may serve as putative mechanosensors [4, 116]. We find that Jurkat cells exhibit mechanosensitivity even without integrin engagement, suggesting that these mechanisms may be quite general. Jurkat cells also lack CasL (a p130Cas homologue), a protein implicated in mechanosensitivity [104, 177, 221, 118]. In conclusion, our studies show that mechanosensitivity may be a general feature of T cells. Our results place constraints on the forces that these cells are able to generate and thereby apply on TCR-ligand linkages to potentially initiate signaling.

# Chapter 4

# Microtubule dynamics at T cell contact regulates stress maintenance through Rho-ROCK-myosin II pathway

# Abstract

T cell receptor (TCR) triggering and subsequent T cell activation are essential for adaptive immune response. Application of mechanical forces to the TCR has been shown to induce signaling events, and conversely, T cell generates and maintains traction forces on the cognate antigen presenting cell during activation. Although actin dynamics have been shown to be essential for force generation, the molecular mechanism regulating these dynamics remain poorly understood. Here, we report traction forces generated by Jurkat T cell to be regulated by microtubule dynamics through Rho activities and nonmuscle myosin II (NMII) light chain phosphorylation at the T cell-substrate interface. These results underscore crosstalk between actin and microtubule cytoskeletal dynamics at the contact and their role in regulating cellular mechanosensing during T cell activation.

## 4.1 Introduction

As a central player in the adaptive immune response, T lymphocytes are activated when T cell receptors (TCRs) on their surface recognize cognate peptide-major histocompatibility complex (pMHC) expressed on surface of antigen-presenting cells (APCs) [95]. A burst of actin polymerization is triggered upon TCR stimulation [23] and T cell spreads over surface of the APC [78], forming a molecular architecture known as the immunological synapse (IS) [148, 79]. This is accompanied by activation of the well-studied TCR signaling pathway [173, 218]. Apart from the actin cytoskeleton, of equal importance is the rapid polarization of the microtubule cytoskeleton that facilitates directional secretion of cytokines and cytolytic factors towards the APC [186, 78, 215, 90].

Since the proposal of the receptor deformation hypothesis [136], there has been keen interest in the role of physical forces during T cell activation, owing to novel techniques to analyze forces T cell experiences and exerts, from molecular scale of single TCRs [111, 131, 132, 46] to cellular scale of the whole T cell [91, 161, 102, 11, 87]. It is now established that T cells are mechanosensitive to substrate stiffness and are able to generate significant traction stresses, albeit relatively weak compared with adherent cells [71]. Actin polymerization/depolymerization dynamics are essential for T cells to maintain dynamic traction stresses, calcium signaling and integrin affinity maturation [87, 8, 38]. However, as the actin cytoskeleton is known to be regulated by multiple factors and molecular pathways,

and forms distinct structures in different zones of the IS [8, 216], it remains challenging to dissect the relative contributions to stresses by individual pathways.

Apart from the well studied phenomenon of microtubule organizing center (MTOC) translocation during IS formation [186, 140, 215], vigorous microtubule dynamics at IS was demonstrated in T cell-APC conjugates by live cell microscopy recently [139, 167]. Interestingly, the microtubule-Rho pathway was shown to regulate T cell migratory polarity [191], and Rho kinase inhibition led to rapid stress relaxation in anti-CD3 stimulated Jurkat T cells [87]. Whether these pathways crosstalk with the actin cytoskeleton and take part in mechanosensing by T cells is poorly understood.

In this report, we propose a molecular mechanism of how traction stresses are generated and maintained at the T cell-substrate interface. Using traction force microscopy (TFM) and quantitative fluorescence imaging, we show that microtubule dynamics at the contact acts as a signaling module that may regulate contractility during activation of both Jurkat cells and human primary $CD4^+$ T cells. Contractility is regulated by bipolar filament assembly of myosin II at the interface, providing a source of traction forces in addition to that from the better understood actin flow.

## 4.2 Results

### 4.2.1 Microtubule network forms a radially emanating dynamic array

In order to visualize the microtubule and actin networks clearly and to reveal the locations of microtubule plus-tips, we permeabilized Jurkat cells after 10 minutes of anti-CD3 stimulation, fixed and stained for tubulin and f-actin [142, 115]. Extraction by 0.1 % Triton-X-100 removed cytosolic proteins efficiently (Figure 4.1a), and the MTOC was preserved and manifested as a focal point from which microtubules emanated. As reported before [216, 8], the f-actin network is organized into distinct zones of lamellipodia (asterisk), actin-arc rich lamella (yellow arrow) and sparse inner actin network (red arrow) (Figure 4.1a). From the overlay, we locate most microtubule plus-tips to be at lamella, where they colocalized with the actin arcs (cyan arrow). This organization of actin and microtubule networks agrees with a recent microscopy study of cytotoxic T cell-APC conjugates [167] and is reminiscent of that in neuronal growth cone [178] and the leading edge of a migrating cell [176], except that the IS is relatively radially symmetric [58].

To characterize microtubule dynamics in live cell, we first established a E6-1 Jurkat cell line of EGFP-actin transfected with retroviruses carrying TagRFP-T-tubulin, and conducted dual color imaging in total internal reflection fluorescence (TIRF) mode. Upon stimulation by surface-bound anti-CD3, the MTOC ap-

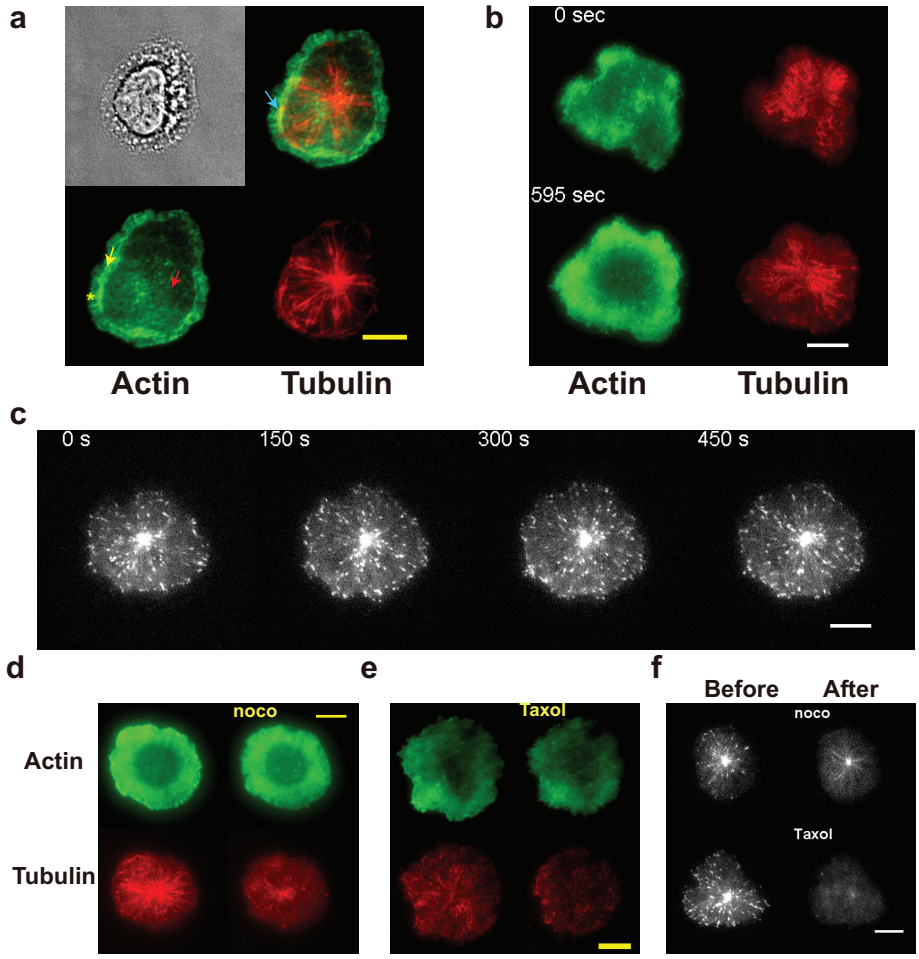


Figure 4.1: **Microtubule dynamics in Jurkat cells upon activation.** (a) E6-1 cell fixed and permeabilized at 10 minutes and stained for tubulin (red) and F-actin (green). (b) E6-1 EGFP-actin TagRFP-T-tubulin cell spreading on anti-CD3$\epsilon$ coated coverslip. Live cell snapshots at 0 and 10 minutes were shown. (c) Montage of E6-1 cells transfected with EB3-tdTomato activated by anti-CD3. (d) and (e) Snapshots of actin (top) and tubulin (bottom) before (left) and 10 minutes after (right) (c) 100 nM nocodazole and (d) 0.5 $\mu$M Taxol application. (f) EB3-tdTomato before (left) and after (right) inhibitor application. Scalebar = 10 $\mu$m.

peared within 1-2 minutes after the cell started spreading, and vigorous microtubule polymerization/depolymerization activities were maintained for at least 10 minutes (Figure 4.1b, Supplemental video 1). We also transfected Jurkat cells with EB3-tdTomato to observe growing plus tips of microtubules. As expected, the MTOC appears as a common starting point of EB3 comets, and we confirmed that the movements of these comets are mostly radially outward, while some comets were observed to travel tangentially at the periphery (Figure 4.1c and Supplemental video 2).

We then proceeded to observe the effects of microtubule-specific drugs on the dynamics of the microtubule array by adding drugs at 10 minutes after cell contact with the coverslip. To avoid disrupting microtubule network structure and to only target on polymerization/depolymerization dynamics, we used a low dose of 100 nM nocodazole for inhibition of microtubule polymerization or 500 nM Taxol for inhibiting microtubule depolymerization, as characterized in [215]. As shown in Figure 4.1d, e and Supplemental video 3 and 4, low doses of nocodazole and Taxol both lead to decreased fluorescence intensity of microtubules suggesting a decreased number of microtubules, while having minimal effects on actin network structure or cell morphology. In addition, both nocodazole and Taxol treatments led to disappearance of EB3 comets, confirming their inhibition of microtubule growth (Figure 4.1f and supplemental video 5).

### 4.2.2 Microtubule dynamics regulate traction stress through Rho activity

To characterize the effect of mcirotubule dynamics inhibition on traction force maintenance, we carried out TFM and observed changes in traction stresses after drug treatment as described before [87]. We observed increases in traction stress upon stabilization of microtubules, as shown in Figure 4.2a (Stress ratio $= 1.42 \pm 0.63$, $n = 20$, $p = 0.0001$ for nocodazole; Stress ratio $= 1.34 \pm 0.32$, $n = 34$, $p = 0.04$ for Taxol).

It was shown before that microtubule dynamics can regulate Rho guanine nucleotide exchange factor (RhoGEF) localization [143] and modulate T cell migration and cytokinesis [191, 67]. We hypothesized the stress enhancement by microtubule dynamics inhibition might be caused by upregulation of Rho activity, which then regulates contractility at the periphery as we found previously that Rho kinase inhibition reduced traction stresses in Jurkat T cells ([87], Figure 4.5f). Therefore, we used the Rho kinase inhibitor Y-27632 together with nocodazole to dissect how microtubule dynamics regulates traction stress in Jurkat cells.

If inhibiting microtubule dynamics enhances contractility through activation of Rho, simultaneous application of Y-27632 and nocodazole would negate stress strengthening effect by nocodazole alone. Consistent with our hypothesis, coapplication of Y-27632 and nocodazole resulted in decrease in stress (Figure 4.2b, stress

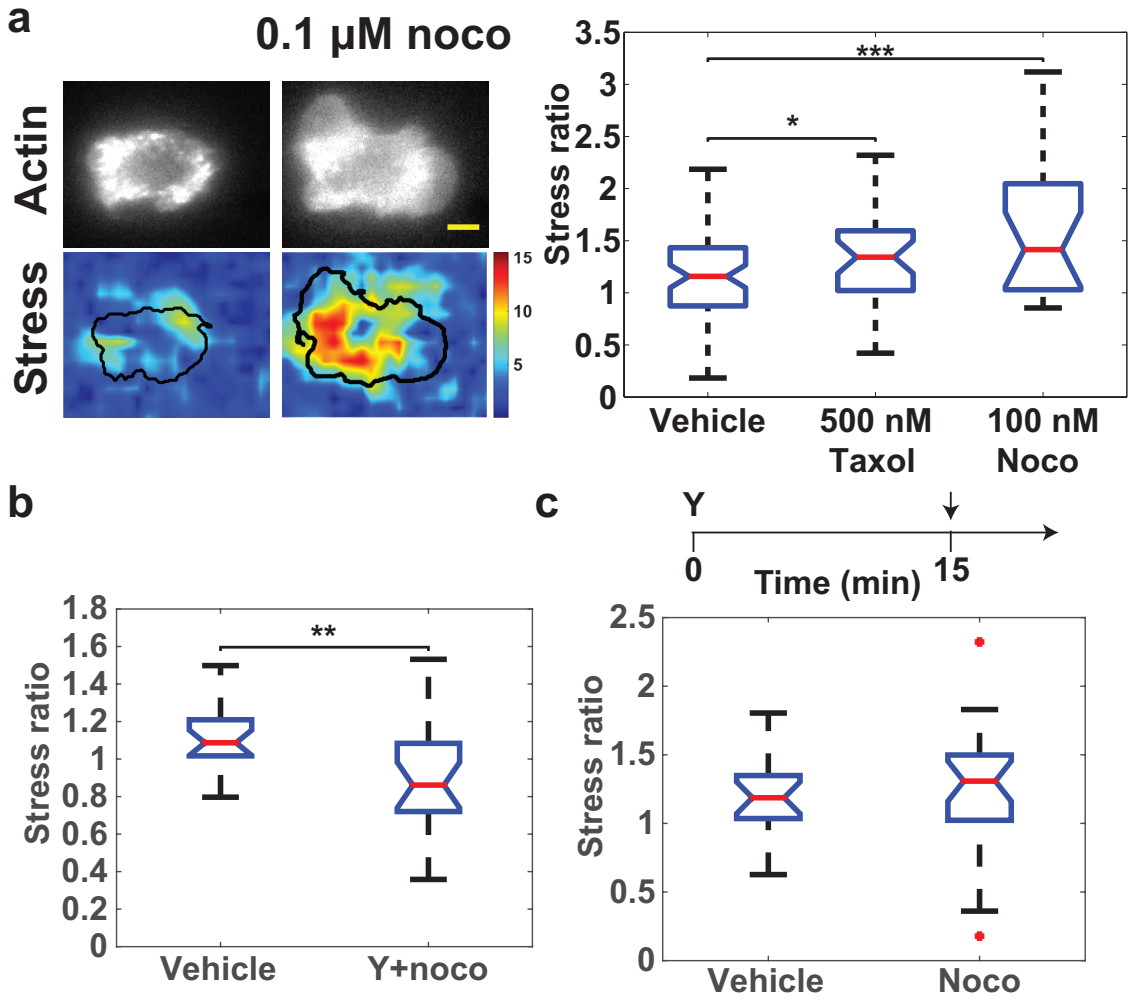


Figure 4.2: **Effects of microtubule inhibitors on traction stress.** (a) Stabilization of microtubule network by 0.1 $\mu$M nocodazole and 0.5 $\mu$M Taxol both led to increase in traction stress. (b) Rho kinase inhibition negated the stress strengthening effect of nocodazole. (c) Stress ratios of vehicle vs. nocodazole treatments at 15 min after Jurkat cell spreading in the presence of 100 $\mu$M Y-27632.

ratio $0.86 \pm 0.22$, $p = 0.003$). In order to rule out the possibility that microtubule dynamics and Rho signaling operate independently but have opposite effects on traction stresses instead of a upstream-downstream relation, we incubated Jurkat cells in 100 $\mu$M Y-27632 for 15 min, activated on elastic substrate in the presence of Y-27632, and then applied nocodazole for 15 min. This allowed us to examine if microtubule stabilization increases traction stress in the absence of Rho activity. We found that for cells already treated with Y-27632, the addition of nocodazole had no effect on the traction stresses (Figure 4.2c, nocodazole stress ratio $1.31 \pm 0.29$; vehicle stress ratio $1.19 \pm 0.17$, $n = 26$, $p = 0.58$). This suggests that the increase in stress observed in the presence of nocodazole is mediated by Rho activity downstream of microtubule dynamics.

### 4.2.3 Rho activation regulates traction maintenance through myosin II

Y-27632 inhibits Rho kinase, whose activation leads to NMII light chain phosphorylation through inhibition of myosin phosphatase [112, 204]. Therefore we used calyculin A (CA), a serine/threonine protein phosphatase inhibitor that inhibits myosin phosphatase activity and enhances NMII light chain phosphorylation [96, 204], to ask whether Rho signaling regulates stress through NMII light chain phosphorylation and bipolar filament assembly [201].

We found that the concentration of CA used in previous literature [224, 214]

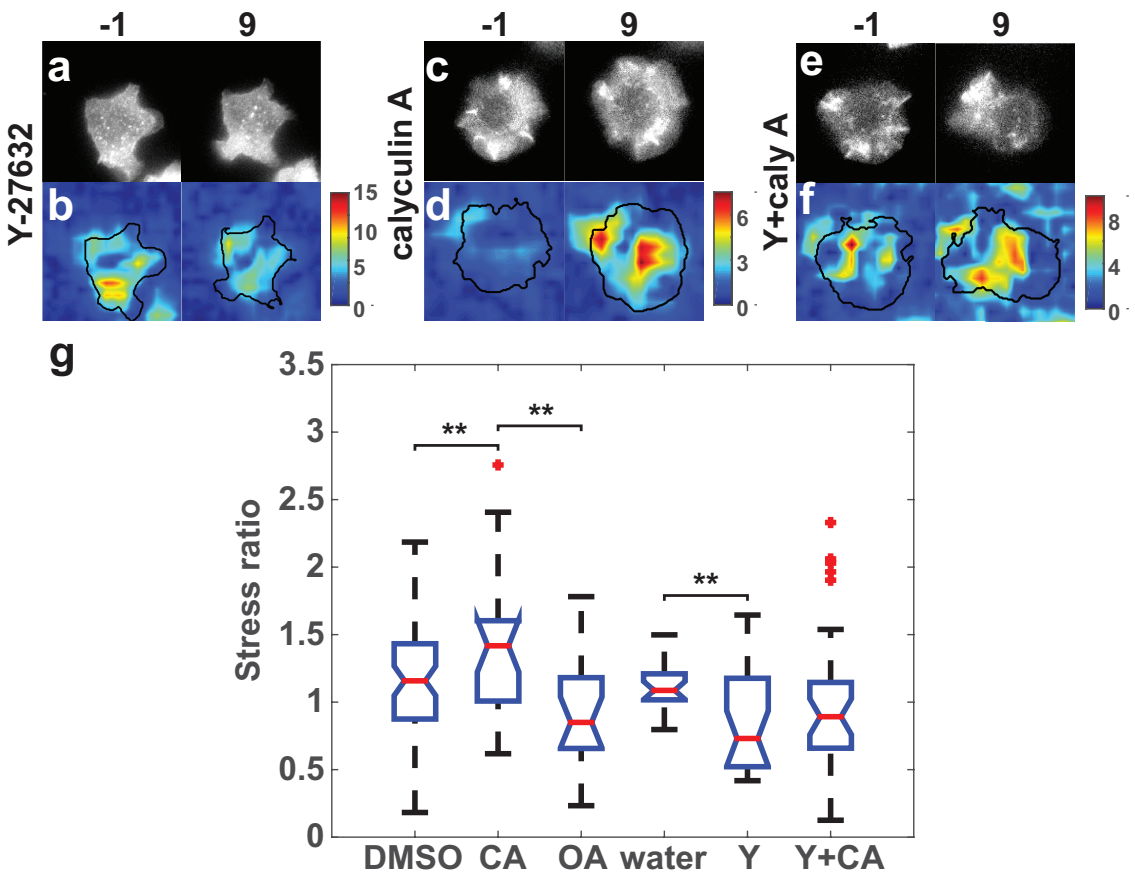


Figure 4.3: **Dissecting the role of myosin II in stress maintenance.** (a-f) (a,c,e) EGFP-actin and (b,d,f) stress exerted by the cell before (top) and after (after) application of (a,b) 100 $\mu$M Y-27632 (Y), (c,d) 5 nM calyculin A (CA) and (e,f) 100 $\mu$M Y-27632 and 5 nM calyculin A (Y+CA) at 15 min. Stress in Pa. (g) Stress ratio of Jurkat cells after application of different myosin II inhibitors at 15 min. DMSO and okadaic acid (OA) are negative controls of CA, and water is negative control of Y and Y+CA.

(20 nM) was too high for the Jurkat cell system, and caused rapid cell retraction from the substrate, drastic rise in traction stress, and cortical oscillations (data not shown). We therefore used a lower dose of 5 nM, which did not cause retraction from substrate within the 15 minute imaging time window for most cells (Figure 4.3c-f). At this dose, CA treatment significantly increased traction stresses after 15 mins (stress ratio = $1.33 \pm 0.39$, $p = 0.037$). As CA inhibits both type 1 and type 2A protein phosphatases, we used okadaic acid (OA), at concentration that preferentially inhibits type 2A phosphatase (20 nM) as a negative control [96]. CA treatment also showed significantly higher stress ratio compared with OA (stress ratio = $0.85 \pm 0.33$, $p = 0.007$). Therefore, we infer that the effect of CA is most likely due to its inhibition of myosin phosphatase [224, 214].

As myosin phosphatase activity lies downstream of Rho activities, we asked if inhibiton of myosin phosphatase can revert the stress relaxation effects of Rho kinase inhibition. We used coapplication of CA and Y-27632 and compare with Y-27632 alone. As shown in Figure 4.3e and f, presence of CA reversed the effect of Y-27632 (Stress ratio = $0.96 \pm 0.52$, $n = 25$, $p = 0.41$). Unfortunately we were not able to address whether myosin phosphatase is strictly downstream of Rho, as CA incubation had a drastic effect on cortical actin structure and inhibited spreading altogether even at a mild dose. Overall, our data suggest positive correlation between NMII light chain phosphorylation and traction stress maintenance in Jurkat cells.

### 4.2.4 Myosin II is recruited during contact formation

The role of NMII in organizing the IS is controversial in the literature [81]. Recent studies show that NMII is dispensable for inward transport of TCR microclusters and formation of IS [98, 221, 12, 216], but TFM data suggest that NMII contributes to traction force build up but not its maintenance [87]. Moreover, NMII ATPase and Rho kinase inhibition experiments showed blebbistatin treatment did not change while Y-27632 treatment decreased the traction force maintenance in Jurkat cells ([87] and Figure 4.3g). This calls for visualization of NMII dynamics and quantification of NMII localization and activation level during T cell spreading.

We cloned and transfected TagRFP-T labelled regulatory light chain (*MYL12B*) into EGFP-actin expressing Jurkat cells. Imaging of these dual-transfected cells indicated that NMII undergoes retrograde flow that spans the lamella region (Figure 4.4a and Supplemental Video 6), as was previously described [8, 216]. More importantly, we observed that NMII is recruited subsequent to initial actin polymerization and cell spreading [23, 120]. To quantify this, we measured actin and light chain TIRF intensity inside the contact as a function of time, as shown in Figure 4.4b. We calculated the ratio between average intensities at 9-10 minutes and 1-2 minutes as the "protein recruitment index" to quantify the level of protein recruitment. Comparison of protein recruitment indices of 13 cells indicated that during cell spreading, the total actin content at the interface remained constant despite vigorous polymerization/depolymerization dynamics (index $= 1.0 \pm 0.2$), but NMII

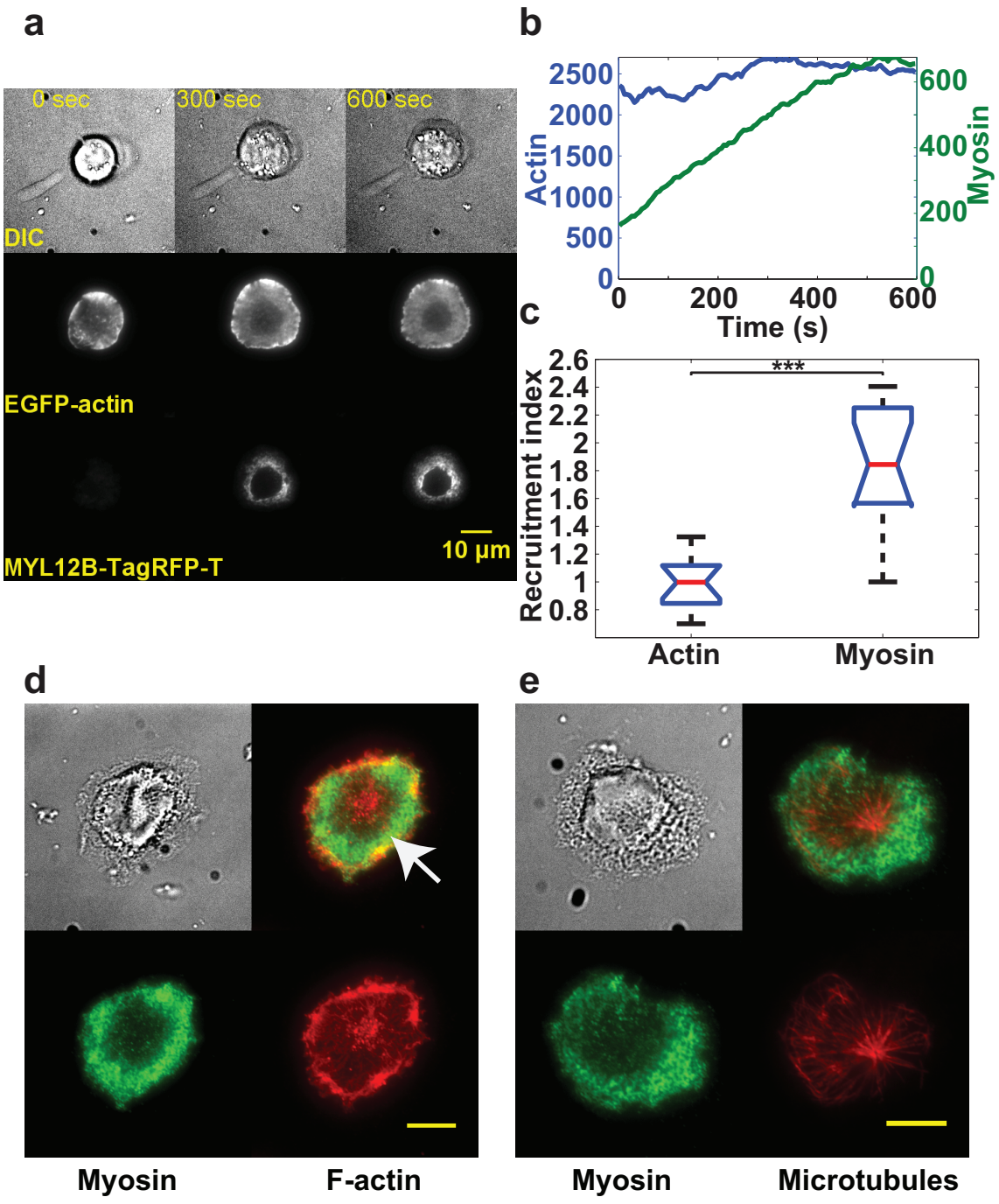


Figure 4.4: **Myosin II dynamics during T cell spreading.** (a) Tracking of intensities of EGFP-actin (blue) and MYL12B-TagRFP-T (green) in cell shown in Figure 4.4a in the first 10 minutes. (b) Myosin II showed significantly higher protein recruitment index than actin. Protein recruitment index is defined to be the ratio of average TIRF intensity between 9-10 minutes to that of 1-2 minutes. (c,d) Immunofluorescence images of Jurkat cells permeabilized and then fixed at 10

is actively recruited into the synapse (Figure 4.4c, index $= 1.8 \pm 0.4$, $p = 6.4 \times 10^{-6}$).

We then used fixation after permeabilization as described before (Figure 4.1b) to visualize actin-bound NMII with F-actin and microtubules respectively. We permeabilized the cells at 10 min after activation for immunostaining, when NMII recruitment has mostly saturated (Figure 4.4b). We found that NMII localizes to the lamella ring behind the cell edge and within actin-sparse central region (arrow in Figure 4.4d). Overlay with microtubules shows that the lamella form a 'cage' to confine the plus-tips of microtubules (Figure 4.4e).

### 4.2.5 Microtubule dynamics and Rho signaling regulate myosin II light chain phosphorylation

We investigated how the small molecules Y-27632 and nocodazole used in force maintenance experiments influence NMII localization and light chain phosphorylation [201]. Jurkat cells were allowed to be activated for 10 minutes, treated with drugs for 10 minutes, permeabilized and fixed (Figure S1a). Quantification of the level of bound NMIIs in the TIRF plane reveals that both nocodazole (NMII intensity: $0.81 \pm 0.17$, $p = 0.0038$) and Y-27632 ($0.82 \pm 0.22$, $p = 1.6 \times 10^{-4}$) treatments increases NMII binding at the interface by 14 % (vehicle: $0.71 \pm 0.18$, Figure S1b,c). To confirm the physiological relevance of this finding, we repeated the experiment with purified human $CD4^+$ T cells and proceeded with the same procedure. As shown in Figure S1e,f, nocodazole (NMII intensity: $1.1 \pm 0.4$, $p = 1.4 \times 10^{-9}$) and

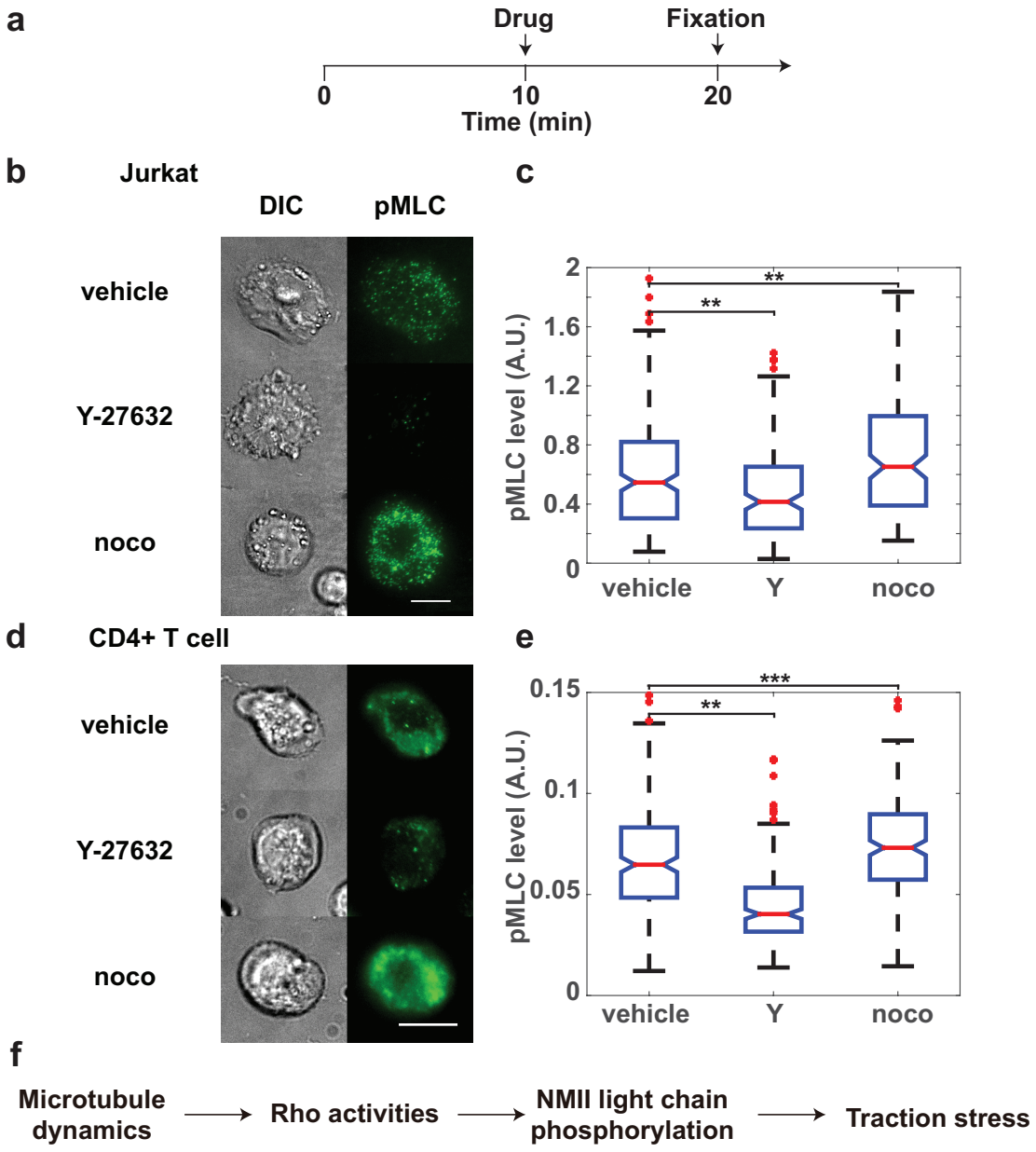


Figure 4.5: **Traction stress maintenance correlates with myosin light chain phosphorylation.** (a) Scheme of experiment. Cells (Jurkat/CD4$^+$) were activated on anti-CD3 and treated with inhibitors for 10 min and fixed. (b,d) Bright Field DIC and pMLC (green) of (b) Jurkats and (d) human CD4$^+$ T cells. (c,e) Quantification of pMLC immunofluorescence intensity of (c) Jurkats and (e) CD4$^+$ human T cells. (f) Working model of microtubule regulated traction force maintenance at T cell contact. Scalebar, 10 $\mu$m.

Y-27632 ($1.1 \pm 0.3$, $p = 3.9 \times 10^{-4}$) both increased bound NMII compared with vehicle ($0.96 \pm 0.24$), with similar percentage increases as in Jurkats. Therefore the opposite effects of Rho kinase and microtubule dynamics inhibitions on stress maintenance cannot be explained by modulation of NMII-actin binding.

We next compared the level of monophosphorylated myosin light chain at serine 19 (pMLC) at contact after different treatments, followed by conventional fixation procedures (Figure 4.5a). For Jurkat cells, Y-27632 treatment reduced pMLC level by 24 % (vehicle: $0.55 \pm 0.27$; Y-27632: $0.42 \pm 0.24$, $p = 0.0038$), while nocodazole treatment resulted in significant 20 % increase in pMLC level ($0.65 \pm 0.34$, $p = 0.0036$, Figure 4.5b,c). We obtained similar results for primary $CD4^+$ cells, in which Y-27632 treatment reduced pMLC level by 40 % (vehicle: $0.065 \pm 0.019$; Y-27632: $0.040 \pm 0.013$, $p = 8 \times 10^{-19}$) and nocodazole treatment resulted in significant 12 % increase in pMLC level ($0.073 \pm 0.016$, $p = 0.0011$, Figure 4.5d,e).

To conclude, the traction stress maintained by T cells at contact is positively correlated with the pMLC level, which is then regulated by microtubule dynamics and Rho activities at the interface (Figure 4.5f), adding a stress-regulatory role to the microtubule network apart from the well known function of secretory granules delivery [186, 167].

## 4.3 Discussion

Physical forces have been observed to take part in multiple cell biological processes [97]. In the context of IS formation, it is not surprising that T cells generate significant traction stresses at contact plane [91, 11, 87], which involves extensive reorganization of surface molecules [148, 79]. In this study, we demonstrated a molecular pathway which originates from microtubule polymerization-depolymerization activities in lamella (Figure 4.1), regulating Rho activities (Figure 4.2), which then regulates myosin light chain phosphorylation and formation of bipolar filaments which correlate with cellular contractility and force generation (Figure 4.3 and 4.5, [201]).

MTOC translocation has been studied extensively [186, 140, 215, 167] and is a hallmark feature of the early phase of T cell activation [16, 90]. The microtubule cytoskeleton is dynamic after translocation to the IS ([139] and Figure 4.1a). The finding that nocodazole and to a lesser extent, Taxol increased traction stress hints that microtubule dynamics serves as a signaling module that regulates stress maintenance. As microtubule dynamics is known to regulate Rho activities through segregation of RhoGEF [209, 143, 144] and Rho kinase inhibition led to decrease in traction stresses in Jurkat cells [87], the microtubule-Rho-NMII pathway is an attractive candidate for the stress maintenance mechanism, adding to their reported role in directing T cell migration polarity [191]. Experiments of nocodazole added to cells already inhibited in Rho kinase and simultaneously with Rho kinase inhi-

bition suggest that microtubule dynamics is an upstream negative regulator of Rho activities, consistent with the role of this pathway in specifying division plane during cytokinesis [67, 63].

The poorly defined role of NMII in maintaining traction prompted us to investigate NMII dynamics directly through live cell imaging. Interestingly, we found that NMII is recruited from the cell body during IS formation rather than being remodelled like actin, a phenomenon underappreciated in the literature. The recruitment took 5-10 minutes in Jurkat cells, and has the same time scale as traction development [11, 87]. This suggests that two different processes involving NMII occur during IS formation, namely, recruitment of NMII and NMII-mediated contractility. In the T cell literature, most studies used either genetic knockdown [93, 12, 118] and/or small molecules [93, 12, 221, 8, 216] to perturb NMII functions. Knockdown experiments reduce the amount of NMII available to be recruited to the interface, while small molecules inhibit NMII acitivities before and when the cell is activated on a stimulatory substrate, therefore might affect both processes differentially. This could be one of the factors that gave rise to inconsistencies between different reports [81].

Immunofluorescence data showed that traction stress maintained by T cells does not correlate with the amount of tightly bound NMII, but correlates with the pMLC level. It is known in the literature that light chain phosphorylation at threonine 18 and serine 19 promotes bipolar filament assembly and ATPase activities

*in vitro* [43, 105], and regulation of the phosphorylation/dephosphorylation cycles maintains tissue integrity during gastrulation [200] and defines the myosin activation zone during cytokinesis [67]. In the latter example, dynamics of astral microtubules and their interaction with the cell cortex operate upstream of Rho and MLC phosphorylation. Our study suggests T cell might use the same mechanism to activate NMII locally at the contact and to generate forces to the TCRs during contact with APC.

Adding to results from our previous report [87], we suggest that Jurkat T cells have two mechanisms to generate and maintain traction stress: firstly, actin polymerization/depolymerization dynamics that generate retrograde flow of f-actin [103, 220]; secondly, phosphorylation of myosin light chain that correlates with cellular contractility [8, 216, 200]. We propose actin dynamics to be the dominant driving force, as T cells can still reorganize and form IS when NMII is knocked down [118] or conditionally knockout [12]. By promoting bipolar filament assembly, light chain phosphorylation increases alignment of actin arcs in the lamella [142, 25, 216], contributing a significant fraction of the stress. Both mechanisms are likely to be physiologically relevant as the effects of Rho kinase and microtubule inhibitions on localization and phosphorylation are observed in both Jurkat and primary human cells.

Unfortunately, spatiotemporal dynamics of the molecular events depicted in Figure 4.5f remains elusive: are Rho activities inhibited during microtubule polymer-

ization or depolymerization? Do NMII-rich zones at the contact represent regions of high Rho activities? Do regions of strong traction stress colocalize with light chain phosphorylation and appearance of new TCR microclusters? To answer these questions, multicolor live cell imaging of EB1 comets [139], RhoA biosensors [163] and tension fluorescent probes [225, 151] will provide a more complete picture of crosstalk between cytoskeletal, signaling and force dynamics at the IS.

## 4.4 Supplementary materials

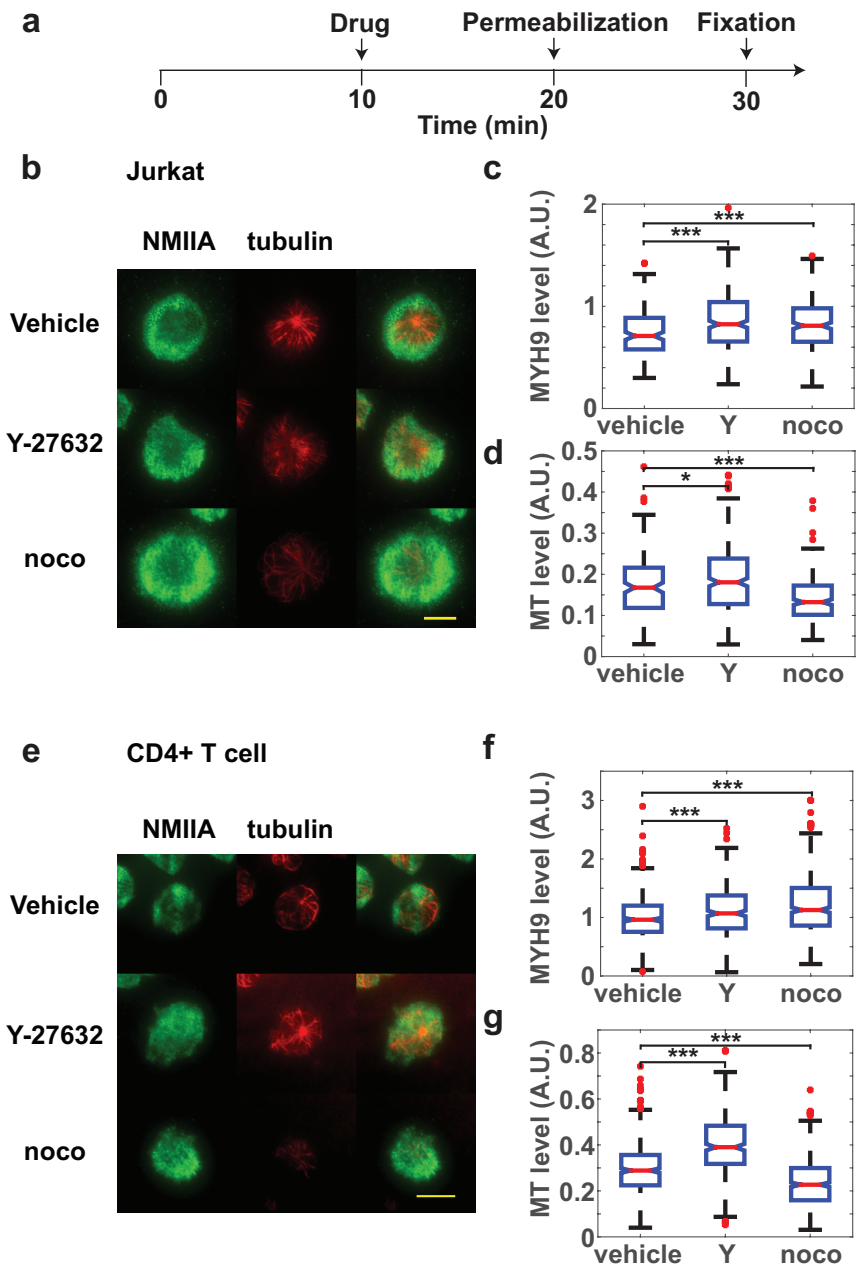


Figure S1: **Traction maintenance does not correlate with level of actin-bound NMII** (a) Scheme of experiment. Cells (Jurkat/CD4$^+$) were activated for 10 mins, treated with inhibitors for 10 mins, permeabilized and fixed. (b,e) Immunofluorescence of NMIIA (green) and tubulin (red) of (b) Jurkats and (e) human CD4$^+$ T cells permeabilized and fixed as shown in (a). (c,d,f,g) Quantification of (c,f) NMII and (d,g) tubulin levels of (c,d) Jurkats and (f,g) CD4$^+$ human T cells. Scalebar: 10 $\mu$m.

# Chapter 5

# Conclusions and Future Directions

## 5.1 Conclusions

T cells, with their specific but wide repertoire of antigen recognition capabilities, are key players in our adaptive immune system. Their roles of carrying out immunosurveillance and mounting immune response upon infection suggest that they routinely contact various tissue cells with significantly different physical properties. In this thesis, we focused on elasticity of the environment as a physical cue that T cells sense and respond to during activation. In chapter 2, we characerized the morphological, membrane and cytoskeletal dynamics during Jurkat T cell spreading on rigid glass substrates. We found the kinetics of contact area expansion follows a universal curve and inclusion of factors that favor membrane undulations gave rise to coupled actin-membrane waves. In chapter 3, we used traction force microscopy to measure the forces generated by Jurkat T cells during activation on elastic substrates, and confirmed that they are weak force generators like the

neuronal growth cone. We found that actin dynamics is essential for generation and maintenance of these forces, while myosin II activity only contributes to build up of the forces but not their maintenance. Importantly, we found that Jurkat T cells sense substrate rigidity by generating more forces on stiffer substrates, while displaying more protrusion/retraction actiivities and more sustained TCR proximal signaling on soft substrates. In chapter 4, we found that the microtubule polymerization/depolymerization dynamics at the T cell-substrate interface regulates traction force maintenance. This was achieved through regulation of Rho activities which promote myosin light chain phosphorylation. Finally in appendix A, we measured calcium influx by Jurkat T cells and found that it varies biphasically with substrate stiffness. The calcium signal was found to decrease and became less sustained as the stiffness approaches 'signaling minimum' around Young's modulus of 5 kPa. In addition, Rho kinase inhibition disrupted both the force generation apparatus and the calcium-stress relation, resulting in significant changes in the calcium-stiffness relation, thereby highlighting the Rho-ROCK pathway as an essential modulator of mechanosensitivity in Jurkat T cells.

The cytoskeletal forces we measured are comparable to that used *in vitro* to trigger the TCR complex and signaling [111, 132]. Combined with the measured relations between stress and stiffness, as well as between calcium influx and stress, these interfacial forces take part in mechanosensing that convert physical signal of stiffness of the opposing substrate into a biochemical signal. As these forces originate from the T cell cytoskeleton rather than an external source and are developed

over time of contact, they might be essential for the T cell to maintain its signaling in *in vivo* immunological synapse.

Different tissues are characterized by varying stiffness. It is unknown whether stiffness could act as a marker of tissue identity in the T cell immune response. Our finding that Jurkat T cells' signaling response being sensitive to substrate stiffness provides a clue that primary T cell might also use stiffness as an input parameter to determine outcome of an immune response, to stay tolerant or to proliferate. This is also important for T cell cancer therapy design, as cancer cells are known to possess significantly different stiffness from healthy tissues [41].

## 5.2 Future directions

### 5.2.1 Primary T cells

Throughout the dissertation, we used the Jurkat E6-1 cell line to carry out imaging experiment with the exception of the immunostaining experiment of primary $CD4^+$ T cells in chapter 4. It is highly desirable to investigate mechanosensitivity in primary T cells for two reasons: firstly, primary T cells are not cancerous, therefore they presumably reflect T cells in the most 'natural' setting. This is particularly important for investigation of cellular signaling, proliferation and gene expression, as pathways regulating these processes are often perturbed in cancer cells. Secondly, different lineages of primary T cells can be effectively sorted

through fluorescence-activated cell sorting (FACS). The sorted pure population of helper, cytotoxic and regulatory T cells allows the exciting possibility to investigate mechanosensing in these different subtypes of T cells.

As preliminary work, we obtained primary $CD4^+$ human T cells transfected with LifeAct-EGFP from our collaborator and conducted TFM of these cells activated on anti-CD3 elastic substrates. We found that similar to Jurkat T cells, they exert significant traction stress during spreading (Figure 5.1a) and is comparable to that of EGFP-actin expressing Jurkat cells.

### 5.2.2 pMHC for activation

We used anti-CD3$\epsilon$ to activate Jurkat T cells throughout the thesis, as the specific antigen Jurkat cells recognize is unknown. Anti-CD3 stimulation might not be the most physiologically relevant way to investigate forces through TCR complex, as forces bypass the $\alpha\beta$TCR and acted through CD3 molecules, hence disallowing study of force transmission through the V$\alpha$ and V$\beta$ domains to the extracellular domain of CD3, which is of keen interest in the mechanical force model of TCR triggering.

Another popular, and more physiological TCR ligand used in the literature is the superantigens conjugated to MHC molecules [174], which allows formation of IS-containing T cell-B cell conjugate without use of any specific peptides [78].

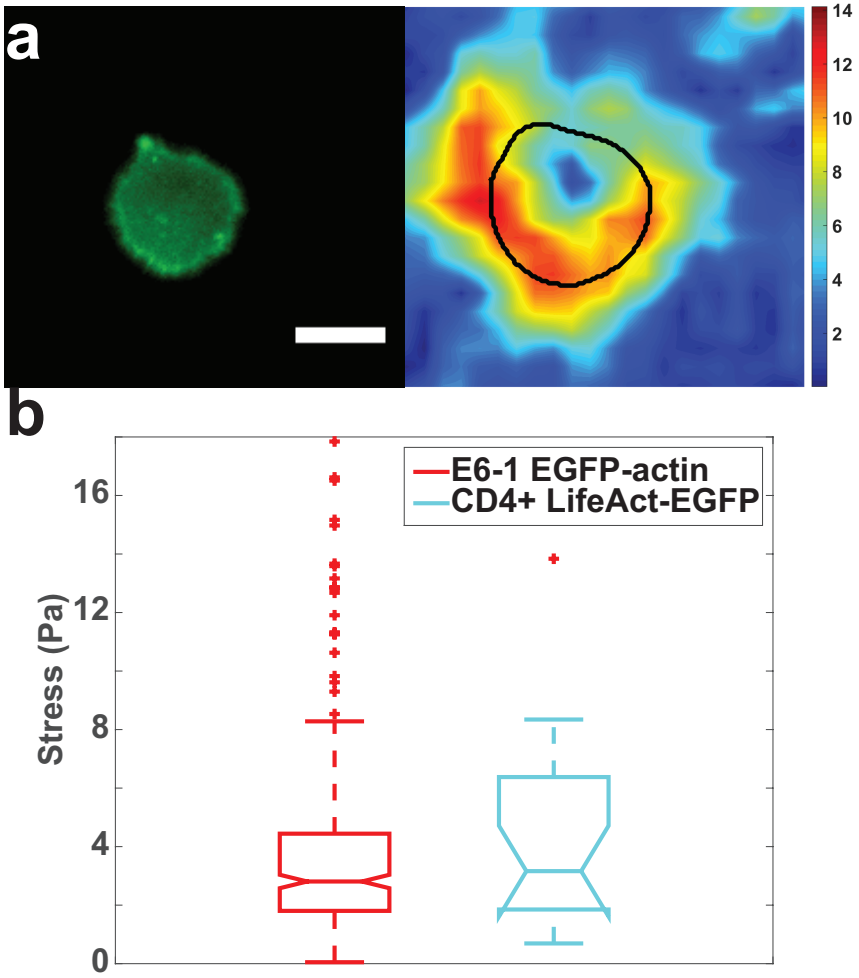


Figure 5.1: **Traction force microscopy of primary human T cells.** (a) Life-Act-EGFP (left) and traction stress map of a $CD4^+$ human T cell activated on a 1 kPa elastic substrate for 15 min. Scale bar: 10 $\mu$m.(b) Comparison of traction stress exerted by $CD4^+$ LifeAct-EGFP primary cells (blue) and EGFP-actin Jurkat cells (red).

The most sophisticated, but natural setting would be the use of mouse T cells from transgenic mice that express TCRs with known peptide antigencity. By activating them on elastic substrates coated with the corresponding pMHC molecules, we can test whether the mechanosensitivity we observed in this dissertation also applies to the TCR-pMHC bond.

Use of pMHC is highly desirable as the TCR-pMHC bond is much weaker than the bond between TCR and its antibody [132]. Recent literature has demonstrated that transgenic mouse T cells are able to generate significant forces on pMHC coated micropillars [11], therefore our system should be easily extensible to measure forces and calcium influx by these transgenic TCR mouse cells.

### 5.2.3 Physiological relevance of membrane undulations and actin waves

The membrane undulations and actin waves we observed in chapter 2 in the presence of FBS are mostly due to weakened cell adhesion to substrate, as we reported that Very Late Antigen-4 (VLA-4, $\alpha_4\beta_1$ integrin) ligation suppressed the undulations [119]. Although live cell imaging of smoothness of T cell-APC interface is beyound the resolution provided by light microscopy, electron micrograph of T cell-APC conjugate often reveals that to be rough [78]. Therefore, it is interesting to investigate how markers of proximal signaling, for example, phosphorylation of ZAP-70, Lck, LAT and SLP-76 etc. and calcium influx are affected by the presence

of FBS as a function of time of cell-substrate contact.

### 5.2.4 Mechanisms of stress generation

In the thesis, we investigated the role of the cytoskeleton, specifically, actin, microtubules and myosin II in regulating traction stresses generated by Jurkat T cell. Our results indicate the most traction stresses are due to actin dynamics, but how different molecular pathways contributed to regulate actin dynamics is still poorly undertstood. We have focused on the small GTPase Rho and Rho kinase pathway that regulates myosin II light chain phosphorylation, but the other small GTPases like Rac1 and Cdc42 can potentially take part in stress regulation as well.

Another interesting direction is to understand whether signaling microclusters take part in mechanosensing. Microclusters, similar to focal adhesions, are multimeric protein complexes where proetein-protein interactions and signal transduction take place [218]. While their nanoarchitecture and dynamics are begun to be revaled by superresolution microscopy [182, 208], to what portion their components being mechanosensitive is unknown. One prominent example is CasL, a homologue of the mechanosensitive protein p130Cas. Myosin IIA knockdown mouse T cells activated by pMHC and intercellular adhesion molecule 1 (ICAM-1) showed significant reduction of phosphorylation of CasL [118].

To dissect the molecular pathways leading to stress generation, it is necessary

to conduct live cell multicolor imaging to detect and distinguish events spatiotemporally [167]. Recent advance of force biosensors that allow simultaneous TIRF imaging of forces and fluorescently tagged proteins [151] opens up the possibility to image actin retrograde flow, EB1 comets, myosin accumulations, microcluster formation etc. together with force patterns, and would greatly speed up the analysis of spatiotemporal dynamics between the phenomenon of interest and forces, as this technique is not limited by availability of fluorescent markers in the vicinity of the cell.

### 5.2.5 Rho modulated mechanosensitivity and calcium-force relation

In appendix A, we showed that Rho kinase inhibition led to significant reduction of calcium influx by Jurkat T cells activated on soft gels. In addition, cells treated with Y-27632 on soft gels have calcium influx profiles similar to control cells activated on stiff gels. It appears that the mechanical (stiffness) and chemical (Rho activity) signals are integrated by the cell that determine the calcium signal. However, it was shown before and confirmed in our hands (data not shown) that Y-27632 treatment has no effect on calcium influx by Jurkat T cells activated on coverslip. To explain the apparent paradox, we hypothesize that Rho kinase inhibition disrupts mechanosensing apparatus of the cell, and possibly softens the cell so that the opposing substrate appears to be stiffer than it really is. Glass substrate is therefore rigid to both control and Y-27632 treated cells, thus results in no change in

calcium influx. This hypothesis would require more data collection of calcium influx of Y-27632 treated cells at the higher stiffness to confirm, as it would predict the 'signaling minimum' stiffness range observed in control cells (around 5 kPa) would also exist in Rho kinase inhibited cells and would be shifted to a lower stiffness.

# Appendices

# Appendix A

# Mechanosensing and signaling during Jurkat T cell activation

# Abstract

T cells, with their role of carrying out immunosurveillance, are routinely exposed to tissues cells with different stiffnesses. Whether and how substrate rigidity regulate T cell signaling remains little known. In this study we carried out calcium imaging of Jurkat T cells activated on elastic substrates with stiffness ranging from 100 Pa to 100,000 Pa, covering the whole range of tissue stiffness including that of professional antigen presenting cells. We discovered a 'signaling minimum' stiffness around 5 kPa and characterized how Rho-ROCK associated contractility modulate mechanosensitivity of these cells. Our results suggest physical force as an essential mediator that connects stiffness sensing to intracellular signaling, which directs gene expression and subsequent immune response.

## A.1 Introduction

Calcium ion ($Ca^{2+}$) acts as an universal second messenger in virtually all eukaryotic cells [65, 2]. Studies have shown that intracellular $Ca^{2+}$ level elevation being an integral part of the T cell receptor (TCR) activation response [89, 111, 132]. The resting T cell cytosolic concentration has been measured to be around 100 nM, but can be elevated to 1 $\mu$M upon TCR stimulation [94, 65]. T cells are extremely sensitive to TCR-peptide-major histocompatibility complex (pMHC) binding such that a single cognate pMHC can trigger calcium influx [95]. Moreover, $Ca^{2+}$ influx upon TCR triggering was recently shown to be correlated with physical forces applied to T cell [111, 132, 46].

At the single cell level, $Ca^{2+}$ influx in T cells is heterogeneous [1, 211, 175]. Primary T cells exhibit $Ca^{2+}$ level oscillations upon stimulation by phytohaemagglutinin (PHA) [83], anti-CD3 crosslinking [36] or antigen presentation by antigen presentating cells (APCs) [1, 211, 175]. These oscillations might enhance signaling efficiency at low stimulation levels [53, 130], as different transcription factors require different $Ca^{2+}$ levels to be activated [52]. Sustained elevation is correlated with peptide antigenicity and dose [1, 211, 175] as well as formation of actin foci in immunological synapse (IS) [117].

Structural findings showed the CD3$\zeta\zeta$ chains were divaricated during TCR complex assembly, and were brought back together as a mechanical pivot upon

cognate pMHC binding [125]. Calcium elevation was suggested to have a role in facilitating the process, as the immunoreceptor tyrosine-based activation motives (ITAMs) of CD3$\epsilon$ and CD3$\zeta$ were exposed to the cytosol upon calcium influx [183], and were otherwise buried inside the hydrophobic lipid bilayer interior in a resting T cell [213]. Therefore, a feedback loop appears to operate between TCR triggering and calcium influx in a healthy T cell, while mechanical force is a possible candidate to induce conformational change in the TCR complex.

The influx of extracellular calcium in T cell is regulated by store-operated calcium entry (SOCE). Upon TCR triggering, a tyrosine phosphorylation cascade [218] leads to phospholipase C$\gamma$1 (PLC$\gamma$1) being phosphorylated at Y783. The resultant activated enzyme catalyzes the hydrolysis of the membrane phospholipid phosphatidylinositol-4,5-biphosphate ($PIP_2$) to inositol 1,4,5-trisphosphate ($IP_3$) and diacylglycerol (DAG). $IP_3$ then acts as a second messenger and binds to $IP_3$ receptors on the endoplasmic reticulum (ER), triggering release of $Ca^{2+}$ from the ER store. The decrease in $Ca^{2+}$ in the ER is detected by stromal interaction molecule 1 (STIM1), which then interacts with calcium release activated current (CRAC) channel protein Orai1 on the plasma membrane. This opens the channel and allows entry of extracellular $Ca^{2+}$. SOCE is essential for activating gene expression after TCR stimulation, notably the transcription factors nuclear factor of activated T cells (NFAT), nuclear factor-$\kappa$B (NF-$\kappa$B) and cyclic-AMP-responsive-element-binding protein (CREB) [65]. Defects in regulating SOCE are associated with immunodeficiencies (severe combined immunodeficiency (SCID) etc.) and autoimmune

diseases (systemic lupus erythemantosus (SLE) and rheumatoid arthritis etc.).

As naïve and memory T cells routinely patrol our body to search for the cognate APCs [141], stiffness of the opposing substrate is a physiologically relevant parameter which could modulate signaling response of different lineages of T cells. We are interested in investigating the relationship between the mechanical properties of the opposing substrate (stiffness), the active response that the T cell generates (traction forces) and the cellular signaling response (SOCE). The first systematic stiffness measurements of professional APCs indicated that macrophages, monocytes and dendritic cells are soft and have Young moduli below 2 kPa [21]. We have previously reported that in this stiffness range, Jurkat T cells display active morphological remodelling and more sustained TCR proximal signaling during activation, compared with higher stiffnesses [87]. Traction force microscopy (TFM) has the advantage of precise control of rigidity of the underlying substrate. When combined with calcium imaging, this allows us to study SOCE on substrates with similar stiffness to APCs, and also on stiffer substrates with elasticity similar to cells of mesenchymal origin [129]. Our simultaneous measurements of traction force and calcium levels allows correlation between these two quantities at the single cell level.

There are a few studies focusing on the relationship between calcium influx and mechanical forces in single cells. One example is keratocytes, in which $Ca^{2+}$ transients were observed to precede traction stress increases during migration [55]. Similarly, fibroblast cells were observed to display $Ca^{2+}$ transients coincident with

traction increase in the direction of local mechanical stretching [153, 155], and on the other hand, application of shear stress can trigger calcium flickers, which were shown to steer cell migration [205]. Here we use the Jurkat cell line to study SOCE on different substate stiffnesses. We have characterized and reported the stress-stiffness relationship in these cells before [87], and in this report, we suggest the close relations between stiffness, forces and SOCE during their activation.

## A.2 Results

### A.2.1 Calcium imaging using widefield OGB-1 fluorescence

We used the nonratiometric calcium dye Oregon Green 488 BAPTA-1 (OGB-1) to image calcium dynamics in Jurkat T cells. The dye has an *in situ* $K_d$ of 430 nM and dynamic range of 2.6 as measured in HeLa cells [192]. We first checked the efficacy of OGB-1 epifluorescence to report relative calcium changes by imaging these cells in wide-field and TIRF simultaneously. TIRF provides a shallow illumination depth of 100-200 nm [7], hence avoids cell body fluorescence and provides a more quantitative measure of dye fluorescent intensity than widefield. We plated Jurkat T cells loaded with OGB-1 on nonstimulatory coverslips coated with poly-L-lysine (PLL), and recorded the fluorescence of the cells as it attached. In all experiments, we started imaging within one minute after plating to ensure consistency between different movies and to include most of the initial calcium spike. Comparison between wide-field (blue) and TIRF (red) intensities shows that the

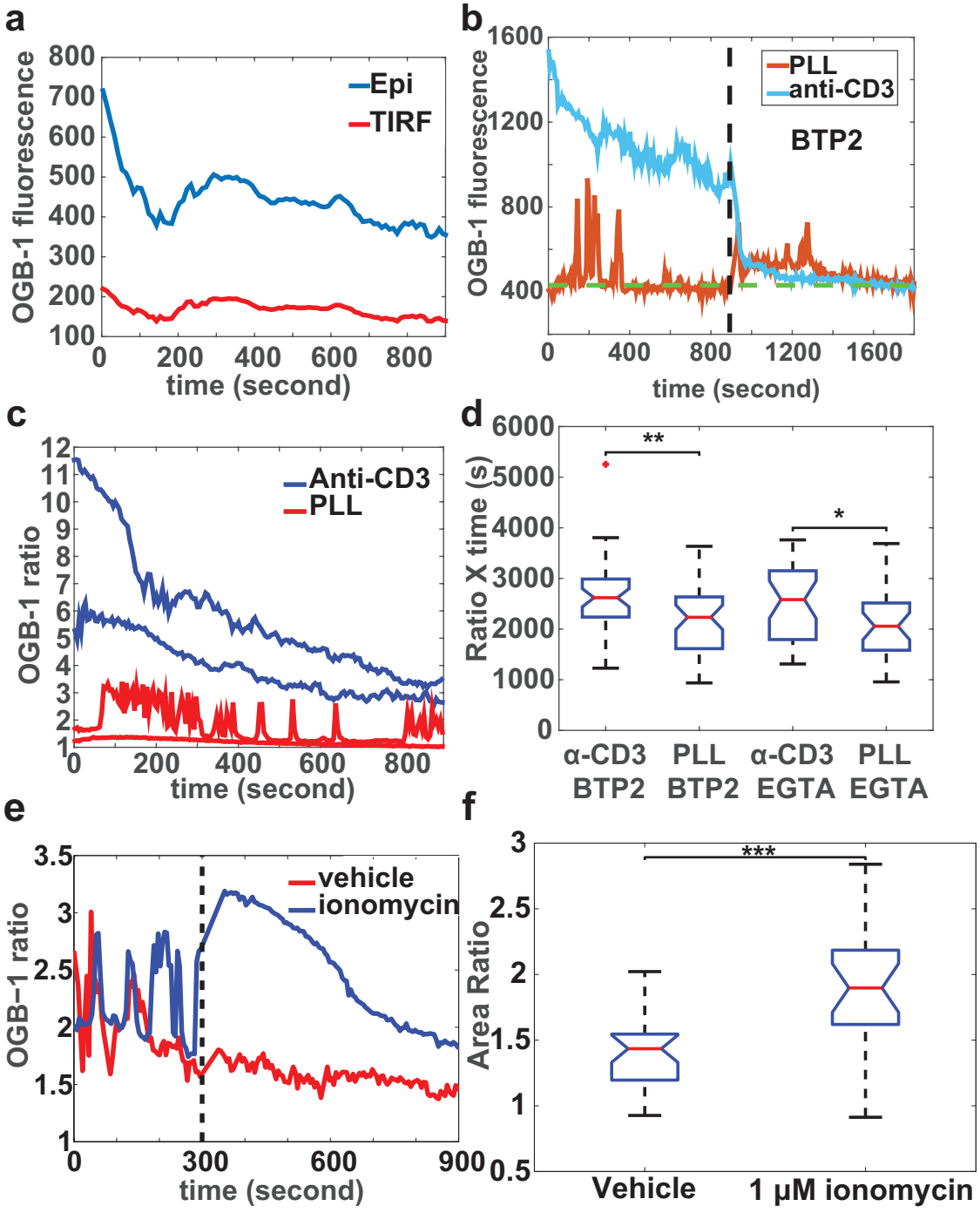


Figure A.1: (Continued on the following page.)

Figure A.1: **Establishment of quantitative calcium imaging with OGB-1.** (a) Wide-field and TIRF OGB-1 intensities of a Jurkat cell attached on nonstimulatory surface. (b) Application of 2 $\mu$M BTP2 at 15 min resulted in decrease of OGB-1 fluorescence for both cells plated on anti-CD3 (blue) or PLL control (red). The baseline can be extracted as indicated (green dash lines). (c) OGB-1 ratio as a function of time, for cells spreading on anti-CD3 (blue) and PLL (red). (d) Area under OGB-1 ratio curve for cells activated on stimulatory ($\alpha$-CD3) vs. nonstimulatory (PLL) and with $Ca^{2+}$ level quenched by BTP2 or 5 mM EGTA. (e) OGB-1 ratios of cells attached on PLL and were treated with 1 $\mu$M ionomycin (blue) or vehicle (red) at 5 minute. (f) Ratio of areas under OGB-1 ratio curve in the 10 minutes after to the 5 minutes before drug treatments.

cell body fluorescence caused significant overshoot of epifluorescence signal in the first minute, most likely because the cell has not yet attached. For the time points afterwards, these two signals followed each other closely (Figure A.1a). Therefore, epifluorescence is a reliable way to measure $Ca^{2+}$ levels in cells.

To account for dye loading heterogeneities, we applied a drug that inhibited SOCE at 15 min after spreading to quench the cytosolic calcium levels back to baseline. We chose BTP2 (or YM 58483) [226] as we found that this drug induced the least effect on cell morphology while quenching OGB-1 fluorescence in most cells efficiently, on both stimulatory and nonstimulatory surfaces (Figure A.1b). By imaging

for a further 15 minutes after BTP2 application, the baseline OGB-1 fluorescence ($F_0$) was extracted from the time series after drug treatment, as shown by the green dash lines in Figure A.1b. The ratio between fluorescence levels before 15 min $F(t)$ and $F_0$m (Figure A.1c) reports calcium levels within single cells quantitatively.

We took two different approachs to show sensitivity of OGB-1 ratio to artificially induced cytosolic $Ca^{2+}$ level changes. First, we compared OGB-1 ratio curves of cells activated on anti-CD3 ($\alpha$-CD3, stimulatory) against poly-L-lysine (PLL, non-stimulatory) and used area under the OGB-1 ratio curve before BTP2 application to measure average calcium influx level. As shown in Figure A.1d, cells spreading on anti-CD3 coated coverslips showed significantly higher area ($n = 43$, $2620 \pm 382$ s) compared with PLL negative control ($n = 44$, $2230 \pm 620$ s) ($p = 0.0025$). To confirm the effectiveness of BTP2 to reveal baseline OGB-1 fluorescence, we applied $Ca^{2+}$ chelator ethylene glycol tetraacetic acid (EGTA), instead of BTP2 and found that the area under ratio curve was also significantly lower on nonstimulatory than stimulatory surface (Figure A.1d). ( Anti-CD3: $n = 33$, $2580 \pm 790$ s; poly-l-lysine: $n = 30$, $2060 \pm 470$ s; $p = 0.015$). No statistically significant difference was found between areas under OGB-1 ratio curves of cells treated with BTP2 and EGTA, on both anti-CD3 coated or uncoated coverslips.

The second approach uses calcium ionosphore ionomycin to artifically increase intracellular $Ca^{2+}$ concentration. We applied ionomycin at 5 min after cells attached to PLL, imaged for 10 min. Example OGB-1 ratio curves of ionomycin (blue) and

vehicle (red) treatments were shown in Figure A.1e. For most cells, OGB-1 fluorescence was increased after ionomycin treatment, but not after vehicle treatment. We computed the area under the OGB-1 ratio curve for 10 minutes after drug treatment and divided that by the area in the 5 minutes prior to treatment. This "area ratio" provides a quantitative readout of $Ca^{2+}$ influx due to ionomycin treatment (Figure A.1f), and we observed a significant increase in area ratio for ionomycin/ vehicle treated cells (ionomycin: $n = 23$, $1.90 \pm 0.29$; vehicle: $n = 28$, $1.43 \pm 0.24$; $p = 5 \times 10^{-6}$). Overall, our OGB-1 imaging method provides a reliable single cell readout of $Ca^{2+}$ levels during Jurkat T cell activation.

### A.2.2 SOCE varies biphasically with substrate stiffness during Jurkat T cell activation

We next studied the calcium influx by Jurkat T cells when activated on anti-CD3 coated polyacrylamide gels [87]. By varying acrylamide-BIS ratio, one can produce elastic substrates that span the whole elasticity range of various tissues (100 Pa - 100 kPa, [188]). The distribution of average influx as a function of substrate stiffness is shown in Figure A.2a. We found that it showed significant decrease as the substrate stiffness increased from 100 Pa to 5 kPa (linear regression: $p = 2.5 \times 10^{-6}$). Above 5 kPa, the $Ca^{2+}$ influx increases with stiffness (linear regression: $p = 0.0094$). For negative control, we measured average influx of Jurkat T cells plated on non-stimulatory PLL substrate with various stiffnesses (Figure A.2a) and observed no

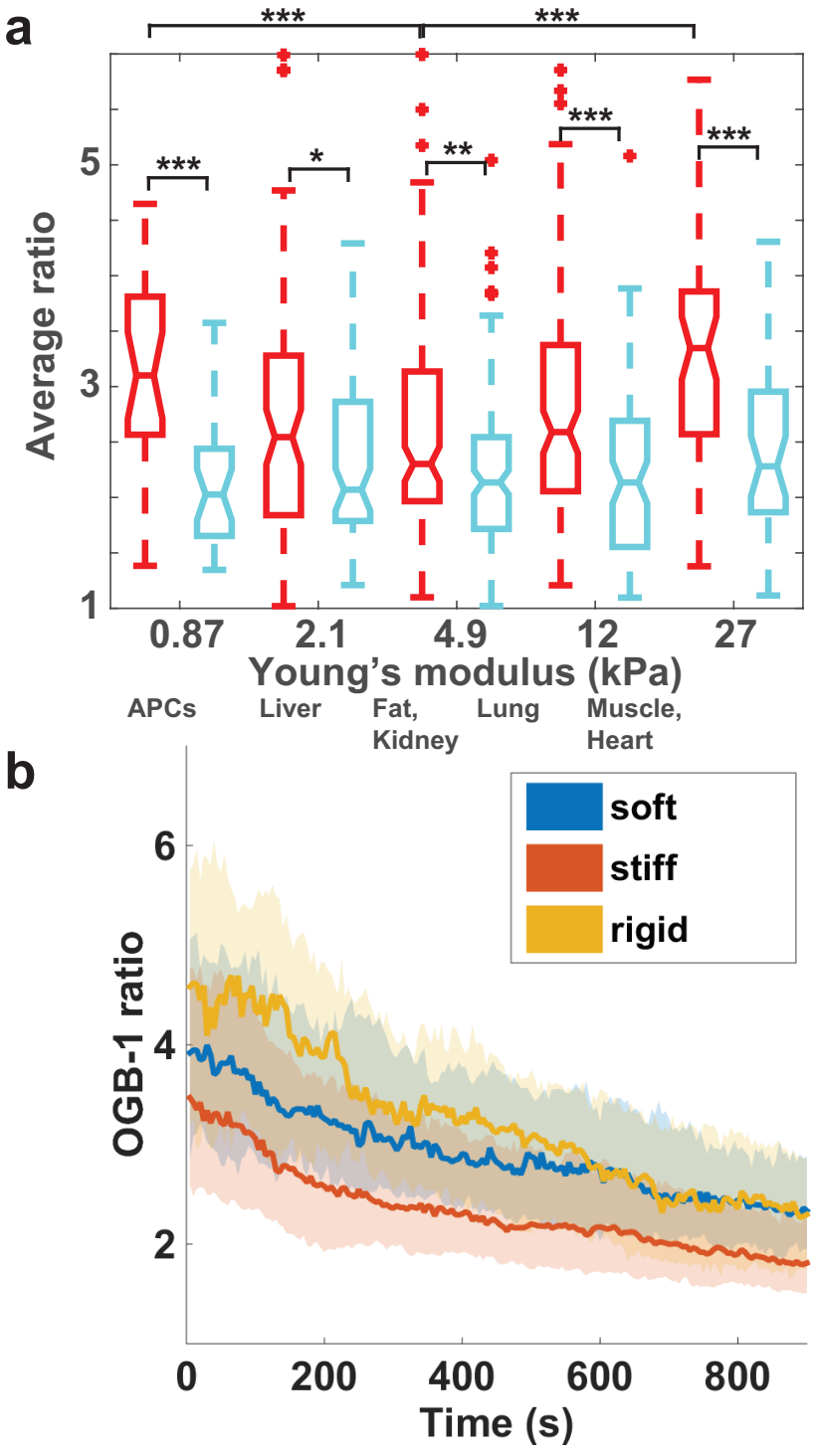


Figure A.2: (Continued on the following page.)

Figure A.2: **$Ca^{2+}$ influx of Jurkat T cells is modulated by substrate rigidity**. (a) Average $Ca^{2+}$ influx as a function of stiffness. Cyan: PLL; Red: anti-CD3. Corresponding tissues with similar stiffnesses were labelled, with information given in a previous report [188]. (b) Population median (bolded lines) and the range between first and third quartiles of cells spreading on soft (blue), stiff (red) and rigid (yellow).

dependence of average influx on substrate stiffness (linear regression: $p = 0.11$). We measured OGB-1 ratio at 15 min and the rate of decrease of OGB-1 ratio as a function of stiffness and observed a similar trend (Figure S1). Therefore, our analysis suggests a biphasic dependence of $Ca^{2+}$ influx on stiffness.

We were interested in how stiffness modulates the temporal dynamics of $Ca^{2+}$ levels. We therefore plotted the population behaviour OGB-1 ratios of cells spreading on soft ($E < 1.3$ kPa), stiff ($3 < E < 7$ kPa) and rigid ($18 < E < 42$ kPa) substrates (Figure A.2b). We observe that the initial $Ca^{2+}$ rise was similar between these three stiffness ranges, as seen from the significant overlap between their midspreads at early time points. However, soft and rigid substrates were better at sustaining $Ca^{2+}$ levels compared with stiff substrates, shown by the overlap of median traces of soft (blue) and rigid (yellow) substrates near 15 min with the stiff trace (red) being significantly lower.

### A.2.3 Rho activities modulate mechanosensitivity of $Ca^{2+}$ influx

How do Jurkat T cells sense stiffness of the stimulatory substrate and modulate their $Ca^{2+}$ influx accordingly? Mechanical force is an attractive candidate because TCR complex was shown to be a mechanosensor [111], and we have previously shown that Jurkat T cells exert stronger traction stresses on stiffer substrates [87]. We focus on the hypothesis that $Ca^{2+}$ influx are regulated through stresses on TCRs, which changes their interaction lifetime with their ligands [132] (Figure A.3a). Also, $Ca^{2+}$ levels could have a regulatory effect on on traction stress generated by the cell. Therefore, it is essential to measure and understand the relation between $Ca^{2+}$ influx and traction stress.

Our TFM setup allows us to simultaneously monitor evolution of $Ca^{2+}$ and traction stress as the cell spreaded. We used $Ca^{2+}$ level at 15 min to correlate with traction stresses exerted by individual cells at that time point regardless of substrate stiffness. We found that cells exerting stronger stresses are worse at sustaining $Ca^{2+}$ influx (Figure A.3b, linear regression: $p = 7.5 \times 10^{-10}$), agreeing with the observation that stress increases but $Ca^{2+}$ influx decreases with stiffness. However, no biphasic relationship (or catch bond behaviour) between $Ca^{2+}$ sustenance and stress was observed, in contrary to the observation in a previous report [132] for the case of mechanical triggering of TCR.

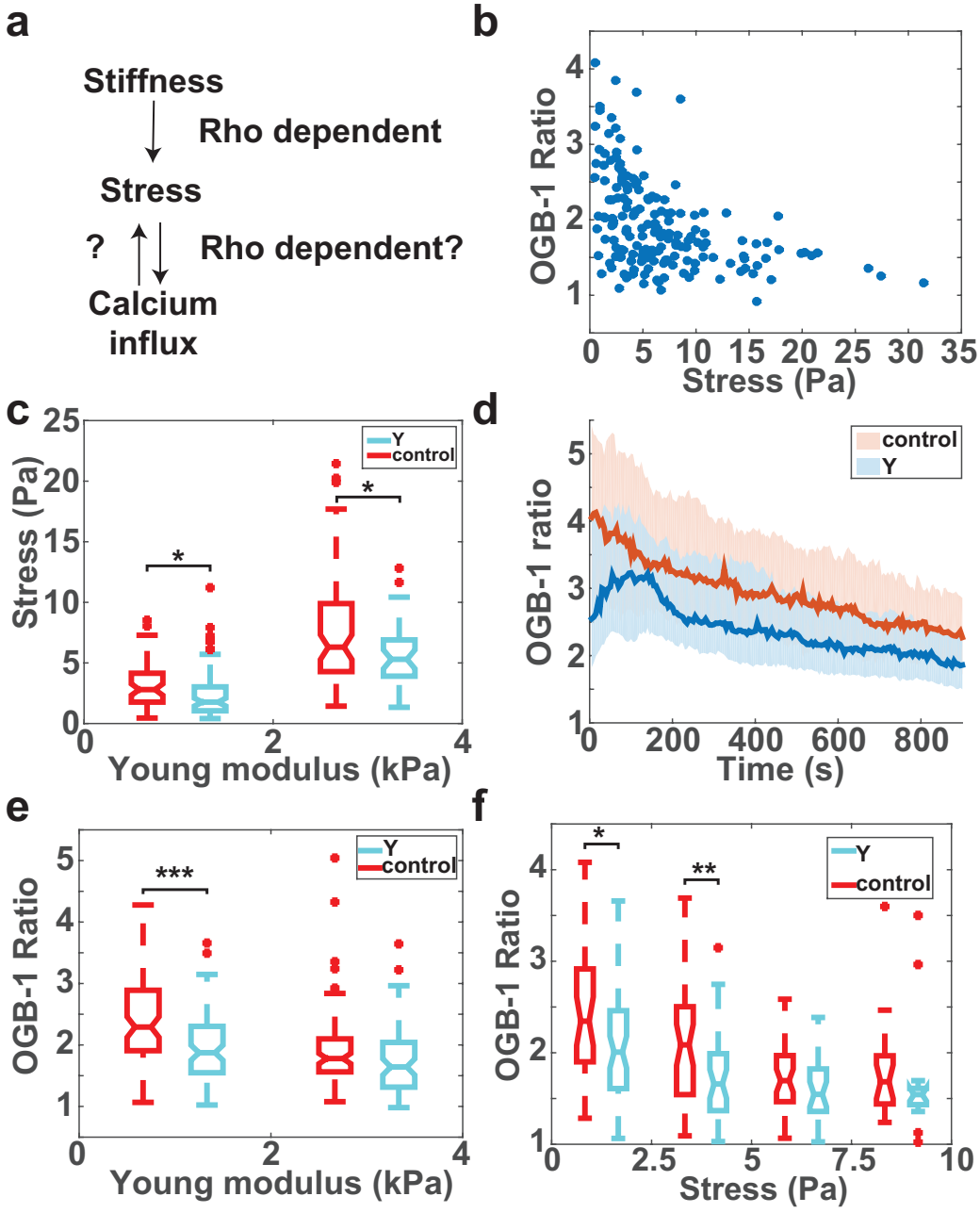


Figure A.3: (Continued on the following page.)

Figure A.3: **Rho signaling regulates both stress-stiffness and $Ca^{2+}$ influx-stress relations**. (a) Hypothesis of mechanosensing mechanism. The cell sense substrate rigidity through generation of physical forces and magnitude of these forces regulate $Ca^{2+}$ influx. (b) Single cell $Ca^{2+}$ sustenance as a function of traction stress. (c) Rho kinase inhibition reduced Jurkat cell's force generation capability. (d,e) Rho kinase inhibition impaired $Ca^{2+}$ sustenance for activation on soft elastic substrate. (f) Rho kinase inhibition significantly changed Jurkat cells' $Ca^{2+}$ influx-stress relation.

We then asked whether and how inhibition of Rho pathway, which is a well known regulator of cellular contractility [123], affects the mechanosensitivity of $Ca^{2+}$ influx. When we allowed Jurkat cells incubated in 100 $\mu$M Y-27632 (Rho kinase inhibitor, [196]) to spread on substrates with various stiffnesses, Rho kinase inhibition consistently resulted in cells generating less traction (Figure A.3c). Therefore, Rho signaling regulates traction stress generation (Figure A.3a, top half). On the other hand, whether and how Rho signaling regulates $Ca^{2+}$ influx is unknown. If the relationship between $Ca^{2+}$ influx and traction stresses is not dependent on Rho signaling, one would expect cells activated in the presence of Y-27632 to have higher $Ca^{2+}$ influx compared with control on similar substrate stiffness, as the Figure A.3b suggests that lower stress leads to higher influx. However, careful examination of $Ca^{2+}$ influx in the absence and presence of Y-27632 on elastic substrates of Young moduli between 0 and 2 kPa showed that Y-27632 reduced $Ca^{2+}$ influx and sus-

tenance (Figure A.3d), indicating that Rho signaling also regulates the relation between $Ca^{2+}$ influx and traction stress. Strikingly, the effect of Rho kinase inhibition is similar to the effect of increased substrate stiffness (Figure A.2b). The difference in $Ca^{2+}$ influx between control and Y-27632 treated cells was the most significant on soft substrates, while on stiffer substrates the difference was only close to significance ($E < 2$ kPa: $p = 2.9 \times 10^{-4}$; $2 < E < 4$ kPa: $p = 0.058$; Figure A.3e).

We finally compared the $Ca^{2+}$ influx-traction relation between control cells and Y-27632 treated cells, as shown in Figure A.3f. For both cases, cells exerting lower tractions have more sustained Ca levels (linear regression: $p = 1.7 \times 10^{-5}$ for Y-27632 treated cells). However, within the same stress range, Rho kinase inhibition significantly reduced both $Ca^{2+}$ sustenance and average influx (data not shown) compared with control. These results highlight Rho-associated contractility as a key regulator of calcium signaling in Jurkat T cell which regulates both how stress depends on stiffness and how the $Ca^{2+}$ signal depends on stress.

## A.3 Discussion

$Ca^{2+}$ influx is a hallmark feature of T cell activation. Previous literature have studied the initial rise and sustenance of the $Ca^{2+}$ signal [211, 22, 95, 219, 12, 175], how different molecular perturbations (knockdowns [157, 93, 118], mutants [190], cytoskeletal inhibitions [199, 8, 117] etc.) influence the signal, and how the signal is generated in the first place [65]. On the other hand, the $Ca^{2+}$ elevations can also

feedback to sustain CD3$\epsilon$ and CD3$\zeta$ chain phosphorylation [213, 183]. As a result, recent works have used $Ca^{2+}$ influx as an easy readout of TCR triggering to correlate with application of mechanical forces to TCR complex [111, 131, 132, 46] and with pushing forces exerted by T cells [91] temporally. In this study, we combined calcium imaging and TFM of the Jurkat Cell anti-CD3 activation system [9], and used the $Ca^{2+}$ signal as a readout of signaling output, in response to different input substrate stiffnesses.

Given T cell's function of immunosurveillance in various body tissues, it is apparent that they routinely encounter cells with various stiffnesses. Mechanobiology research has hightlighted the importance of substrate stiffness in driving cell migration [134], mesenchymal stem cell differentiation [61] and development of metastatic potential of tumor cells [133]. Two studies in the literature have addressed T cell activation on soft elastic substrates, but they found contradictory results: one suggested soft substrate enhanced interleukin 2 (IL-2) production [161] while the second suggested the converse [102]. Unfortunately, the range of substrate stiffness investigated (minimum of 10 kPa) was much higher than that typical of APCs in both studies ($<$ 2 kPa, [21]). The stiffness range used in this and our previous study [87] employed polyacrylamide gels ranging 3 orders of magnitude from 100 Pa up to 100 kPa, spanning the whole stiffness range of living tissues [129].

While ratiometric dyes like Fura-2 are commonly used for calcium imaging in T cells, OGB-1 is a gold standard for imaging action potentials in neuroscience [35].

We prefer it over Fura-2 for a few reasons: firstly, its superior optical and chemical properties that provide brightness and sensitivity to changes in $Ca^{2+}$ levels, and secondly, its green emission allows use of the same optical setup as imaging GFP, hence avoiding UV optics and reduced microscope objective magnification which is important for simultaneous TFM. The drawback is the need to quench $Ca^{2+}$ level at the end of imaging to obtain the baseline fluorescence. Photobleaching was minimal as we seldom see cells with steadily decaying fluorescence when its $Ca^{2+}$ level is quenched. Our characterization of the system suggests that this approach is suitable for large scale calcium imaging and comparison between cells activated on different substrates and at different dates.

We and other groups have previously characterized the polyacrylamide system's capability to provide a chemically identical environment with stiffness as the only changing parameter [87]. Our results suggests a biphasic relation between $Ca^{2+}$ influx and stiffness in Jurkat cells. The existence of "signaling minimum" around the stiffness of fat, kidney and lung (Figure A.2c) is surprising. Close look of cells activated on these stiffnesses revealed weakened $Ca^{2+}$ signal sustenance (Figure A.2d). This is in accordance with our previous result that tyrosine phosphorylation of TCR signaling kinases and adaptors is less sustained on these stiffnesses [87]. Furthermore, the rise of $Ca^{2+}$ sustenance as stiffness is increased agrees with observation that TCR proximal signaling increased with stiffness from 10 to 200 kPa [102]. Compared with previous studies, our result has given a more complete picture of how signaling varies from typical stiffness of APCs (100-1000 Pa) to more rigid tissue

stiffness of bones and muscles.

Physical forces and stiffness sensing form the basis of mechanobiology [97]. It is natural to hypothesize that mechanosensing by Jurkat cells is mediated by physical forces the cells exert on the opposing substrate (Figure A.3a), as previous results by us and other groups [87, 91] has shown that T cells exert higher traction forces on stiffer substrate. Further, TCR-pMHC interaction was shown to be via catch-bond in which forces can enhance interaction lifetime [132, 46]. We therefore asked whether and how inhibition of Rho pathway, a well-known pathway that regulates cellular contractility, influences the mechanosensing behaviour of Jurkat cells. We found that in a Rho kinase inhibited environment, Jurkat T cells were less capable of sustaining $Ca^{2+}$ influx on soft substrates, and show strikingly similar $Ca^{2+}$ signal as control cells spreading on stiff substrate. Our finding echoes to that of a previous study, which the investigators cultured various adherent cell types on substrate stiffness ranging from 0.3 kPa to that of glass [146], and observed that inhibition of myosin II-associated contractility could promote cell proliferation on soft substrates, mimicking the effect of increasing stiffness. Our data also showed Y-27632 treatment changed the $Ca^{2+}$ influx-stress relation significantly (Figure A.3f), together indicating Rho signaling as a regulator of mechanosensing of Jurkat cells.

Although Jurkat cells are not ideal for investigation of physiological T cell signaling [88], our study nevertheless highlights an nontrivial role of substrate stiffness during T cell activation. Our system could be easily extended to primary T

cells, in which different subtypes of T cells (e.g. naïve, helper, cytotoxic, regulatory, memory) could have substantially different stiffness dependence in their signaling response. Also, the similar $Ca^{2+}$ influx behaviour of Y-27632 treated cells spreading on a soft gel and a control cell spreading on a stiff gel suggests mechanical (stiffness) and chemical (Rho) signals can be integrated for mechanochemical information processing at the cellular scale. Finally, whether the $Ca^{2+}$ influx-stress relation is causal and bidirectional is still open to investigation. Overall, our study highlights tissue stiffness as a key regulator of Jurkat T cell signaling, and a more holistic undertstanding of the mechanobiology of T cell activation might be essential for tackling autoimmune diseases and designing T cell cancer therapy.

## A.4 Supplementary materials

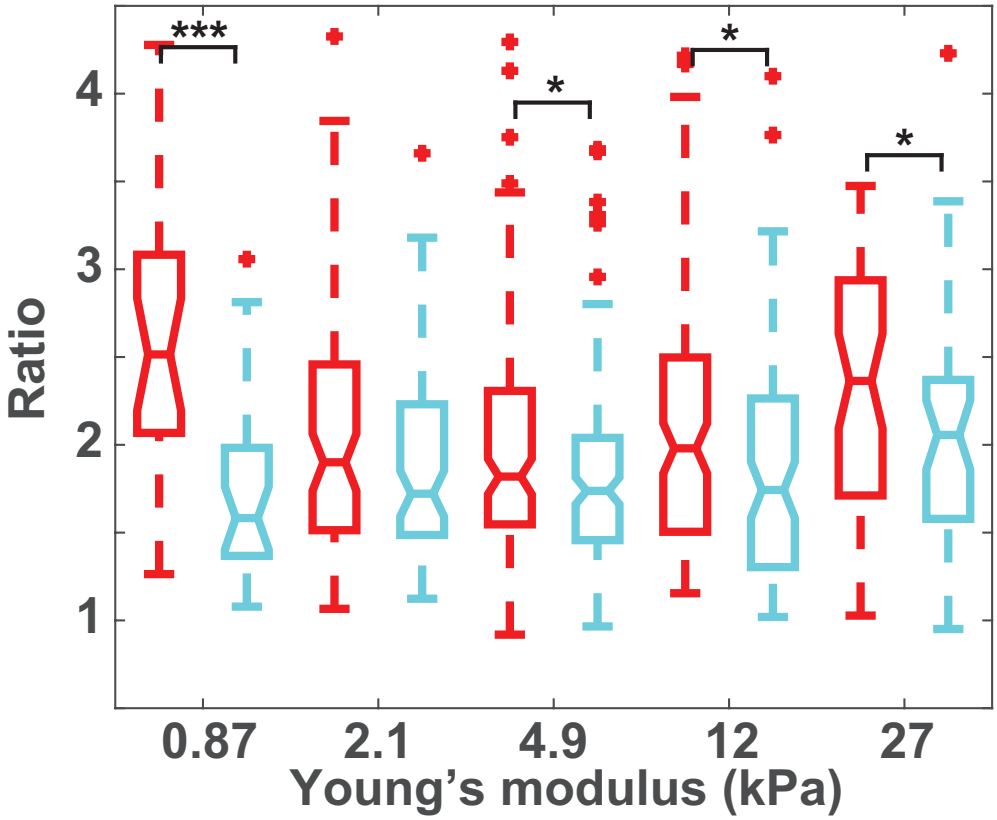


Figure S1: **Calcium influx is less sustained on stiff substrate.**

# Appendix B

# Materials and Methods

## B.1 Cells and reagents

### B.1.1 Reagents

Anti-CD3 was purchased from eBioscience (San Diego, CA). Antibody against tubulin, NMIIA and monophosphorylated NMII light chain were purchased from Abcam (Cambridge, MA). Calyculin A and antibody against doubly phosphorylated NMII light chain were purchased from Cell Signaling Technology (Danvers, MA).Okadaic acid was purchased from Santa Cruz Biotechnology (Dallas, TX). Y27632 was purchased from SelleckChem (Houston, TX). BTP2 and Taxol were purchased from Cayman Chemicals (Ann Arbor, MI). Jasplakinolide, (-)-blebbistatin and ionomycin were purchased from Calbiochem (Billerica, MA). 40 % acrylamide, 2 % Bis-acrylamide, ammonium persulfate, and tetramethylethylenediamine were purchased from Bio-Rad (Hercules, CA). FluoSphereRed microspheres, 0.2 $\mu$m, were

purchased from Molecular Probes (Eugene, OR). Poly-l-lysine, latrunculin-A and nocodazole were purchased from Sigma-Aldrich (St. Louis, MO). Sylgard 164 elastomers were purchased from Ellsworth Adhesives (Germantown, WI). Stainless steel microspheres were purchased from Salem Balls (Canton, CT). Polystyrene microspheres were purchased from Polysciences (Warrington, PA). Hydrazine hydrate and colchicine were purchased from Acros (Pittsburgh, PA). L-15 medium was purchased from Life Technologies (Grand Island, NY). All oligos were purchased from Integrated DNA Technologies (Coralville, Iowa).

### B.1.2 Cell culture

E6-1 and E6-1 EGFP-actin Jurkat T cells were a gift from the lab of L. Samelson (National Cancer Institute, National Institute of Health) Primary peripheral $CD4^+$ T cells were generous gift from Dr. Janis Burkhardt, Children's Hospital of Philadelphia, Philadelphia, PA. They are cultured in RPMI 1640 supplemented with 10 % fetal bovine serum and 1 % penicillin-streptomycin. Briefly, cells were grown in RPMI medium at 37 °C in a $CO_2$ incubator. Before imaging, 1 ml of cells was centrifuged at 240 g for 5 min. The supernatant was removed and the cells were resuspended in imaging buffer (L-15, Invitrogen, Carlsbad, CA). For experiments with serum, 10 % fetal bovine serum (FBS) (Invitrogen) was added to the imaging buffer. For drug inhibitions, drugs were added to the imaging buffer and the cells were incubated at 37 °C for 15 min before imaging.

### B.1.3 Molecular cloning and transfections

TagRFP-T sequence was cloned from pcass TagRFP-T (a gift from Morgan Huse, Rockefeller University, New York, NY) into pIRES-neo2-PAGFP-tubulin (a gift from Patricia Wadsworth, Addgene plasmid # 12297, [195]) by polymerase chain reaction (PCR) with forward primer: GATTAAGCTAGCGGCCGCAGGTG and backward primer: GTAATCCGGACTTGTACAGCTCGTC to create pIRES-neo2-TagRFP-T-tubulin. The TagRFP-T-tubulin fragment was then further cloned into pMSCV-IRES-hygro to create pMSCV-TagRFP-T-tubulin-IRES-hygro, allowing retroviral bicistronic expression of TagRFP-T-tubulin and hygromycin-resistance gene. *MYL12B* was cloned by whole cell reverse transcriptase polymerase chain reaction (RT-PCR) from Jurkat cells [113] with the forward primer: CAACTCGAGAATTAAACAACCACCATG and reverse primer: CATAGCGGCCGCGTCATCTTTGTCTTTGG, and cloned into Z4-MSCV-TagRFP-T (a gift from Morgan Huse, Rockefeller University, New York, NY). Retroviruses were generated according to standard protocol [189] with Phoenix Amphotropic cells and were transduced into Jurkat cells by spin infection. The cells were then selected in 12.5 $\mu$g/ml zeocin for 2 weeks, and sorted with fluorescence-activated cell sorting (FACS) to obtain high expression clones. Monoclonal cell lines were finally generated by limiting dilution of the sorted polyclonal population.

## B.2 Substrate preparation

### B.2.1 Glass substrates for TIRF imaging

Chambered coverslips (LabTek) were cleaned with 1 M HCl and 70 % ethanol for 30 min and dried at 37 °C for 1 h. Chambers were treated for 10 min with 0.01 % (weight/volume) poly-L-lysine solution (Sigma- Aldrich), drained, and dried for 1 h at 37 °C. Chambers were coated with 10 $\mu$g/ml anti-CD3$\epsilon$ antibody (Hit-3a, eBiosciences, San Diego, CA) overnight at 4 °C. Excess antibody was removed by extensive washing with phosphate-buffered saline. To test the effect of substrate coverage on spreading kinetics, the solution antibody concentration was varied over 0.01-10 $\mu$g/ml. Cells were seeded onto chambers in the appropriate imaging medium.

### B.2.2 Elastic substrates for TFM and characterization

Bulk fabrication of polyacrylamide gels with diameter of 12 mm was followed as described in [45], with a slight modification to form a thin and dense layer of fluorescent beads trapped on top of the polyacrylamide gel [19]. Gel stiffness ranges from 100 Pa to 100 kPa, by varying acrylamide from 2 to 12 % and keeping BIS at 0.1 %. Before coating of proteins, the top of the gel was observed under an epifluorescence microscope (TE2000; Nikon, Tokyo, Japan) at 20× magnification in rhodamine channel to ensure that a monolayer of densely spaced beads was present. Suitable gels were then attached to the bottom of MatTek 35-mm dishes with a 20 mm diameter microwell (MatTek, Ashland, MA) with Sylgard 164 silicone elastomer (Dow Corning, Midland, MI). 0.01 % poly-l-lysine was coated on polyacrylamide

with hydrazine hydrate method [5]. Afterwards, the gels were washed three times with Dulbecco's phosphate buffered saline (DPBS), and 10 $\mu$g/ml anti-human CD3 (Hit3a) was added to the gel and incubated at 4 °C overnight.

Fluorescently labeled Hit3a was used to verify that antibody coating did not depend on substrate stiffness (unpublished data). After each image acquisition, gel height was determined by microscope's focusing mechanism and corrected for axial scaling [99]. Stainless steel balls (1/64-, 1/32-, and 3/64-in. diameter) or polystyrene balls (for gels with Young modulus $< 300$ Pa) were then added to where the time series was taken. Steel balls were removed by a magnetic stir bar, and polystyrene balls were removed by bulb aspiration for a few times. The indentation caused by the ball and the gel height at that spot were recorded. The Young's modulus of each individual gel used for the experiments was calculated using a Hertz model for an elastic substrate with finite thickness [49]. Typically, gels with acrylamide/Bis ratios of 2:0.1, 3:0.1, 4:0.1, and 5:0.1 were measured to have an average stiffness of 0.4, 2, 4, and 9 kPa, respectively.

## B.3 Microscopy

### B.3.1 Live cell imaging

Live-cell movies of cell spreading were taken over 15 min at a frame rate of 5 s per frame in bright-field differential interference contrast (DIC), FluoSphereRed,

and GFP channels. Images were collected using an inverted microscope (TE2000 PFS; Nikon, Melville, NY) with a cooled charge-coupled device camera (CoolSNAP HQ2; Photometrics, Tucson, AZ). EGFP-actin and fluorescent beads were imaged using a 60×/1.49 numerical aperture objective lens and a mercury lamp excitation for TFM. For TIRF microscopy, the light source were 491 nm and 561 nm lasers from Andor Technology (Belfast, UK).

The imaging medium used was Leibovitz's medium L-15 without phenol red [128], and the dish was kept at 37 °C throughout data acquisition by means of an airstream incubator (Nevtek, Williamsville, VA). Illumination wavelength and exposure times were controlled using a multibandpass dichromatic mirror (Chroma, Rockingham, VT) and bandpass excitation and emission filters (Chroma) in electronic filterwheel/shutter devices (Sutter Instruments, Novato, CA). In inhibitor addition experiments and calcium imaging, data acquisition was paused at 15 min. drugs at double of target concentration were added at an equal volume as the imaging medium, and data acquisition was resumed for 15 min. The carrier solvent was maintained at 0.1 % for DMSO and 1 % water.

### B.3.2 Immunofluorescence imaging

Conventional fixation was carried out by fixing the cells at 2.4 % paraformaldehyde (PFA) for 30 minutes at 37 °C, permeabilizing cells at 0.1 % Triton-X-100 for

4 minutes at room temperature, blocked with 2 % normal goat serum for 30 minutes at room temperature, incubated with primary antibodies overnight at 4 °C and finally incubated in secondary antibodies for 45 minutes at room temperature.

Permeabilization before fixation protocol was adopted from previous studies [142, 115], with the modification of using a much lower percentage of Triton-X-100 (0.1 %) than previous studies (1 %), so that cell morphology was kept intact during permeabilization. Cells were activated for specified time period, and a 2× permabilization buffer (10 mM 2-(N-morpholino)ethanesulfonic acid (MES), 130 mM potassium chloride (KCl), 3 mM magnesium chloride ($MgCl_2$), 10 mM ethylene glycol tetraacetic acid (EGTA), 0.2 % Triton-X-100, 8 % Polyethylene glycol (PEG) 8000, 2 % bovine serum albumin(BSA)) were added at equal volume to the buffer the cells were in for 10 minutes at 37 °C. The cells were then washed in wash buffer (10 mM MES, 130 mM KCl, 3 mM $MgCl_2$, 5 mM EGTA, 4 % PEG 8000, 1 % BSA) and fixed in 2.4 % PFA in DPBS.

In immunofluorescence experiments, images of four different channels, namely, interference reflection (IRM), bright field DIC, green and red TIRF fluorescence were acquired. At the end of experiment, one image of fluorescent dextran solution was taken for shading correction, and one image with all light sources turned off was taken for dark noise removal.

## B.4 Image analysis

### B.4.1 Tracking of fluorescent beads

For TFM data, the image sequences in FluoSphereRed channel were background-subtracted with the background estimated from morphological opening and then input into the freely available MATLAB package MatPIV for particle image velocimetry analysis [187]. The first image in the sequence before the cells contacted the substrate was taken as the zero-displacement image, and sample drift was corrected for by tracking the displacements of fiduciary beads far away from any cells. The method was sufficiently sensitive to detect bead displacements in gels up to 6-8 kPa, as verified by single-particle tracking (Figure B.1).

### B.4.2 Fourier-transform traction cytometry

To obtain traction forces exerted by the cell, Boussinesq solution of infinite half space in linear elasticity theory was used, neglecting displacements and forces in the $z$ direction: [122]:

$$\begin{pmatrix} u_x \\ u_y \end{pmatrix} = \frac{1+\nu}{\pi E r^3} \begin{pmatrix} r^2 - \nu y^2 & \nu xy \\ \nu xy & r^2 - \nu x^2 \end{pmatrix} \begin{pmatrix} F_x \\ F_y \end{pmatrix} \tag{B.1}$$

Here a point force $F_x\hat{x} + F_y\hat{y}$ is applied at origin, $u_x\hat{x} + u_y\hat{y}$ is the resultant displacement at $(x, y)$, and $r = \sqrt{x^2 + y^2}$. Hence, below is the Green's function of the Boussineq solution:

$$G(x, y) = \frac{1+\nu}{\pi E r^3} \begin{pmatrix} r^2 - \nu y^2 & \nu xy \\ \nu xy & r^2 - \nu x^2 \end{pmatrix} \tag{B.2}$$

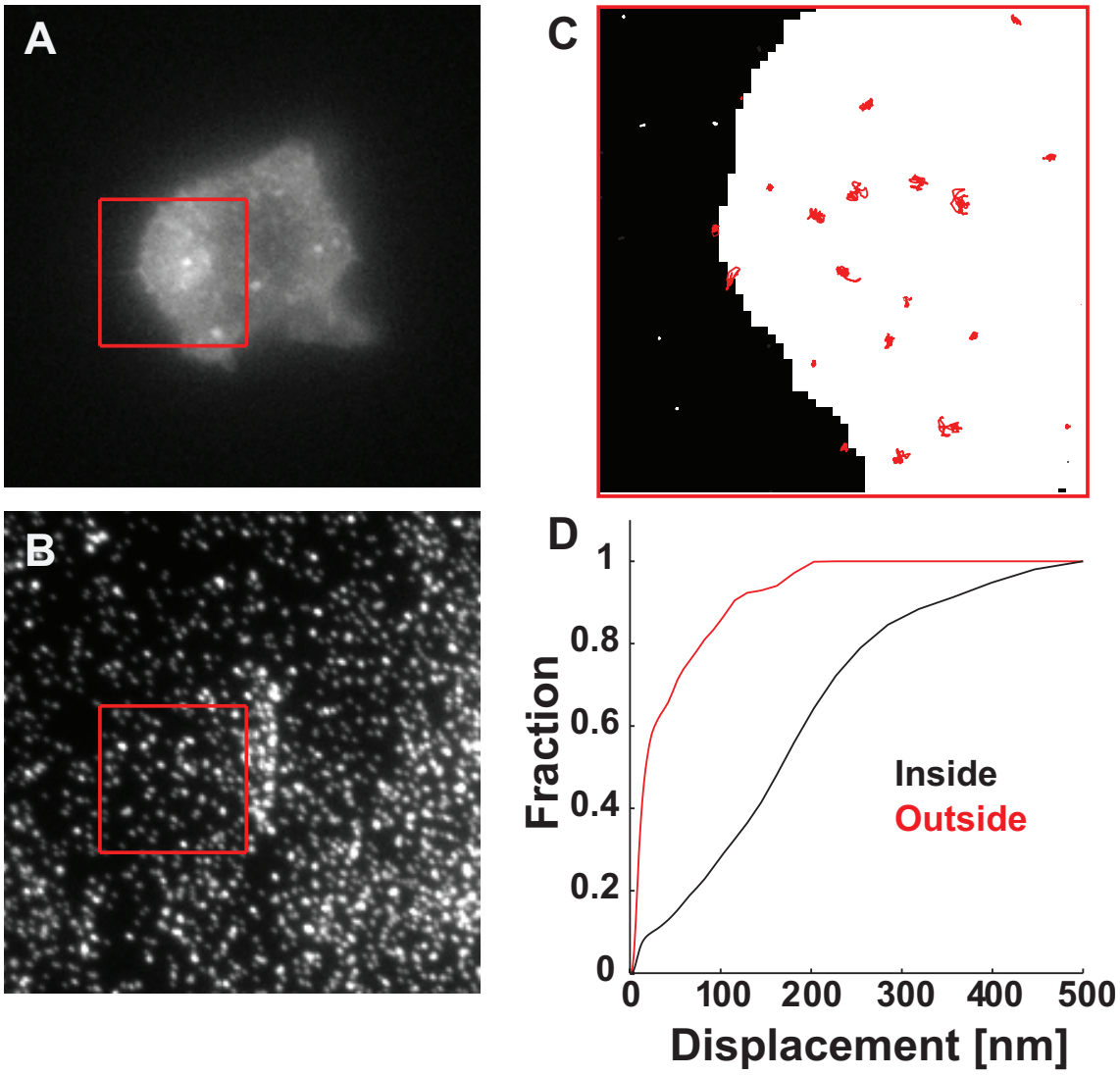


Figure B.1: **Particle tracking velocimetry can detect bead displacements on stiff gels.** A. Jurkat cell expressing EGFP-actin spreading on a stiff (6 kPa) gel. B. Image of 200 nm fluorescent bead. C. Zoomed in view of ROI shown in A,B with bead tracks superimposed on binary image of cell. Tracks for beads under the cell are shown in red while external beads are shown in white. D. Cumulative histogram of multiple beads tracked over 15 min. of cell spreading.

and given a stress profile of $\vec{\sigma}(x,y) = \sigma_x(x,y)\hat{x} + \sigma_y(x,y)\hat{y}$, the resultant displacement profile is given by:

$$\begin{pmatrix} u_x \\ u_y \end{pmatrix} = \int\int dx'dy' G(x-x', y-y') \begin{pmatrix} \sigma_x(x',y') \\ \sigma_y(x',y') \end{pmatrix} \tag{B.3}$$

Therefore, 2D TFM is to solve the above integral equation. By convolution theorem, convolution integral is much simplified in the frequency space. We take 2D Fourier transform of equation B.3:

$$\begin{pmatrix} \tilde{u}_x \\ \tilde{u}_y \end{pmatrix} = \tilde{G} \begin{pmatrix} \tilde{\sigma}_x \\ \tilde{\sigma}_y \end{pmatrix} \tag{B.4}$$

$$\begin{pmatrix} \tilde{\sigma}_x \\ \tilde{\sigma}_y \end{pmatrix} = \tilde{G}^{-1} \begin{pmatrix} \tilde{u}_x \\ \tilde{u}_y \end{pmatrix} \tag{B.5}$$

where $\tilde{u}_x$, $\tilde{u}_y$, $\tilde{\sigma}_x$, $\tilde{\sigma}_y$, $\tilde{G}$ are the Fourier transform of the vectors and matrices and $\tilde{G}^{-1}$ is inverse of $\tilde{G}$.

$$\tilde{G} = \frac{2(1+\nu)}{Ek^3} \begin{pmatrix} k^2 - \nu k_x^2 & -\nu k_x k_y \\ -\nu k_x k_y & k^2 - \nu k_y^2 \end{pmatrix} \tag{B.6}$$

$$\tilde{G}^{-1} = \frac{E}{2(1-\nu^2)k} \begin{pmatrix} k^2 - \nu k_y^2 & \nu k_x k_y \\ \nu k_x k_y & k^2 - \nu k_x^2 \end{pmatrix} \tag{B.7}$$

Here $k_x$, $k_y$ and $k^2 = k_x^2 + k_y^2$ are the wave vector components and magnitude. This method is known as Fourier Transform Traction Cytometry (FTTC) [26, 172].

In TFM carried out in this disseration, displacement vector maps generated were then input into an unconstrained FTTC algorithm implemented in MATLAB

[26] at resolution of 1.6 $\mu$m and extended to include finite-thickness correction [193]. The analysis was carried out for every frame in the image sequence, and the analyzed traction stress data were presented as traction stress magnitude and vector maps image sequences, respectively. Cells showing significant above-background displacements and traction were chosen by visual observation for cell edge tracking.

Cell boundaries and edge velocities were extracted using techniques described in [120, 137]. Stress vectors calculated at each grid point from FTTC were linearly interpolated to each neighboring pixel, and average traction stress magnitude was obtained by integrating the magnitudes of stress vectors at every pixel inside the cell boundary, irrespective of the stress direction. The stress curve for individual cell was smoothed by robust lowess before statistical analysis. Finally, we used the traction stress measured at the first frame as an estimate of the background stress noise and was subtracted from the stresses at later times to obtain the effective traction stress exerted by the cell.

### B.4.3 Cell edge dynamics quantification

The centroid of the tracked cell area in the first frame was treated as the cell center. At each frame, the radial distance $r$ and angle of each piece of the cell edge from the centroid $\theta$ was recorded. The radial edge profile $R(\theta, t)$ of the cell at each time point $t$ was represented by the average $r$ in each bin angle of 6°. Pearson

correlation coefficient between the radial edge profiles at 15 minutes ($t$) and before ($t'$) was calculated by the following formula:

$$\rho(t,t') = \frac{E[R(\theta,t)R(\theta,t')] - E[R(\theta,t)]E[R(\theta,t')]}{\sqrt{E[R^2(\theta,t)] - (E[R(\theta,t)])^2}\sqrt{E[R^2(\theta,t')] - (E[R(\theta,t')])^2}} \tag{B.8}$$

Here expectation is taken over $\theta$. This calculation was carried out by corr function in MATLAB.

### B.4.4 Quantitative imaging

To analyze immunofluorescence images quantitatively, dark noise was first subtracted from each image. Secondly the image was corrected for illumination shading, by dividing with dark noise subtracted TIRF image of fluorescent dextran solution acquired at the end of imaging. Background fluorescence was then estimated from morphological opening and was subtracted from the corrected image to give the final quantitative image. Edge of single cells was tracked using cell edge tracking software on the IRM image. The average intensity in the tracked region was calculated for the channels of interest (green, red or both).

### B.4.5 Densitometry analysis

For densitometry analysis, we first normalized the intensity within the 35- to 40 kDa band (pLAT) and 70 kDa (pZAP70/pSLP-76) by tubulin intensity respectively at every time point, giving ratio $R$.

# Bibliography

[1] NG Agrawal and Jennifer J Linderman. Calcium response of helper t lymphocytes to antigen-presenting cells in a single-cell assay. *Biophysical journal*, 69(3):1178–1190, 1995.

[2] B. Alberts. *Molecular Biology of the Cell: Reference edition*. Number 1 in Molecular Biology of the Cell: Reference Edition. Garland Science, 2008.

[3] John S Allingham, Robert Smith, and Ivan Rayment. The structural basis of blebbistatin inhibition and specificity for myosin ii. *Nature structural & molecular biology*, 12(4):378–379, 2005.

[4] Ronen Alon and Michael L Dustin. Force as a facilitator of integrin conformational changes during leukocyte arrest on blood vessels and antigen-presenting cells. *Immunity*, 26(1):17–27, 2007.

[5] Yvonne Aratyn-Schaus, Patrick W Oakes, Jonathan Stricker, Stephen P Winter, and Margaret L Gardel. Preparation of complaint matrices for quantifying cellular contraction. *Journal of visualized experiments: JoVE*, (46), 2010.

[6] Yukako Asano, Akira Nagasaki, and Taro QP Uyeda. Correlated waves of actin filaments and pip3 in dictyostelium cells. *Cell motility and the cytoskeleton*, 65(12):923–934, 2008.

[7] Daniel Axelrod. Cell-substrate contacts illuminated by total internal reflection fluorescence. *The Journal of cell biology*, 89(1):141–145, 1981.

[8] Alexander Babich, Shuixing Li, Roddy S O'Connor, Michael C Milone, Bruce D Freedman, and Janis K Burkhardt. F-actin polymerization and retrograde flow drive sustained plc$\gamma$1 signaling during t cell activation. *The Journal of cell biology*, 197(6):775–787, 2012.

[9] L. Balagopalan, E. Sherman, V.A. Barr, and L.E. Samelson. Imaging techniques for assaying lymphocyte activation in action. *Nature Reviews Immunology*, 11(1):21–33, 2010.

[10] Mira Barda-Saad, Alex Braiman, Rachel Titerence, Stephen C Bunnell, Valarie A Barr, and Lawrence E Samelson. Dynamic molecular interactions linking the t cell antigen receptor to the actin cytoskeleton. *Nature immunology*, 6(1):80–89, 2005.

[11] Keenan T Bashour, Alexander Gondarenko, Haoqian Chen, Keyue Shen, Xin Liu, Morgan Huse, James C Hone, and Lance C Kam. Cd28 and cd3 have complementary roles in t-cell traction forces. *Proceedings of the National Academy of Sciences*, 111(6):2241–2246, 2014.

[12] Peter Beemiller, Jordan Jacobelli, and Matthew F Krummel. Integration of the movement of signaling microclusters with cellular motility in immunological synapses. *Nature Immunology*, 13(8):787–795, 2012.

[13] Peter Beemiller and Matthew F Krummel. Mediation of t-cell activation by actin meshworks. *Cold Spring Harbor perspectives in biology*, 2(9), 2010.

[14] Karen A Beningo, Kozue Hamao, Micah Dembo, Yu-li Wang, and Hiroshi Hosoya. Traction forces of fibroblasts are regulated by the rho-dependent kinase but not by the myosin light chain kinase. *Archives of biochemistry and biophysics*, 456(2):224–231, 2006.

[15] Timo Betz, Daniel Koch, Yun-Bi Lu, Kristian Franze, and Josef A Käs. Growth cones as soft and weak force generators. *Proceedings of the National Academy of Sciences*, 108(33):13420–13425, 2011.

[16] Daniel D Billadeau, Jeffrey C Nolz, and Timothy S Gomez. Regulation of t-cell activation by the cytoskeleton. *Nature Reviews Immunology*, 7(2):131–143, 2007.

[17] Till Bretschneider, Kurt Anderson, Mary Ecke, Annette Müller-Taubenberger, Britta Schroth-Diez, Hellen C Ishikawa-Ankerhold, and Günther Gerisch. The three-dimensional dynamics of actin waves, a model of cytoskeletal self-organization. *Biophysical journal*, 96(7):2888–2900, 2009.

[18] Till Bretschneider, Stefan Diez, Kurt Anderson, John Heuser, Margaret Clarke, Annette Müller-Taubenberger, Jana Köhler, and Günther Gerisch.

Dynamic actin patterns and arp2/3 assembly at the substrate-attached surface of motile cells. *Current Biology*, 14(1):1–10, 2004.

[19] Paul C Bridgman, Sonya Dave, Clara F Asnes, Antonella N Tullio, and Robert S Adelstein. Myosin iib is required for growth cone motility. *The Journal of Neuroscience*, 21(16):6159–6169, 2001.

[20] Volker Brinkmann, Ulrike Reichard, Christian Goosmann, Beatrix Fauler, Yvonne Uhlemann, David S Weiss, Yvette Weinrauch, and Arturo Zychlinsky. Neutrophil extracellular traps kill bacteria. *science*, 303(5663):1532–1535, 2004.

[21] Nathalie Bufi, Michael Saitakis, Stéphanie Dogniaux, Oscar Buschinger, Armelle Bohineust, Alain Richert, Mathieu Maurin, Claire Hivroz, and Atef Asnacios. Human primary immune cells exhibit distinct mechanical properties that are modified by inflammation. *Biophysical Journal*, 108(9):2181–2190, 2015.

[22] Stephen C Bunnell, David I Hong, Julia R Kardon, Tetsuo Yamazaki, C Jane McGlade, Valarie A Barr, and Lawrence E Samelson. T cell receptor ligation induces the formation of dynamically regulated signaling assemblies. *The Journal of cell biology*, 158(7):1263–1275, 2002.

[23] Stephen C Bunnell, Veena Kapoor, Ronald P Trible, Weiguo Zhang, and Lawrence E Samelson. Dynamic actin polymerization drives t cell receptor–

induced spreading: a role for the signal transduction adaptor lat. *Immunity*, 14(3):315–329, 2001.

[24] Janis K Burkhardt, Esteban Carrizosa, and Meredith H Shaffer. The actin cytoskeleton in t cell activation. *Annu. Rev. Immunol.*, 26:233–259, 2008.

[25] Dylan T Burnette, Suliana Manley, Prabuddha Sengupta, Rachid Sougrat, Michael W Davidson, Bechara Kachar, and Jennifer Lippincott-Schwartz. A role for actin arcs in the leading-edge advance of migrating cells. *Nature cell biology*, 13(4):371–382, 2011.

[26] James P Butler, Iva Marija Tolić-Nørrelykke, Ben Fabry, and Jeffrey J Fredberg. Traction fields, moments, and strain energy that cells exert on their surroundings. *American Journal of Physiology-Cell Physiology*, 282(3):C595–C605, 2002.

[27] Yunfei Cai, Nicolas Biais, Gregory Giannone, Monica Tanase, Guoying Jiang, Jake M Hofman, Chris H Wiggins, Pascal Silberzan, Axel Buguin, Benoit Ladoux, et al. Nonmuscle myosin iia-dependent force inhibits cell spreading and drives f-actin flow. *Biophysical journal*, 91(10):3907–3920, 2006.

[28] Gabriele Campi, Rajat Varma, and Michael L Dustin. Actin and agonist mhc–peptide complex–dependent t cell receptor microclusters as scaffolds for signaling. *The Journal of experimental medicine*, 202(8):1031–1036, 2005.

[29] Lindsay B Case and Clare M Waterman. Adhesive f-actin waves: a novel integrin-mediated adhesion complex coupled to ventral actin polymerization. *PloS one*, 6(11):e26631, 2011.

[30] Lindsay B. Case and Clare M. Waterman. Integration of actin dynamics and cell adhesion by a three-dimensional, mechanosensitive molecular clutch. *Nat Cell Biol*, 17(8):955–963, Aug 2015. Review.

[31] F Chamaraux, S Fache, F Bruckert, and B Fourcade. Kinetics of cell spreading. *Physical review letters*, 94(15):158102, 2005.

[32] François Chamaraux, Olivier Ali, Sébastien Keller, Franz Bruckert, and Bertrand Fourcade. Physical model for membrane protrusions during spreading. *Physical biology*, 5(3):036009, 2008.

[33] Clarence E Chan and David J Odde. Traction dynamics of filopodia on compliant substrates. *Science*, 322(5908):1687–1691, 2008.

[34] Guillaume T Charras, Justin C Yarrow, Mike A Horton, L Mahadevan, and TJ Mitchison. Non-equilibration of hydrostatic pressure in blebbing cells. *Nature*, 435(7040):365–369, 2005.

[35] Tsai-Wen Chen, Trevor J Wardill, Yi Sun, Stefan R Pulver, Sabine L Renninger, Amy Baohan, Eric R Schreiter, Rex A Kerr, Michael B Orger, Vivek Jayaraman, et al. Ultrasensitive fluorescent proteins for imaging neuronal activity. *Nature*, 499(7458):295–300, 2013.

[36] Susan N Christo, Kerrilyn R Diener, Robert E Nordon, Michael P Brown, Hans J Griesser, Krasimir Vasilev, Farid C Christo, and John D Hayball. Scrutinizing calcium flux oscillations in t lymphocytes to deduce the strength of stimulus. *Scientific reports*, 5, 2015.

[37] Corina Ciobanasu, Bruno Faivre, and Christophe Le Clainche. Actomyosin-dependent formation of the mechanosensitive talin–vinculin complex reinforces actin anchoring. *Nature communications*, 5, 2014.

[38] William A Comrie, Alexander Babich, and Janis K Burkhardt. F-actin flow drives affinity maturation and spatial organization of lfa-1 at the immunological synapse. *The Journal of cell biology*, 208(4):475–491, 2015.

[39] Max D Cooper and Matthew N Alder. The evolution of adaptive immune systems. *Cell*, 124(4):815–822, 2006.

[40] Max D Cooper and Brantley R Herrin. How did our complex immune system evolve? *Nature Reviews Immunology*, 10(1):2–3, 2010.

[41] Thomas R Cox and Janine T Erler. Remodeling and homeostasis of the extracellular matrix: implications for fibrotic diseases and cancer. *Disease models & mechanisms*, 4(2):165–178, 2011.

[42] Erin M Craig, David Van Goor, Paul Forscher, and Alex Mogilner. Membrane tension, myosin force, and actin turnover maintain actin treadmill in the nerve growth cone. *Biophysical journal*, 102(7):1503–1513, 2012.

[43] Roger Craig, Robin Smith, and John Kendrick-Jones. Light-chain phosphorylation controls the conformation of vertebrate non-muscle and smooth muscle myosin molecules. 1983.

[44] Damien Cuvelier, Manuel Théry, Yeh-Shiu Chu, Sylvie Dufour, Jean-Paul Thiéry, Michel Bornens, Pierre Nassoy, and L Mahadevan. The universal dynamics of cell spreading. *Current biology*, 17(8):694–699, 2007.

[45] V. Damljanovic, B.C. Lagerholm, and K. Jacobson. Bulk and micropatterned conjugation of extracellular matrix proteins to characterized polyacrylamide substrates for cell mechanotransduction assays. *Biotechniques*, 39(6):847, 2005.

[46] Dibyendu Kumar Das, Yinnian Feng, Robert J Mallis, Xiaolong Li, Derin B Keskin, Rebecca E Hussey, Sonia K Brady, Jia-Huai Wang, Gerhard Wagner, Ellis L Reinherz, et al. Force-dependent transition in the t-cell receptor $\beta$-subunit allosterically regulates peptide discrimination and pmhc bond lifetime. *Proceedings of the National Academy of Sciences*, page 201424829, 2015.

[47] Micah Dembo and Yu-Li Wang. Stresses at the cell-to-substrate interface during locomotion of fibroblasts. *Biophysical journal*, 76(4):2307–2316, 1999.

[48] Andrew L DeMond, Kaspar D Mossman, Toby Starr, Michael L Dustin, and Jay T Groves. T cell receptor microcluster transport through molecular mazes reveals mechanism of translocation. *Biophysical journal*, 94(8):3286–3292, 2008.

[49] Emilios K Dimitriadis, Ferenc Horkay, Julia Maresca, Bechara Kachar, and Richard S Chadwick. Determination of elastic moduli of thin layers of soft material using the atomic force microscope. *Biophysical journal*, 82(5):2798–2810, 2002.

[50] Hans-Günther Döbereiner, Benjamin Dubin-Thaler, Grégory Giannone, Harry S Xenias, and Michael P Sheetz. Dynamic phase transitions in cell spreading. *Physical review letters*, 93(10):108105, 2004.

[51] Hans-Günther Döbereiner, Benjamin J Dubin-Thaler, Jake M Hofman, Harry S Xenias, Tasha N Sims, Grégory Giannone, Michael L Dustin, Chris H Wiggins, and Michael P Sheetz. Lateral membrane waves constitute a universal dynamic pattern of motile cells. *Physical review letters*, 97(3):038102, 2006.

[52] Ricardo E Dolmetsch, Richard S Lewis, Christopher C Goodnow, and James I Healy. Differential activation of transcription factors induced by ca2+ response amplitude and duration. 1997.

[53] Ricardo E Dolmetsch, Keli Xu, and Richard S Lewis. Calcium oscillations increase the efficiency and specificity of gene expression. *Nature*, 392(6679):933–936, 1998.

[54] Adam D Douglass and Ronald D Vale. Single-molecule microscopy reveals plasma membrane microdomains created by protein-protein networks that exclude or trap signaling molecules in t cells. *Cell*, 121(6):937–950, 2005.

[55] Andrew Doyle, William Marganski, and Juliet Lee. Calcium transients induce spatially coordinated increases in traction force during the movement of fish keratocytes. *Journal of cell science*, 117(11):2203–2214, 2004.

[56] Glenn Dranoff. Cytokines in cancer pathogenesis and cancer therapy. *Nature Reviews Cancer*, 4(1):11–22, 2004.

[57] Benjamin J Dubin-Thaler, Gregory Giannone, Hans-Günther Döbereiner, and Michael P Sheetz. Nanometer analysis of cell spreading on matrix-coated surfaces reveals two distinct cell states and steps. *Biophysical journal*, 86(3):1794–1806, 2004.

[58] Michael L Dustin. Cell adhesion molecules and actin cytoskeleton at immune synapses and kinapses. *Current opinion in cell biology*, 19(5):529–533, 2007.

[59] Michael L Dustin and Jay T Groves. Receptor signaling clusters in the immune synapse. *Annual review of biophysics*, 41:543, 2012.

[60] M.L. Dustin and A.C. Chan. Signaling takes shape in review the immune system. *Cell*, 103:283–294, 2000.

[61] Adam J Engler, Shamik Sen, H Lee Sweeney, and Dennis E Discher. Matrix elasticity directs stem cell lineage specification. *Cell*, 126(4):677–689, 2006.

[62] MA Fardin, OM Rossier, P Rangamani, PD Avigan, NC Gauthier, W Vonnegut, A Mathur, J Hone, R Iyengar, and MP Sheetz. Cell spreading as a hydrodynamic process. *Soft Matter*, 6(19):4788–4799, 2010.

[63] Juan Pablo Fededa and Daniel W Gerlich. Molecular control of animal cell cytokinesis. *Nature cell biology*, 14(5):440–447, 2012.

[64] Joseph Fenner, Amanda C Stacer, Frank Winterroth, Timothy D Johnson, Kathryn E Luker, and Gary D Luker. Macroscopic stiffness of breast tumors predicts metastasis. *Scientific reports*, 4, 2014.

[65] Stefan Feske. Calcium signalling in lymphocyte activation and disease. *Nature Reviews Immunology*, 7(9):690–702, 2007.

[66] Andrew Fire, SiQun Xu, Mary K Montgomery, Steven A Kostas, Samuel E Driver, and Craig C Mello. Potent and specific genetic interference by double-stranded rna in caenorhabditis elegans. *nature*, 391(6669):806–811, 1998.

[67] Victoria E Foe and George von Dassow. Stable and dynamic microtubules coordinately shape the myosin activation zone during cytokinetic furrow formation. *The Journal of cell biology*, 183(3):457–470, 2008.

[68] Maxime F Fournier, Roger Sauser, Davide Ambrosi, Jean-Jacques Meister, and Alexander B Verkhovsky. Force transmission in migrating cells. *The Journal of cell biology*, 188(2):287–297, 2010.

[69] K Christopher Garcia. Reconciling views on t cell receptor germline bias for mhc. *Trends in immunology*, 33(9):429–436, 2012.

[70] K Christopher Garcia, Massimo Degano, Robyn L Stanfield, Anders Brunmark, Michael R Jackson, Per A Peterson, Luc Teyton, and Ian A Wilson.

An $\alpha\beta$ t cell receptor structure at 2.5 å and its orientation in the tcr-mhc complex. *Science*, 274(5285):209–219, 1996.

[71] Margaret L Gardel, Benedikt Sabass, Lin Ji, Gaudenz Danuser, Ulrich S Schwarz, and Clare M Waterman. Traction stress in focal adhesions correlates biphasically with actin retrograde flow speed. *The Journal of cell biology*, 183(6):999–1005, 2008.

[72] Nicholas RJ Gascoigne. Do t cells need endogenous peptides for activation? *Nature Reviews Immunology*, 8(11):895–900, 2008.

[73] Günther Gerisch, Till Bretschneider, Annette Müller-Taubenberger, Evelyn Simmeth, Mary Ecke, Stefan Diez, and Kurt Anderson. Mobile actin clusters and traveling waves in cells recovering from actin depolymerization. *Biophysical journal*, 87(5):3493–3503, 2004.

[74] Günther Gerisch, Mary Ecke, Britta Schroth-Diez, Silke Gerwig, Ulrike Engel, Lucinda Maddera, and Margaret Clarke. Self-organizing actin waves as planar phagocytic cup structures. *Cell adhesion & migration*, 3(4):373–382, 2009.

[75] Grégory Giannone, Benjamin J Dubin-Thaler, Hans-Günther Döbereiner, Nelly Kieffer, Anne R Bresnick, and Michael P Sheetz. Periodic lamellipodial contractions correlate with rearward actin waves. *Cell*, 116(3):431–443, 2004.

[76] Elizabeth S Gold, David M Underhill, Naomi S Morrissette, Jian Guo, Mark A McNiven, and Alan Aderem. Dynamin 2 is required for phagocytosis in macrophages. *The Journal of experimental medicine*, 190(12):1849–1856, 1999.

[77] Erin D Goley and Matthew D Welch. The arp2/3 complex: an actin nucleator comes of age. *Nature reviews Molecular cell biology*, 7(10):713–726, 2006.

[78] Timothy S Gomez, Karan Kumar, Ricardo B Medeiros, Yoji Shimizu, Paul J Leibson, and Daniel D Billadeau. Formins regulate the actin-related protein 2/3 complex-independent polarization of the centrosome to the immunological synapse. *Immunity*, 26(2):177–190, 2007.

[79] Arash Grakoui, Shannon K Bromley, Cenk Sumen, Mark M Davis, Andrey S Shaw, Paul M Allen, and Michael L Dustin. The immunological synapse: a molecular machine controlling t cell activation. *Science*, 285(5425):221–227, 1999.

[80] Carsten Grashoff, Brenton D Hoffman, Michael D Brenner, Ruobo Zhou, Maddy Parsons, Michael T Yang, Mark A McLean, Stephen G Sligar, Christopher S Chen, Taekjip Ha, et al. Measuring mechanical tension across vinculin reveals regulation of focal adhesion dynamics. *Nature*, 466(7303):263–266, 2010.

[81] John A Hammer and Janis K Burkhardt. Controversy and consensus regarding myosin ii function at the immunological synapse. *Current opinion in immunology*, 25(3):300–306, 2013.

[82] Niña C Hartman, Jeffrey A Nye, and Jay T Groves. Cluster size regulates protein sorting in the immunological synapse. *Proceedings of the National Academy of Sciences*, 106(31):12729–12734, 2009.

[83] SD Hess, M Oortgiesen, and MD Cahalan. Calcium oscillations in human t and natural killer cells depend upon membrane potential and calcium influx. *The Journal of Immunology*, 150(7):2620–2633, 1993.

[84] Philippe Horvath and Rodolphe Barrangou. Crispr/cas, the immune system of bacteria and archaea. *Science*, 327(5962):167–170, 2010.

[85] Jon CD Houtman, Richard A Houghtling, Mira Barda-Saad, Yoko Toda, and Lawrence E Samelson. Early phosphorylation kinetics of proteins involved in proximal tcr-mediated signaling pathways. *The Journal of Immunology*, 175(4):2449–2458, 2005.

[86] Ke Hu, Lin Ji, Kathryn T Applegate, Gaudenz Danuser, and Clare M Waterman-Storer. Differential transmission of actin motion within focal adhesions. *Science*, 315(5808):111–115, 2007.

[87] King Lam Hui, Lakshmi Balagopalan, Lawrence E Samelson, and Arpita Upadhyaya. Cytoskeletal forces during signaling activation in jurkat t cells. *Molecular biology of the cell*, pages mbc–E14, 2014.

[88] J.B. Huppa, M.M. Davis, et al. T-cell-antigen recognition and the immunological synapse. *Nature Reviews Immunology*, 3(12):973–983, 2003.

[89] J.B. Huppa, M. Gleimer, C. Sumen, M.M. Davis, et al. Continuous t cell receptor signaling required for synapse maintenance and full effector potential. *Nature immunology*, 4(8):749–755, 2003.

[90] Morgan Huse. Microtubule-organizing center polarity and the immunological synapse: protein kinase c and beyond. *Frontiers in immunology*, 3, 2012.

[91] Julien Husson, Karine Chemin, Armelle Bohineust, Claire Hivroz, and Nelly Henry. Force generation upon t cell receptor engagement. *PLoS One*, 6(5):e19680, 2011.

[92] Callen Hyland, Aaron F Mertz, Paul Forscher, and Eric Dufresne. Dynamic peripheral traction forces balance stable neurite tension in regenerating aplysia bag cell neurons. *Scientific reports*, 4, 2014.

[93] T. Ilani, G. Vasiliver-Shamis, S. Vardhana, A. Bretscher, and M.L. Dustin. T cell antigen receptor signaling and immunological synapse stability require myosin iia. *Nature immunology*, 10(5):531–539, 2009.

[94] JB Imboden and A Weiss. The t-cell antigen receptor regulates sustained increases in cytoplasmic free ca2+ through extracellular ca2+ influx and ongoing intracellular ca2+ mobilization. *Biochem. J*, 247:695–700, 1987.

[95] Darrell J Irvine, Marco A Purbhoo, Michelle Krogsgaard, and Mark M Davis. Direct observation of ligand recognition by t cells. *Nature*, 419(6909):845–849, 2002.

[96] H Ishihara, BL Martin, DL Brautigan, H Karaki, H Ozaki, Y Kato, N Fusetani, S Watabe, K Hashimoto, D Uemura, et al. Calyculin a and okadaic acid: inhibitors of protein phosphatase activity. *Biochemical and biophysical research communications*, 159(3):871–877, 1989.

[97] Thomas Iskratsch, Haguy Wolfenson, and Michael P Sheetz. Appreciating force and shape [mdash] the rise of mechanotransduction in cell biology. *Nature Reviews Molecular Cell Biology*, 2014.

[98] J. Jacobelli, S.A. Chmura, D.B. Buxton, M.M. Davis, and M.F. Krummel. A single class ii myosin modulates t cell motility and stopping, but not synapse formation. *Nature immunology*, 5(5):531–538, 2004.

[99] H. Jacobsen and S.W. Hell. Effect of the specimen refractive index on the imaging of a confocal fluorescence microscope employing high aperture oil immersion lenses. *Bioimaging*, 3(1):39–47, 1995.

[100] John R James and Ronald D Vale. Biophysical mechanism of t-cell receptor triggering in a reconstituted system. *Nature*, 2012.

[101] Paul A Janmey and Christopher A McCulloch. Cell mechanics: integrating cell responses to mechanical stimuli. *Annu. Rev. Biomed. Eng.*, 9:1–34, 2007.

[102] Edward Judokusumo, Erdem Tabdanov, Sudha Kumari, Michael L Dustin, and Lance C Kam. Mechanosensing in t lymphocyte activation. *Biophysical journal*, 102(2):L5–L7, 2012.

[103] Yoshihisa Kaizuka, Adam D Douglass, Rajat Varma, Michael L Dustin, and Ronald D Vale. Mechanisms for segregating t cell receptor and adhesion molecules during immunological synapse formation in jurkat t cells. *Proceedings of the National Academy of Sciences*, 104(51):20296–20301, 2007.

[104] Kenjiro Kamiguchi, Kouichi Tachibana, Satoshi Iwata, Yoshiyuki Ohashi, and Chikao Morimoto. Cas-l is required for $\beta$1 integrin-mediated costimulation in human t cells. *The Journal of Immunology*, 163(2):563–568, 1999.

[105] H Kamisoyama, Y Araki, and M Ikebe. Mutagenesis of the phosphorylation site (serine 19) of smooth muscle myosin regulatory light chain and its effects on the properties of myosin. *Biochemistry*, 33(3):840–847, 1994.

[106] Pakorn Kanchanawong, Gleb Shtengel, Ana M. Pasapera, Ericka B. Ramko, Michael W. Davidson, Harald F. Hess, and Clare M. Waterman. Nanoscale architecture of integrin-based cell adhesions. *Nature*, 468(7323):580–584, 2010. 10.1038/nature09621.

[107] Karen E Kasza, Amy C Rowat, Jiayu Liu, Thomas E Angelini, Clifford P Brangwynne, Gijsje H Koenderink, and David A Weitz. The cell as a material. *Current opinion in cell biology*, 19(1):101–107, 2007.

[108] Karen E Kasza and Jennifer A Zallen. Dynamics and regulation of contractile actin–myosin networks in morphogenesis. *Current opinion in cell biology*, 23(1):30–38, 2011.

[109] Kinneret Keren, Patricia T. Yam, Anika Kinkhabwala, Alex Mogilner, and Julie A. Theriot. Intracellular fluid flow in rapidly moving cells. *Nat Cell Biol*, 11(10):1219–1224, 2009. 10.1038/ncb1965.

[110] Sun Taek Kim, Yongdae Shin, Kristine Brazin, Robert J Mallis, Zhen-Yu J Sun, Gerhard Wagner, Matthew J Lang, and Ellis L Reinherz. Tcr mechanobiology: torques and tunable structures linked to early t cell signaling. *Frontiers in immunology*, 3, 2012.

[111] Sun Taek Kim, Koh Takeuchi, Zhen-Yu J Sun, Maki Touma, Carlos E Castro, Amr Fahmy, Matthew J Lang, Gerhard Wagner, and Ellis L Reinherz. The $\alpha\beta$ t cell receptor is an anisotropic mechanosensor. *Journal of Biological Chemistry*, 284(45):31028–31037, 2009.

[112] Kazushi Kimura, Masaaki Ito, Mutsuki Amano, Kazuyasu Chihara, Yuko Fukata, Masato Nakafuku, Bunpei Yamamori, Jianhua Feng, Takeshi Nakano, Katsuya Okawa, et al. Regulation of myosin phosphatase by rho and rho-associated kinase (rho-kinase). *Science*, 273(5272):245–248, 1996.

[113] RJ Klebe, GM Grant, AM Grant, MA Garcia, TA Giambernardi, and GP Taylor. Rt-pcr without rna isolation. *Biotechniques*, 21(6):1094–1100, 1996.

[114] Daniel Koch, William J Rosoff, Jiji Jiang, Herbert M Geller, and Jeffrey S Urbach. Strength in the periphery: growth cone biomechanics and substrate rigidity response in peripheral and central nervous system neurons. *Biophysical journal*, 102(3):452–460, 2012.

[115] Stefan A Koestler, Klemens Rottner, Frank Lai, Jennifer Block, Marlene Vinzenz, and J Victor Small. F-and g-actin concentrations in lamellipodia of moving cells. *PloS one*, 4(3):e4810, 2009.

[116] Fang Kong, Andrés J García, A Paul Mould, Martin J Humphries, and Cheng Zhu. Demonstration of catch bonds between an integrin and its ligand. *The Journal of cell biology*, 185(7):1275–1284, 2009.

[117] Sudha Kumari, David Depoil, Roberta Martinelli, Edward Judokusumo, Guillaume Carmona, Frank B Gertler, Lance C Kam, Christopher V Carman, Janis K Burkhardt, Darrell J Irvine, et al. Actin foci facilitate activation of the phospholipase c-$\gamma$ in primary t lymphocytes via the wasp pathway. *eLife*, 4:e04953, 2015.

[118] Sudha Kumari, Santosha Vardhana, Michael Cammer, Silvia Curado, Luis Santos, Michael P Sheetz, and Michael L Dustin. T lymphocyte myosin iia is required for maturation of the immunological synapse. *Frontiers in immunology*, 3, 2012.

[119] King Lam Hui, Sae In Kwak, and Arpita Upadhyaya. Adhesion-dependent modulation of actin dynamics in jurkat t cells. *Cytoskeleton*, 71(2):119–135, 2014.

[120] King Lam Hui, Chenlu Wang, Brian Grooman, Jessica Wayt, and Arpita Upadhyaya. Membrane dynamics correlate with formation of signaling clusters during cell spreading. *Biophysical journal*, 102(7):1524–1533, 2012.

[121] Tim Lämmermann and Michael Sixt. Mechanical modes of amoeboidcell migration. *Current opinion in cell biology*, 21(5):636–644, 2009.

[122] Lev Davidovitch Landau and Evgeniĭ Lifshit?s? *Course of theoretical physics: theory of elasticity*.

[123] Douglas A Lauffenburger and Alan F Horwitz. Cell migration: a physically integrated molecular process. *Cell*, 84(3):359–369, 1996.

[124] Kyeong-Hee Lee, Amy D Holdorf, Michael L Dustin, Andrew C Chan, Paul M Allen, and Andrey S Shaw. T cell receptor signaling precedes immunological synapse formation. *Science*, 295(5559):1539–1542, 2002.

[125] Mark S Lee, Caleb R Glassman, Neha R Deshpande, Hemant B Badgandi, Heather L Parrish, Chayasith Uttamapinant, Philipp S Stawski, Alice Y Ting, and Michael S Kuhns. A mechanical switch couples t cell receptor triggering to the cytoplasmic juxtamembrane regions of cd3$\zeta\zeta$. *Immunity*, 2015.

[126] Wesley R Legant, Colin K Choi, Jordan S Miller, Lin Shao, Liang Gao, Eric Betzig, and Christopher S Chen. Multidimensional traction force microscopy reveals out-of-plane rotational moments about focal adhesions. *Proceedings of the National Academy of Sciences*, 110(3):881–886, 2013.

[127] Wesley R Legant, Jordan S Miller, Brandon L Blakely, Daniel M Cohen, Guy M Genin, and Christopher S Chen. Measurement of mechanical tractions exerted by cells in three-dimensional matrices. *Nature methods*, 7(12):969–971, 2010.

[128] Albert Leibovitz. The growth and maintenance of tissue–cell cultures in free gas exchange with the atmosphere. *American Journal of Epidemiology*, 78(2):173–180, 1963.

[129] Ilya Levental, Penelope C Georges, and Paul A Janmey. Soft biological materials and their impact on cell function. *Soft Matter*, 3(3):299–306, 2007.

[130] RS Lewis. Calcium oscillations in t-cells: mechanisms and consequences for gene expression. *Biochemical Society Transactions*, 31(5):925–929, 2003.

[131] Ya-Chen Li, Bing-Mae Chen, Pei-Chun Wu, Tian-Lu Cheng, Lung-Sen Kao, Mi-Hua Tao, Andre Lieber, and Steve R Roffler. Cutting edge: mechanical forces acting on t cells immobilized via the tcr complex can trigger tcr signaling. *The Journal of Immunology*, 184(11):5959–5963, 2010.

[132] Baoyu Liu, Wei Chen, Brian D Evavold, and Cheng Zhu. Accumulation of dynamic catch bonds between tcr and agonist peptide-mhc triggers t cell signaling. *Cell*, 157(2):357–368, 2014.

[133] Jing Liu, Youhua Tan, Huafeng Zhang, Yi Zhang, Pingwei Xu, Junwei Chen, Yeh-Chuin Poh, Ke Tang, Ning Wang, and Bo Huang. Soft fibrin gels promote selection and growth of tumorigenic cells. *Nature materials*, 11(8):734–741, 2012.

[134] Chun-Min Lo, Hong-Bei Wang, Micah Dembo, and Yu-li Wang. Cell movement is guided by the rigidity of the substrate. *Biophysical journal*, 79(1):144–152, 2000.

[135] Zhengyu Ma and Terri H Finkel. T cell receptor triggering by force. *Trends in immunology*, 31(1):1–6, 2010.

[136] Zhengyu Ma, Paul A Janmey, and Terri H Finkel. The receptor deformation model of tcr triggering. *The FASEB Journal*, 22(4):1002–1008, 2008.

[137] M. Machacek and G. Danuser. Morphodynamic profiling of protrusion phenotypes. *Biophysical journal*, 90(4):1439, 2006.

[138] Philippe Marcq, Natsuhiko Yoshinaga, and Jacques Prost. Rigidity sensing explained by active matter theory. *Biophysical journal*, 101(6):L33–L35, 2011.

[139] Noa B Martín-Cófreces, Francesc Baixauli, María J López, Diana Gil, Alicia Monjas, Balbino Alarcón, and Francisco Sánchez-Madrid. End-binding protein 1 controls signal propagation from the t cell receptor. *The EMBO journal*, 31(21):4140–4152, 2012.

[140] Noa B Martín-Cófreces, Javier Robles-Valero, J Román Cabrero, María Mittelbrunn, Mónica Gordón-Alonso, Ching-Hwa Sung, Balbino Alarcón, Jesús Vázquez, and Francisco Sánchez-Madrid. Mtoc translocation modulates is formation and controls sustained t cell signaling. *The Journal of cell biology*, 182(5):951–962, 2008.

[141] David Masopust and Jason M Schenkel. The integration of t cell migration, differentiation and function. *Nature Reviews Immunology*, 13(5):309–320, 2013.

[142] Nelson A Medeiros, Dylan T Burnette, and Paul Forscher. Myosin ii functions in actin-bundle turnover in neuronal growth cones. *Nature cell biology*, 8(3):216–226, 2006.

[143] David Meiri, Christopher B Marshall, Melissa A Greeve, Bryan Kim, Marc Balan, Fernando Suarez, Chris Bakal, Chuanjin Wu, Jose LaRose, Noah Fine, et al. Mechanistic insight into the microtubule and actin cytoskeleton coupling through dynein-dependent rhogef inhibition. *Molecular cell*, 45(5):642–655, 2012.

[144] David Meiri, Christopher B Marshall, Daphna Mokady, Jose LaRose, Michael Mullin, Anne-Claude Gingras, Mitsuhiko Ikura, and Robert Rottapel. Mechanistic insight into gpcr-mediated activation of the microtubule-associated rhoa exchange factor gef-h1. *Nature communications*, 5, 2014.

[145] Aaron F Mertz, Yonglu Che, Shiladitya Banerjee, Jill M Goldstein, Kathryn A Rosowski, Stephen F Revilla, Carien M Niessen, M Cristina Marchetti, Eric R Dufresne, and Valerie Horsley. Cadherin-based intercellular adhesions organize epithelial cell–matrix traction forces. *Proceedings of the National Academy of Sciences*, 110(3):842–847, 2013.

[146] Justin D Mih, Aleksandar Marinkovic, Fei Liu, Asma S Sharif, and Daniel J Tschumperlin. Matrix stiffness reverses the effect of actomyosin tension on cell proliferation. *Journal of cell science*, 125(24):5974–5983, 2012.

[147] Emad Moeendarbary, Léo Valon, Marco Fritzsche, Andrew R Harris, Dale A Moulding, Adrian J Thrasher, Eleanor Stride, L Mahadevan, and Guillaume T Charras. The cytoplasm of living cells behaves as a poroelastic material. *Nature materials*, 12(3):253–261, 2013.

[148] Colin RF Monks, Benjamin A Freiberg, Hannah Kupfer, Noah Sciaky, and Abraham Kupfer. Three-dimensional segregation of supramolecular activation clusters in t cells. *Nature*, 395(6697):82–86, 1998.

[149] James J Moon, H Hamlet Chu, Marion Pepper, Stephen J McSorley, Stephen C Jameson, Ross M Kedl, and Marc K Jenkins. Naive cd4$^+$ t cell frequency varies for different epitopes and predicts repertoire diversity and response magnitude. *Immunity*, 27(2):203–213, 2007.

[150] Simon W Moore, Pere Roca-Cusachs, and Michael P Sheetz. Stretchy proteins on stretchy substrates: the important elements of integrin-mediated rigidity sensing. *Developmental cell*, 19(2):194–206, 2010.

[151] Masatoshi Morimatsu, Armen H Mekhdjian, Alice C Chang, Steven J Tan, and Alexander R Dunn. Visualizing the interior architecture of focal adhesions with high-resolution traction maps. *Nano letters*, 15(4):2220–2228, 2015.

[152] Kaspar D Mossman, Gabriele Campi, Jay T Groves, and Michael L Dustin. Altered tcr signaling from geometrically repatterned immunological synapses. *Science Signaling*, 310(5751):1191, 2005.

[153] Steven Munevar, Yu-li Wang, and Micah Dembo. Regulation of mechanical interactions between fibroblasts and the substratum by stretch-activated ca2+ entry. *Journal of cell science*, 117(1):85–92, 2004.

[154] K. Nguyen, N.R. Sylvain, and S.C. Bunnell. T cell costimulation via the integrin vla-4 inhibits the actin-dependent centralization of signaling microclusters containing the adaptor slp-76. *Immunity*, 28(6):810–821, 2008.

[155] Wagner Shin Nishitani, Taher A Saif, and Yingxiao Wang. Calcium signaling in live cells on elastic gels under mechanical vibration at subcellular levels. *PloS one*, 6(10):e26181, 2011.

[156] BJ Nolen, N Tomasevic, A Russell, DW Pierce, Z Jia, CD McCormick, J Hartman, R Sakowicz, and TD Pollard. Characterization of two classes of small molecule inhibitors of arp2/3 complex. *Nature*, 460(7258):1031–1034, 2009.

[157] Jeffrey C Nolz, Timothy S Gomez, Peimin Zhu, Shuixing Li, Ricardo B Medeiros, Yoji Shimizu, Janis K Burkhardt, Bruce D Freedman, and Daniel D Billadeau. The wave2 complex regulates actin cytoskeletal reorganization and crac-mediated calcium entry during t cell activation. *Current biology*, 16(1):24–34, 2006.

[158] Leann L Norman, Jan Brugés, Kheya Sengupta, Pierre Sens, and Helim Aranda-Espinoza. Cell blebbing and membrane area homeostasis in spreading and retracting cells. *Biophysical journal*, 99(6):1726–1733, 2010.

[159] Patrick W Oakes, Dipan C Patel, Nicole A Morin, Daniel P Zitterbart, Ben Fabry, Jonathan S Reichner, and Jay X Tang. Neutrophil morphology and migration are affected by substrate elasticity. *Blood*, 114(7):1387–1395, 2009.

[160] Joshua J Obar, Kamal M Khanna, and Leo Lefrançois. Endogenous naive cd8$^+$ t cell precursor frequency regulates primary and memory responses to infection. *Immunity*, 28(6):859–869, 2008.

[161] Roddy S OConnor, Xueli Hao, Keyue Shen, Keenan Bashour, Tatiana Akimova, Wayne W Hancock, Lance C Kam, and Michael C Milone. Substrate rigidity regulates human t cell activation and proliferation. *The Journal of Immunology*, 189(3):1330–1339, 2012.

[162] P.J. Paddison, M. Cleary, J.M. Silva, K. Chang, N. Sheth, R. Sachidanandam, and G.J. Hannon. Cloning of short hairpin rnas for gene knockdown in mammalian cells. *Nature Methods*, 1(2):163–167, 2004.

[163] Olivier Pertz, Louis Hodgson, Richard L. Klemke, and Klaus M. Hahn. Spatiotemporal dynamics of rhoa activity in migrating cells. *Nature*, 440(7087):1069–1072, 2006. 10.1038/nature04665.

[164] Jeffrey R Peterson and Timothy J Mitchison. Small molecules, big impact: a history of chemical inhibitors and the cytoskeleton. *Chemistry & biology*, 9(12):1275–1285, 2002.

[165] Ryan J Petrie, Hyun Koo, and Kenneth M Yamada. Generation of compartmentalized pressure by a nuclear piston governs cell motility in a 3d matrix. *Science*, 345(6200):1062–1065, 2014.

[166] Anne Pierres, Philippe Eymeric, Emmanuelle Baloche, Dominique Touchard, Anne-Marie Benoliel, and Pierre Bongrand. Cell membrane alignment along adhesive surfaces: contribution of active and passive cell processes. *Biophysical journal*, 84(3):2058–2070, 2003.

[167] Alex T Ritter, Yukako Asano, Jane C Stinchcombe, NMG Dieckmann, Bi-Chang Chen, C Gawden-Bone, Schuyler van Engelenburg, Wesley Legant, Liang Gao, Michael W Davidson, et al. Actin depletion initiates events leading to granule secretion at the immunological synapse. *Immunity*, 42(5):864–876, 2015.

[168] Michael J Rosenbluth, Ailey Crow, Joshua W Shaevitz, and Daniel A Fletcher. Slow stress propagation in adherent cells. *Biophysical journal*, 95(12):6052–6059, 2008.

[169] Michael J Rosenbluth, Wilbur A Lam, and Daniel A Fletcher. Force microscopy of nonadherent cells: a comparison of leukemia cell deformability. *Biophysical journal*, 90(8):2994–3003, 2006.

[170] Markus G Rudolph, John G Luz, and Ian A Wilson. Structural and thermodynamic correlates of t cell signaling. *Annual review of biophysics and biomolecular structure*, 31(1):121–149, 2002.

[171] Gillian L Ryan, Heather M Petroccia, Naoki Watanabe, and Dimitrios Vavylonis. Excitable actin dynamics in lamellipodial protrusion and retraction. *Biophysical journal*, 102(7):1493–1502, 2012.

[172] Benedikt Sabass, Margaret L Gardel, Clare M Waterman, and Ulrich S Schwarz. High resolution traction force microscopy based on experimental and computational advances. *Biophysical Journal*, 94(1):207–220, 2008.

[173] Karen Sachs, Omar Perez, Dana Pe'er, Douglas A Lauffenburger, and Garry P Nolan. Causal protein-signaling networks derived from multiparameter single-cell data. *Science*, 308(5721):523–529, 2005.

[174] Maria Saline, Karin EJ Rödström, Gerhard Fischer, Vladislav Yu Orekhov, B Göran Karlsson, and Karin Lindkvist-Petersson. The structure of superantigen complexed with tcr and mhc reveals novel insights into superantigenic t cell activation. *Nature communications*, 1:119, 2010.

[175] Audrey Salles, Cyrille Billaudeau, Arnauld Sergé, Anne-Marie Bernard, Marie-Claire Phélipot, et al. Barcoding t cell calcium response diversity with methods for automated and accurate analysis of cell signals (maaacs). *PLoS Comput. Biol*, 9:e1003245, 2013.

[176] Wendy C Salmon, Michael C Adams, and Clare M Waterman-Storer. Dual-wavelength fluorescent speckle microscopy reveals coupling of microtubule and actin movements in migrating cells. *The Journal of cell biology*, 158(1):31–37, 2002.

[177] Yasuhiro Sawada, Masako Tamada, Benjamin J Dubin-Thaler, Oksana Cherniavskaya, Ryuichi Sakai, Sakae Tanaka, and Michael P Sheetz. Force sensing by mechanical extension of the src family kinase substrate p130cas. *Cell*, 127(5):1015–1026, 2006.

[178] Andrew W Schaefer, Nurul Kabir, and Paul Forscher. Filopodia and actin arcs guide the assembly and transport of two populations of microtubules with unique dynamic parameters in neuronal growth cones. *The Journal of cell biology*, 158(1):139–152, 2002.

[179] Britta Schroth-Diez, Silke Gerwig, Mary Ecke, Reiner Hegerl, Stefan Diez, and Günther Gerisch. Propagating waves separate two states of actin organization in living cells. *HFSP journal*, 3(6):412–427, 2009.

[180] Kheya Sengupta, Helim Aranda-Espinoza, Lee Smith, Paul Janmey, and Daniel Hammer. Spreading of neutrophils: from activation to migration. *Biophysical journal*, 91(12):4638–4648, 2006.

[181] VB Shenoy and LB Freund. Growth and shape stability of a biological membrane adhesion complex in the diffusion-mediated regime. *Proceedings of the National Academy of Sciences of the United States of America*, 102(9):3213–3218, 2005.

[182] E. Sherman, V. Barr, S. Manley, G. Patterson, L. Balagopalan, I. Akpan, C.K. Regan, R.K. Merrill, C.L. Sommers, J. Lippincott-Schwartz, et al. Functional

nanoscale organization of signaling molecules downstream of the t cell antigen receptor. *Immunity*, 2011.

[183] Xiaoshan Shi, Yunchen Bi, Wei Yang, Xingdong Guo, Yan Jiang, Chanjuan Wan, Lunyi Li, Yibing Bai, Jun Guo, Yujuan Wang, et al. Ca2+ regulates t-cell receptor activation by modulating the charge property of lipids. *Nature*, 493(7430):111–115, 2013.

[184] Scott H Soderling. Grab your partner with both hands: cytoskeletal remodeling by arp2/3 signaling. *Science signaling*, 2(55):pe5.

[185] Martin P Stewart, Jonne Helenius, Yusuke Toyoda, Subramanian P Ramanathan, Daniel J Muller, and Anthony A Hyman. Hydrostatic pressure and the actomyosin cortex drive mitotic cell rounding. *Nature*, 469(7329):226–230, 2011.

[186] Jane C Stinchcombe, Endre Majorovits, Giovanna Bossi, Stephen Fuller, and Gillian M Griffiths. Centrosome polarization delivers secretory granules to the immunological synapse. *Nature*, 443(7110):462–465, 2006.

[187] J.K. Sveen. An introduction to matpiv v. 1.6. 1. *World Wide Web Internet And Web Information Systems*, 2004.

[188] Joe Swift, Irena L Ivanovska, Amnon Buxboim, Takamasa Harada, PC Dave P Dingal, Joel Pinter, J David Pajerowski, Kyle R Spinler, Jae-Won Shin, Manorama Tewari, et al. Nuclear lamin-a scales with tissue stiffness and enhances matrix-directed differentiation. *Science*, 341(6149):1240104, 2013.

[189] Susan Swift, James Lorens, Philip Achacoso, and Garry P Nolan. Rapid production of retroviruses for efficient gene delivery to mammalian cells using 293t cell–based systems. *Current protocols in immunology*, pages 10–17.

[190] M Szabo, T Czompoly, K Kvell, G Talaber, D Bartis, P Nemeth, T Berki, and F Boldizsar. Fine-tuning of proximal tcr signaling by zap-70 tyrosine residues in jurkat cells. *International immunology*, 24(2):79–87, 2012.

[191] Aya Takesono, Sarah J Heasman, Beata Wojciak-Stothard, Ritu Garg, and Anne J Ridley. Microtubules regulate migratory polarity through rho/rock signaling in t cells. *PLoS One*, 5(1):e8774, 2010.

[192] D Thomas, SC Tovey, TJ Collins, MD Bootman, MJ Berridge, and P Lipp. A comparison of fluorescent ca¡ sup¿ 2+¡/sup¿ indicator properties and their use in measuring elementary and global ca¡ sup¿ 2+¡/sup¿ signals. *Cell calcium*, 28(4):213–223, 2000.

[193] X. Trepat, M.R. Wasserman, T.E. Angelini, E. Millet, D.A. Weitz, J.P. Butler, and J.J. Fredberg. Physical forces during collective cell migration. *Nature physics*, 5(6):426–430, 2009.

[194] Léa Trichet, Jimmy Le Digabel, Rhoda J Hawkins, Sri Ram Krishna Vedula, Mukund Gupta, Claire Ribrault, Pascal Hersen, Raphaël Voituriez, and Benoît Ladoux. Evidence of a large-scale mechanosensing mechanism for cellular adaptation to substrate stiffness. *Proceedings of the National Academy of Sciences*, 109(18):6933–6938, 2012.

[195] US Tulu, NM Rusan, and P Wadsworth. Peripheral, non-centrosome-associated microtubules contribute to spindle formation in centrosome-containing cells. *Current biology*, 13(21):1894–1899, 2003.

[196] Masayoshi Uehata, Toshimasa Ishizaki, Hiroyuki Satoh, Takashi Ono, Toshio Kawahara, Tamami Morishita, Hiroki Tamakawa, Keiji Yamagami, Jun Inui, Midori Maekawa, et al. Calcium sensitization of smooth muscle mediated by a rho-associated protein kinase in hypertension. *Nature*, 389(6654):990–993, 1997.

[197] P Anton van der Merwe and Omer Dushek. Mechanisms for t cell receptor triggering. *Nature Reviews Immunology*, 11(1):47–55, 2011.

[198] David Van Goor, Callen Hyland, Andrew W Schaefer, and Paul Forscher. The role of actin turnover in retrograde actin network flow in neuronal growth cones. *PloS one*, 7(2):e30959, 2012.

[199] Rajat Varma, Gabriele Campi, Tadashi Yokosuka, Takashi Saito, and Michael L Dustin. T cell receptor-proximal signals are sustained in peripheral microclusters and terminated in the central supramolecular activation cluster. *Immunity*, 25(1):117–127, 2006.

[200] Claudia G Vasquez, Mike Tworoger, and Adam C Martin. Dynamic myosin phosphorylation regulates contractile pulses and tissue integrity during epithelial morphogenesis. *The Journal of cell biology*, 206(3):435–450, 2014.

[201] Miguel Vicente-Manzanares, Xuefei Ma, Robert S Adelstein, and Alan Rick Horwitz. Non-muscle myosin ii takes centre stage in cell adhesion and migration. *Nature reviews Molecular cell biology*, 10(11):778–790, 2009.

[202] Michael G Vicker. Eukaryotic cell locomotion depends on the propagation of self-organized reaction–diffusion waves and oscillations of actin filament assembly. *Experimental cell research*, 275(1):54–66, 2002.

[203] Tetsuro Wakatsuki, Robert B Wysolmerski, and Elliot L Elson. Mechanics of cell spreading: role of myosin ii. *Journal of cell science*, 116(8):1617–1625, 2003.

[204] Toshiyuki Watanabe, Hiroshi Hosoya, and Shigenobu Yonemura. Regulation of myosin ii dynamics by phosphorylation and dephosphorylation of its light chain in epithelial cells. *Molecular biology of the cell*, 18(2):605–616, 2007.

[205] Chaoliang Wei, Xianhua Wang, Min Chen, Kunfu Ouyang, Long-Sheng Song, and Heping Cheng. Calcium flickers steer cell migration. *Nature*, 457(7231):901–905, 2009.

[206] Orion D Weiner, William A Marganski, Lani F Wu, Steven J Altschuler, and Marc W Kirschner. An actin-based wave generator organizes cell motility. *PLoS biology*, 5(9):e221, 2007.

[207] Matthew D Welch and R Dyche Mullins. Cellular control of actin nucleation. *Annual review of cell and developmental biology*, 18(1):247–288, 2002.

[208] David J Williamson, Dylan M Owen, Jérémie Rossy, Astrid Magenau, Matthias Wehrmann, J Justin Gooding, and Katharina Gaus. Pre-existing clusters of the adaptor lat do not participate in early t cell signaling events. *Nature immunology*, 12(7):655–662, 2011.

[209] Torsten Wittmann and Clare M Waterman-Storer. Cell motility: can rho gtpases and microtubules point the way? *Journal of cell science*, 114(21):3795–3803, 2001.

[210] Christoph Wülfing and Mark M Davis. A receptor/cytoskeletal movement triggered by costimulation during t cell activation. *Science*, 282(5397):2266–2269, 1998.

[211] Christoph Wülfing, Joshua D Rabinowitz, Craig Beeson, Michael D Sjaastad, Harden M McConnell, and Mark M Davis. Kinetics and extent of t cell activation as measured with the calcium signal. *The Journal of experimental medicine*, 185(10):1815–1825, 1997.

[212] Zhen Xia, Huabiao Chen, Seung-gu Kang, Tien Huynh, Justin W Fang, Pedro A Lamothe, Bruce D Walker, and Ruhong Zhou. The complex and specific pmhc interactions with diverse hiv-1 tcr clonotypes reveal a structural basis for alterations in ctl function. *Scientific reports*, 4, 2014.

[213] Chenqi Xu, Etienne Gagnon, Matthew E Call, Jason R Schnell, Charles D Schwieters, Christopher V Carman, James J Chou, and Kai W Wucherpfennig.

Regulation of t cell receptor activation by dynamic membrane binding of the cd3$\epsilon$ cytoplasmic tyrosine-based motif. *Cell*, 135(4):702–713, 2008.

[214] Patricia T Yam, Cyrus A Wilson, Lin Ji, Benedict Hebert, Erin L Barnhart, Natalie A Dye, Paul W Wiseman, Gaudenz Danuser, and Julie A Theriot. Actin–myosin network reorganization breaks symmetry at the cell rear to spontaneously initiate polarized cell motility. *The Journal of cell biology*, 178(7):1207–1221, 2007.

[215] Jason Yi, Xufeng Wu, Andrew H Chung, James K Chen, Tarun M Kapoor, and John A Hammer. Centrosome repositioning in t cells is biphasic and driven by microtubule end-on capture-shrinkage. *The Journal of cell biology*, 202(5):779–792, 2013.

[216] Jason Yi, Xufeng S Wu, Travis Crites, and John A Hammer. Actin retrograde flow and actomyosin ii arc contraction drive receptor cluster dynamics at the immunological synapse in jurkat t cells. *Molecular biology of the cell*, 23(5):834–852, 2012.

[217] Yiyuan Yin, Xin Xiang Wang, and Roy A Mariuzza. Crystal structure of a complete ternary complex of t-cell receptor, peptide–mhc, and cd4. *Proceedings of the National Academy of Sciences*, 109(14):5405–5410, 2012.

[218] Tadashi Yokosuka and Takashi Saito. The immunological synapse, tcr microclusters, and t cell activation. In *Immunological Synapse*, pages 81–107. Springer, 2010.

[219] Tadashi Yokosuka, Kumiko Sakata-Sogawa, Wakana Kobayashi, Michio Hiroshima, Akiko Hashimoto-Tane, Makio Tokunaga, Michael L Dustin, and Takashi Saito. Newly generated t cell receptor microclusters initiate and sustain t cell activation by recruitment of zap70 and slp-76. *Nature immunology*, 6(12):1253–1262, 2005.

[220] Cheng-han Yu, Hung-Jen Wu, Yoshihisa Kaizuka, Ronald D Vale, and Jay T Groves. Altered actin centripetal retrograde flow in physically restricted immunological synapses. *PloS one*, 5(7):e11878, 2010.

[221] Yan Yu, Nicole C Fay, Alexander A Smoligovets, Hung-Jen Wu, and Jay T Groves. Myosin iia modulates t cell receptor transport and casl phosphorylation during early immunological synapse formation. *PloS one*, 7(2):e30704, 2012.

[222] Yan Yu, Alexander A Smoligovets, and Jay T Groves. Modulation of t cell signaling by the actin cytoskeleton. *Journal of cell science*, 126(5):1049–1058, 2013.

[223] A Zemel, F Rehfeldt, AEX Brown, DE Discher, and SA Safran. Optimal matrix rigidity for stress-fibre polarization in stem cells. *Nature physics*, 6(6):468–473, 2010.

[224] Xiao-Feng Zhang, Andrew W Schaefer, Dylan T Burnette, Vincent T Schoonderwoert, and Paul Forscher. Rho-dependent contractile responses in

the neuronal growth cone are independent of classical peripheral retrograde actin flow. *Neuron*, 40(5):931–944, 2003.

[225] Yun Zhang, Chenghao Ge, Cheng Zhu, and Khalid Salaita. Dna-based digital tension probes reveal integrin forces during early cell adhesion. *Nature communications*, 5, 2014.

[226] Christof Zitt, Bettina Strauss, Eva C Schwarz, Nicola Spaeth, Georg Rast, Armin Hatzelmann, and Markus Hoth. Potent inhibition of ca2+ release-activated ca2+ channels and t-lymphocyte activation by the pyrazole derivative btp2. *Journal of Biological Chemistry*, 279(13):12427–12437, 2004.